

The Pennsylvania State University
The Graduate School
Department of Electrical Engineering

ACTIVE ENERGY HARVESTING

A Thesis in
Electrical Engineering

by
Yiming Liu

© 2006 Yiming Liu

Submitted in Partial Fulfillment
of the Requirements
for the Degree of

Doctor of Philosophy

December 2006

The thesis of Yiming Liu was reviewed and approved* by the following:

Heath F. Hofmann
Associate Professor of Electrical Engineering
Thesis Advisor
Chair of Committee

Qiming Zhang
Professor of Electrical Engineering

George A. Lesieutre
Professor and Head of Aerospace Engineering

Jeffrey Mayer
Associate Professor of Electrical Engineering

W. Kenneth Jenkins
Professor and Head of Electrical Engineering

*Signatures are on file in the Graduate School

ABSTRACT

Harvesting energy from the ambient environment is an enabling technology for wide deployment of wireless sensor networks. Converting mechanical energy to electrical energy using piezoelectric and electrostrictive materials has been the choice for many energy harvesting applications. The energy harvesting circuit is the interface between a piezoelectric/electrostrictive device and electrical load. A conventional view of energy harvesting circuitry is based on power conditioning concepts, which often involve AC to DC conversion and voltage regulation. In fact, an energy harvesting circuit also applies electrical boundary conditions to the device during energy conversion which are crucial for optimizing the harvested energy. This thesis presents a study of a relatively new type of energy harvesting approach: active energy harvesting.

In this thesis, energy harvesting using both piezoelectric and electrostrictive materials is investigated. For each type of material, a theoretical model of energy conversion process is established, based on the electro-mechanical boundary conditions applied to the device by different energy harvesting circuits. This modeling technique has certain advantages over a harmonic analysis approach. First, it gives a more intuitive picture in terms of understanding the energy harvesting process than the harmonic analysis approach. Second, it is more general in its conclusions, that is the input mechanical excitation and electrical boundary conditions are not constrained to sinusoidal form but instead represented by several critical states of the electro-mechanical boundary conditions. Finally, for nonlinear materials, such as electrostrictive polymer, a linear

harmonic analysis is no longer applicable, while the presented technique does not have this limitation.

As a result of better understanding the importance of electromechanical boundary conditions in the energy conversion process, questions were raised: what is the best electrical boundary condition for a given mechanical excitation? And how to achieve the maximum power conversion? This thesis answers these questions by presenting the relatively new concept of active energy harvesting, which uses switch-mode power electronics to control the voltage and/or current of the piezoelectric/electrostrictive devices. Two control strategies, voltage control and charge control mode of operation are presented.

Practically, power electronic circuits are not 100 percent power efficient, which greatly influences the performance of active energy harvesting system. We also address this issue by taking into account the loss due to reactive power flow between the piezoelectric/electrostrictive device and the energy storage unit.

Experimental results of active energy harvesting are also presented for both piezoelectric and electrostrictive polymers. The model is validated by comparing theoretical prediction with experimental data. The experimental results also demonstrated superior energy harvesting performance over conventional diode rectifier circuits.

TABLE OF CONTENTS

LIST OF FIGURES	viii
LIST OF TABLES	xi
ACKNOWLEDGEMENTS	xii
Chapter 1 Introduction	1
1.1 Motivation.....	1
1.2 Contribution of the Thesis	3
1.3 Thesis Overview	4
Chapter 2 Energy Harvesting Background	6
2.1 Resources	6
2.1.1 Electromagnetic (EM) radiation	6
2.1.2 Thermal energy.....	8
2.1.3 Kinetic energy	8
2.1.4 Comparison.....	9
2.2 Mechanical energy harvesting methods.....	11
2.2.1 Electromagnetic generator	11
2.2.2 Electrostatic system	13
2.2.3 Piezoelectric materials and devices	14
2.2.4 Electrostrictive polymers.....	16
2.2.5 Comparison.....	17
2.3 Mechanical energy harvesting applications.....	18
2.3.1 Quasi-static excitation applications.....	19
2.3.2 Harmonic excitation	21
2.3.3 Impulsive mechanical excitation	22
2.4 Energy harvesting system	23
2.4.1 The power flow of the system	23
2.4.2 Control of the energy harvesting circuit	28
Chapter 3 Quasi-static Linear Energy Harvesting Theory.....	31
3.1 Piezoelectric material and device	31
3.2 Passive and Semi-passive Energy harvesting circuits	37
3.2.1 Passive circuits	39
3.2.1.1 Diode rectifier	39
3.2.1.2 Synchronous Charge Extraction.....	45
3.2.2 Semi-passive energy harvesting circuit	48
3.2.2.1 Serial SSHI circuit.....	49

3.2.2.2 Parallel SSHI circuit.....	55
3.3 Active energy harvesting.....	59
3.3.1 Fundamental limitation.....	60
3.3.2 Voltage controlled mode.....	62
3.3.3 Charge control.....	66
3.3.4 Inefficiency of power electronics.....	68
3.4 Theoretical Comparison of energy harvesting circuits.....	71
Chapter 4 Active Energy Harvesting Experiment Using Piezoelectric.....	75
4.1 Mechanical excitation.....	75
4.2 Determination of Device Parameters.....	76
4.3 The power electronic circuit.....	80
4.4 Controller.....	83
4.5 Results.....	84
4.6 Comparison and conclusion.....	88
Chapter 5 Quasi-static Electrostrictive Energy Harvesting Theory.....	89
5.1 Electrostrictive materials and devices.....	90
5.2 Energy Harvesting Cycle and Boundary Conditions.....	91
5.2.1 Coupling Factor Determined from Linearized Model of Electrostriction.....	94
5.2.2 Energy Harvesting Cycle #1: Constant Field and Open-Circuit Electrical Boundary Conditions.....	95
5.2.3 Energy Harvesting Cycle #2: Constant-Field Boundary Conditions During stressing and Unstressing of Material.....	98
5.2.4 Energy Harvesting Cycle #3: Open-Circuit Boundary Conditions During Stressing and Unstressing of Material.....	100
5.2.5 Energy Harvesting Cycle #4: Passive Diode Circuit for Energy Harvesting.....	101
5.2.6 Sinusoidal excitation.....	103
5.3 Comparison of Different Boundary Conditions.....	105
Chapter 6 Quasi-static Electrostrictive Energy Harvesting Experiment.....	109
6.1 Experimental.....	109
6.1.1 MECHANICAL SYSTEM AND EXPERIMENTAL SETUP.....	109
6.1.2 Experiment and results.....	111
6.1.2.1 Determined the loss.....	112
6.1.2.2 Energy harvesting.....	114
Chapter 7 Conclusions and Future Work.....	121
7.1 Summary.....	121

7.2 Future Work.....	122
Bibliography	123

LIST OF FIGURES

Figure 2.1: Amirtharajah and Chandrabasan 1998 [29].....	12
Figure 2.2: Capacitive energy harvesting device	14
Figure 2.3: Lead Zirconate Titanate (PZT) unit cell.....	15
Figure 2-4: Vibration energy harvesting using an attached piezoelectric device (Left) and using proof-mass (Right)	22
Figure 2.5: Energy harvesting system.....	25
Figure 2.6: Control flow of energy harvesting system	30
Figure 3.1: Energy harvesting cycle for coupling coefficient defination	35
Figure 3.2: Energy conversion loop.....	38
Figure 3.3: Full bridge diode rectifier (a) and half bridge diode rectifier circuit (b)...	39
Figure 3.4: Voltage wave of full bridge (left) and half bridge (right) rectifier.....	40
Figure 3.5: Experimental comparison of full bridge and half bridge rectifier. Half bridge rectifier has more optimized power and doubled optimized voltage.	41
Figure 3.6: Energy conversion cycle for full bridge rectifier circuit (a) electrical domain, (b) mechanical domain	42
Figure 3.7: Synchronous charge extraction circuit	46
Figure 3.8: The energy conversion cycle of the synchronous charge extraction circuit. (a) electrical domain, (b) mechanical domain. The dash line is the full-bridge rectifier circuit under same force excitation, their enclosed area are one forth that of synchronous charge extraction.....	47
Figure 3.9: (a) serial synchronized switch harvesting on inductor circuit (b) implementation of serial synchronized switch harvesting on inductor circuit using bidirectional switch made of two back to back PMOS transistors	49
Figure 3.10: A simplifier synchronized switch harvesting on inductor circuit (a) and its single PMOS transistor implementation	50
Figure 3.11: Conversion cycle of serial synchronized switch harvesting on inductor circuit (a) electric domain, (b) mechanical domain.....	51

Figure 3.12: Equivalent circuit of serial synchronized switch harvesting on inductor circuit during transition	52
Figure 3.13: Parallel SSHI circuit and its implementation	56
Figure 3.14: Energy conversion cycle of Parallel SSHI circuit (a) electrical domain (b) mechanical domain	57
Figure 3.15: Equivalent Parallel SSHI discharging circuit, where diode blocks the reversion of the current	57
Figure 3.16: Mechanical limits bound the optimized energy conversion.....	61
Figure 3.17: Voltage and displacement bounded energy harvesting cycle.....	63
Figure 3.18: Voltage control of voltage controlled active energy harvesting.....	64
Figure 3.19: Charge controlled energy conversion cycle bounded by both electrical charge and the mechanical displacement	66
Figure 3.20: Charge controlled energy conversion cycle bounded only by both electrical charge	67
Figure 3.21: The voltage and charge controlled energy harvesting loops that have a equal amount of harvested energy. The shaded area represents the input electrical energy in one cycle	69
Figure 3.22: The performance of active energy harvesting as function of its efficiency	71
Figure 4.1: The mechanical setup for quasi-static energy harvesting.....	76
Figure 4.2: The open-circuit voltage at different levels of mechanical force	78
Figure 4.3: The piezoelectric coefficient changes under different mechanical load ...	79
Figure 4.4: Half bridge converter used for active energy harvesting	81
Figure 4.5: Active energy harvesting control using Simulink for Dspace system implimentation.....	84
Figure 4.6: The voltage controlled mode operation. Channel 3 is the sinusoidal force (at 600lbf/V), while AC coupling of oscilloscope is used. Channel 1 is voltage across piezoelectric device,.....	85

Figure 4.7: Sinusoidal wave is measured force (at 600lbf/V), triangular like wave is voltage across piezoelectric device. The charge controlled mode operation....	86
Figure 4.8: Active energy harvesting compared to diode rectifier circuit. Sinusoidal wave is measured force (at 600lbf/V), trapezoid wave is voltage across piezoelectric device.	87
Figure 5.1: Type Caption Here	92
Figure 5.2: Energy harvesting cycle under constant field 1-2 and open circuit 2-3 electrical boundary conditions.....	96
Figure 5.4: Energy harvesting cycle under open-circuit conditions as stress is applied and removed.....	100
Figure 5.5: Passive diode circuit for energy harvesting.....	101
Figure 5.6: Energy harvesting cycle for passive diode circuit.....	102
Figure 5.7: Theoretical prediction of Electrostrictive energy harvesting under different harvesting circuits	106
Figure 6.1: Experiment setup for electrostrictive materials.....	110
Figure 6.2: The power loss under different electrical excitation when the fixed strain mechanical boundary condition is applied.....	112
Figure 6.3: Curve fitting of loss measurement data to Equation 6.2	114
Figure 6.4: The energy harvesting cycle of electrical field and flux density.....	115
Figure 6.5: Strain stress plot of electrostrictive energy harvesting	116
Figure 6.6: Theoretical and experimental results, in which the solid lines are theoretical prediction	117
Figure 6.7: Mechanical force and voltage wave on the sample during active energy harvesting experiment.....	118
Figure 6.8: Frequency domain of current and voltage wave during active energy harvesting.....	119

LIST OF TABLES

Table 2.1: Energy harvesting performance comparison	10
Table 3.1: Comparison of energy harvesting circuit.....	73
Table 4.1: material properties and geometric information of the single crystal	77
Table 5.1: Electrostrictive Material Parameters and Their Operation Limitations.....	106
Table 5.2: Maximum Energy Harvesting Density and Associated Coupling Factor for Various Electrical Boundary Conditions, Terpolymer Material.....	107
Table 5.3: Maximum Energy Harvesting Density and Associated Coupling Factor for Various Electrical Boundary Conditions, Polyurethane Material.....	107
Table 6.1: Electrostrictive energy harvesting experimental results comparsion	120

ACKNOWLEDGEMENTS

I would like to express my appreciation for those who have guided and supported me through my educational experience. In particular, I would like to thank my adviser Heath Hofmann for imparting his ingenious and optimistic research approach upon me. I also cherished this exciting research opportunity on energy harvesting that Professor Qiming Zhang was instrumental in creating. I am extremely thankful for Professor George Lesieutre for his support and the direction that he has provided to the project from the beginning. Thanks also to Professor Jeffrey Mayer for the inspirational discussion that kept me focused.

I greatly appreciate the help of Dr Jeremy Frank, who has been helped me to understand the mechanical side of energy harvesting systems, as well as help me in other innumerable ways.

My interaction with the many lab mates and colleagues (Jae Do Park, Danhong Zhong, Richard Geiger, Jacob Loverich) with whom I have worked has made my time in graduate school a very enjoyable one.

I am ever grateful to my parents for their constant love and confidence in me.

My most heart felt gratitude goes to my wife Qian. She has been always loving, supportive, and understanding. For her support and partnership I will be always in debt.

Finally, thanks go to my daughter, Emily, who lift my spirits by being such a smart and understanding baby, and serves as a continual reminder to me that my research work is not all that important.

Chapter 1

Introduction

This dissertation is on the use of piezoelectric and electrostrictive materials to generate electrical energy from mechanical excitations. “Energy harvesting” is a process that converts otherwise wasted energy into usable energy, often in the form of electric power. This thesis focus primarily on the study of active energy harvesting, an approach that utilizes a bidirectional switching inverter to actively control the voltage or charge of a piezoelectric or electrostrictive device in certain relation to mechanical input to maximize power conversion. This relatively novel concept for piezoelectric and electrostrictive energy harvesting has not been systematically studied before. Through theoretical analysis and experimental investigation, the active energy harvesting is presented as an effective way to increase output power without modification of the mechanical system relative to other energy harvesting circuits.

1.1 Motivation

Recent years have seen a proliferation of portable electronics and wireless sensor networks [1][2]. Such electronics traditionally are powered by electrochemical batteries. Although the energy density of these batteries has been increasing gradually, it is unlikely they will experience dramatic improvement in the near future [3]. Batteries need to be replaced or replenished regularly, which significantly undermines the convenience and

economical benefits wireless sensor networks and portable devices are supposed to bring. Billions of batteries used every year also pose a huge negative impact on the environment because many of them are not appropriately recycled.

Fortunately, the exponential reduction of power requirements of electronic components in recent years[4], particularly the integrated circuits and MEMS sensors, have enabled what was once negligible sub-milliwatt power to become useful for many applications. For example, a wireless sensor node developed by GE uses only 200 microwatts of average power, and a similar crossbow sensor node consumes about 400 microwatts on average, based on our measurements. Thus, energy harvesting that generates small amounts of power from ambient environment sources creates opportunities for more and more applications. It has been established as an economically viable, environmentally amiable, and technically feasible alternative to batteries as a power source for many applications [5][6]

Researchers and engineers have made enormous progress in energy harvesting technologies in the last decade, including new active materials [7], better device design [8][9][10], and new circuits and controls [11]; however, current technologies still do not meet the requirements of many demanding applications, such as harvesting power from low mechanical vibrations. First, the current technologies do not generate enough power, especially under size and weight restrictions. Second, for a vibration power harvester, the power harvesting bandwidth is usually narrowed down to a few Hz around its resonance frequency, and a slight frequency shift results in a steep power output reduction [12].

In both academia and industry, prevailing energy harvesting circuits under investigation are passive and semi-passive [13][14][15]. However, research on active

vibration control has not only been long established as one of the major research topics, but also has already been adopted for many applications [16][17]. Among these studies, the power regeneration effect has been observed in some active structural damping systems, and researchers have gained a fairly deep understanding of this process [18]. An active energy harvesting which might have been a counterpart of active vibration control, on the other hand, has not drawn deserved attention from either academia or industry. As this dissertation means to be an advocate of active energy harvesting not just for academic reasons, I believe it will be a widely adopted technology in the near future, enabled by technologies such as efficient power electronics, ultra-low power digital signal processors (DSP), and application specific integrated circuits (ASIC).

1.2 Contribution of the Thesis

This thesis research study is the first systematic study of active energy harvesting approaches from mechanical excitations using piezoelectric and electrostrictive materials. First, a model-based analysis of existing energy harvesting circuits and active energy harvesting for linear (Piezoelectricity) and non-linear (Electrostrictive) harvester under quasi-static assumptions is presented. Unlike the conventional equivalent circuit modeling technique, our model emphasizes the importance of electro-mechanical boundary conditions in energy conversion cycle, revealing a fundamental role that the electric circuit plays in energy conversion.

Second, experiments are performed for quasi-static piezoelectric and electrostriction energy harvesting, showing significant improvement of power harvesting.

These results match well with theoretical predictions. Control algorithms and power electronic designs used in these experiments could be further developed into practical standalone energy harvesting circuits.

Finally, some practical limitations of active energy harvesting are discussed for all systems, including maximum voltage or charge on the device or electrical circuit. The optimum operating condition is presented considering the efficiency of the power electronic circuit. These results also serve as a general design guideline for active energy harvesting design.

1.3 Thesis Overview

Chapter 2 is a background review of energy harvesting. First, we discuss energy harvesting resources in general. Then, as our focus, mechanical energy harvesting is covered for both quasi-static and dynamic applications. Secondly, different mechanical-electric conversion mechanisms are presented based on their advantages and disadvantages. Finally, we look at the energy harvesting system from both energy flow and control system points of view, addressing how to optimize the interaction between mechanical input and a system to maximize the harvested power.

Piezoelectric ceramic, polymer and single crystal are usually considered to have a linear electrical-mechanical coupling. In Chapter 3, we first introduce the properties that are closely related to energy harvesting. Then a quasi-static energy conversion cycle is shown for three types of energy harvesting; namely passive, semi-passive, and active

approaches. In this chapter, we also investigate the effect of the efficiency of power electronics on the active energy harvesting.

Chapter 4 discusses an experimental demonstration of quasi-static active energy harvesting using piezoelectric single crystal (PMN-PT). The experiment results are compared to the theoretical model that is developed in Chapter 3.

Non-linear systems, including electrostrictive material, electroelastomer and electrostatic generators, are highly interesting for their superior performance over conventional ceramic piezoelectric materials in certain applications. A common characteristic of these non-linear systems is that they all need sustained electric bias fields to be functional. Chapter 5 models the energy conversion of electrostrictive polymers.

In Chapter 6, a very high energy conversion density has been achieved experimentally in electrostrictive polymers using the active approach. The experiment is explained by the modeling of the previous chapter. The theoretical calculation matches well with the experimental results.

Chapter 7 concludes the thesis with general conclusions, and proposes future work that could be done with active energy harvesting.

Chapter 2

Energy Harvesting Background

Energy harvesting is not a new idea. It dates back to 1770, when Abraham-Louis Perrelet, a French scientist, invented a completely autonomous, self-winding pedometer watch that gathers power from an individual's arm movements. However, the development of energy harvesting had been somewhat slow until recent research began seeking alternative power sources for wireless sensor networks and portable electronics. The dramatic reduction in power consumption of these circuits makes various forms of energy meaningful to be harvested.

2.1 Resources

Energy in ambient surroundings exists in three forms. These include electromagnetic (EM), thermal, chemical and mechanical energies.

2.1.1 Electromagnetic (EM) radiation

Electromagnetic (EM) radiation of light and radio waves are of particular interest for harvesting. The energy of electromagnetic waves propagates at the speed of light, and its power density is related to the Poynting vector given by:

$$P = \frac{1}{2} \operatorname{Re} [E \times H^*], \quad (2.1)$$

where E and H are electric and magnetic fields components of the wave.

Photovoltaic systems [19], often known as solar cells, are an older technology that could generate electrical power directly from sunlight, making it useful for a wide range of applications. A state-of-the-art solar cell could convert 20 percent of solar power directly into electricity. Further improvement of the efficiency of solar cells is, however, unlikely to be dramatic in the near future [20].

Invisible to the naked eye, radio frequency (RF) waves are ubiquitous. In cities and very populated areas there are a large number of potential RF sources: broadcast radio and TV, mobile telephones, wireless networks, etc. The challenge of harvesting energy from these sources lies in collecting energy from these disparate sources with moderately sized antennas. An often-used technology is based on a rectifying antenna [21], constructed with a Schottky diode located between the antenna dipoles. Usually the harvestable power is small unless there is an operating cell phone in the vicinity. Researchers have successfully scavenged power from radio waves that radiated from nearby cell phone towers [22].

A recent application of radio-frequency energy harvesting is the so-called passive radio frequency tag. It uses printed circuit antennas to collect power from a nearby transmission antenna. An integrated circuit with built-in flash memory and controls logic can send back the important information about the product, which the Radio Frequency Identification (RFID) [23] is attached to. This technology is also known as 'smarter bar code'.

2.1.2 Thermal energy

If close to thermal sources, thermoelectric devices can generate electrical power from temperature differences. A solid-state thermoelectric generator is usually comprised of a p-type and n-type semiconductor connected electrically in series and thermally in parallel. It produces an electrical current proportional to the temperature difference between the hot and cold junctions. The ideal power conversion efficiency can be driven through the Carnot cycle. If the heat flow from high T_H to low T_L temperatures source is Q , then the maximum useable power is calculated as

$$P = Q \frac{T_H - T_L}{T_H} \quad (2.2)$$

In practice, the conversion efficiency of current technologies is much poorer than this theoretical limit. On a larger scale, geothermal and oceanic temperature gradients are abundant and mostly renewable resources that can generate megawatts of power. Researchers of energy harvesting, however, are more interested in the other end of these extremes: generating power from relative low temperature differences, such as a human's body temperature and the ambient environment. It has been demonstrated that human body temperature is able to generate enough power for a wristwatch at room temperature [24].

2.1.3 Kinetic energy

Motions of all kinds contain kinetic energy. The power is generally related to the force F and its displacement x . Its average power is given by:

$$P = \frac{1}{T} \int_0^T F \dot{x} dt \quad (2.3)$$

And the instantaneous power is given as:

$$P = F \dot{x} \quad (2.4)$$

Mechanical power that is applicable for energy harvesting includes sound, structural vibration, wind, water waves and fluid flow. Human activities, such as walking, are also highly interesting because the energy source becomes portable in nature. Mechanical energy harvesting is the primary topic of this thesis research.

2.1.4 Comparison

Some often used energy harvesting resources is summarized in Table 2.1 as a general comparison.

Table 2.1: Energy harvesting performance comparison

	Power	Conversion	Note
Radio frequency	$1\mu\text{W}/\text{cm}^2$	Antenna	[25]
Light	$100\text{mW}/\text{cm}^2$	Solar cell	17% efficient directly under sun
Vibration	$375\mu\text{W}/\text{cm}^2$	Piezo generator	
Thermo	$60\mu\text{W}/\text{cm}^2$	Thermopile	$T_H=40^\circ\text{C}$, $T_L=35^\circ\text{C}$ Efficient <1%
Airflow	$1\text{mW}/\text{cm}^2$	Micro Turbine	[26]
Heel Strike	7W	Potential available	[27]
	800mW	Elastomer	[28]
	250-700mW	Piezoelectric	

It is unlikely that a single approach to energy harvesting meets the needs of all applications, because energy harvesting is very application specific. The widely used solar power energy harvesting, for example, would be rendered useless in complete darkness. Vibration energy harvesting might be applicable only beyond a certain threshold of vibration levels. Among all the power sources, mechanical to electrical energy conversion was chosen for this dissertation because it is relatively higher power, readily available and potentially low cost, and suitable for many applications, including building automation, transportation, condition based maintenance, etc.

2.2 Mechanical energy harvesting methods

The end product of energy harvesting is usually electrical power. Methods that convert kinetic power to electrical power include electromagnetic induction, electrostatic force, piezoelectric and electrostrictive effects.

2.2.1 Electromagnetic generator

When a closed-loop circuit is immersed in a changing magnetic field, a current will be induced. If the circuit, on the other hand, is open-circuited, a voltage will be generated across the terminals of the circuit. This is mathematically described by the famous Faraday's law in Equation 2.5:

$$\oint E \cdot dl = -\frac{d}{dt} \int B \cdot dA \quad (2.5)$$

Based on Faraday's law, a typical inertial vibration-based generator consists of an oscillating spring and mass system, as shown in the electromagnetic generator for vibration energy harvesting in Figure 2.1. The vibration of the base induces the wire coil to move relative to the permanent magnet. As the magnetic flux moves through the coils an AC current/voltage is generated.

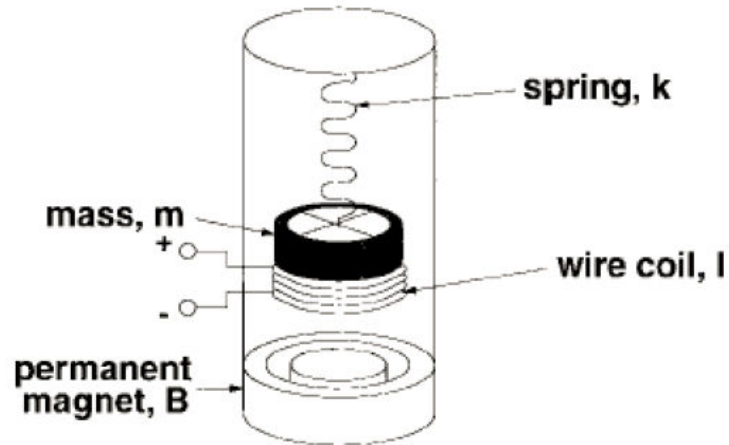


Figure 2.1: Amirtharajah and Chandrabasan 1998 [29]

A theoretical limit on the power such a system could generate could be related to the magnetic energy density in Equation 2.6.

$$u_B = \frac{B^2}{2\mu_0} \quad (2.6)$$

The remanent static magnetic field of the neodymium magnet ($\text{Nd}_2\text{Fe}_{14}\text{B}$) is 1.38 T, and hence the resulting energy density is calculated as $1.38^2 / (2 \times 4\pi \times 10^{-7}) = 0.75 \times 10^6 \text{ J/m}^3$.

An idealistic estimation of how much power an electromagnetic generator could produce for given volume V at excitation angular frequency ω is given as:

$$P = u_B V \frac{\omega}{2\pi} \quad (2.7)$$

2.2.2 Electrostatic system

Electrostatic force is attraction or repulsion of electric charges, which is summarized in Coulomb's law in Equation 2.8:

$$F_{12} = \frac{kq_1q_2}{r^2} \quad (2.8)$$

Where q_1 and q_2 are charges, and $k = 9 \times 10^9 \text{ N} \cdot \text{m}^2 / \text{C}^2$. The force F_{12} is inversely proportional to the square of the distance r between them. For distributed charge and complex geometry, electrostatic force is often mathematically related to Maxwell tensor. In Equation 2.9, we assumed the magnetic field to be zero:

$$\vec{T} = \varepsilon_0 \left(E_i E_j - \frac{1}{2} \delta_{ij} E_k E_k \right) \quad (2.9)$$

Two types of electrostatic generators are variable capacitors and electroelastomers. Shown in Figure 2.2 is a parallel capacitor generator [30]. If electrical voltage has two plates pre-charged, there will be an attractive force between the two. Suppose an external force F moves the plate for a displacement of x . In the meantime, mechanical work is converted to electrical energy [31] according to the conservation of energy. Similarly, if a highly compliant dielectric material is inserted between two plates, not only could the distance between the plates change, but the electrodes could also strain along the direction perpendicular to the electric field, effectively changing the surface area of the parallel capacitor. Dielectric material is chosen so that the electric field established can be much higher than the breakdown field of air.

The theoretical maximum energy density of an electrostatic device is related to its highest electric field. The energy density, therefore, is formulated as Equation 2.10:

$$u_E = \frac{1}{2} \epsilon E^2 \quad (2.10)$$

For an often used dielectric material, acrylic, the energy density is $3.4 \times 10^6 J/m^3$, while the maximum possible energy density for air is about $450 J/m^3$ before electric field breakdown occurs. Since a dielectric material is chosen, the electric field established could be much higher than the breakdown field of air, and the required voltage for a practical device is usually as high as a few thousands volts.

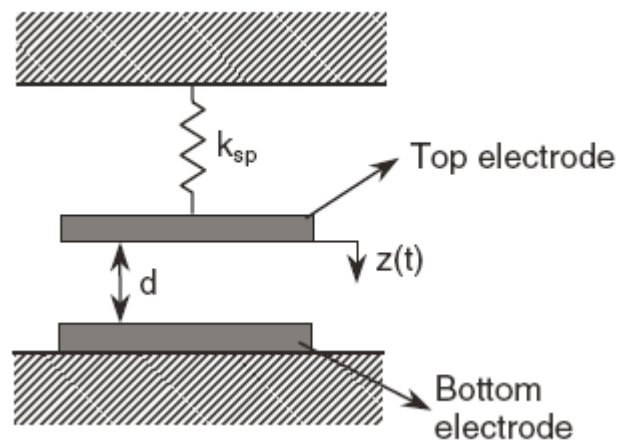


Figure 2.2: Capacitive energy harvesting device

2.2.3 Piezoelectric materials and devices

Piezoelectric materials [38] exhibit the unique property known as the piezoelectric effect. When these materials are subjected to a compressive or tensile stress, an electric field is generated across the material, creating a voltage gradient and subsequently a current flow if a current path exists. This effect stems from the asymmetric nature of their

unit cells when a stress is applied. As seen in Figure 2.3, the unpolarized Lead Zirconate Titanate (PZT) unit cell contains a small positively charged particle in the center, shown as black dot. When the material is poled under an electrical field, the positive charge will stabilize at an offset center position. Only poled PZT has piezoelectricity. Under strain, the positive charge will move away from its equilibrium position, creating an internal field across the crystal. If the surface of the piezoelectric material has electrodes, the free charge in the metal will tend to compensate the internal electrical field. Further more, if an electrical return path is established through an external circuit, then a current is usually generated.

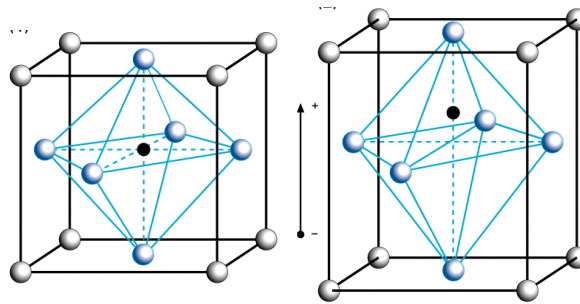


Figure 2.3: Lead Zirconate Titanate (PZT) unit cell

Utilizing piezoelectric material, mechanical energy can be converted to electric energy. Since the input mechanical energy could be stored as elastic energy, the elastic energy density is expressed as Equation 2.11:

$$u_m = \frac{1}{2} s T^2 \quad (2.11)$$

However not all of the elastic energy can be converted to electric energy; it generally depends on the coupling coefficient of the material, and electromechanical boundary conditions. Further discussion will be given in chapter 3.

2.2.4 Electrostrictive polymers

Electrostrictive polymer differ from the piezoelectric material in that it is central symmetric without a bias field. A recently discovered copolymer P(VDF-TrFE) [32] is not only a superior actuator material, it is also well-suited for energy harvesting applications. Its work mechanism is complex, and its details have not been fully understood. A simplified explanation is that it is a strain-induced phase transition that results from electric dipole movement on the molecular level; the dipole motion, in turn, generates an internal electric field. Therefore, it differs fundamentally from electrostatic force in an electroelastomer. Furthermore their intrinsic properties and electrostatic effects both contribute positively to energy harvesting effects. An electrostrictive polymer is a potentially better candidate than an electroelastomer for energy harvesting applications.

2.2.5 Comparison

Each type of energy conversion method has its own characteristics. Electromagnetic systems often require certain mechanisms, such as gearing or resonance with high quality factor, to enhance the relative speed between rotor and stator because the efficiency is directly related to the rate of change of the magnetic field. It also usually produces low voltage output. On the other hand, piezoelectric systems often borrow cantilevers and other mechanisms to amplify the force because the voltage is proportional to the strain and the piezoelectric material is relatively stiff. The electrical output of piezoelectric devices often tends to consist of higher voltage and lower current than that of electromagnetic system.

The sizing effect also determines which system is suitable for specific applications. Electromagnetic motors of ten kilowatts could probably easily beat any other electrical-mechanical energy conversion system of that power level in efficiency and power density. It is difficult to use electromagnetic systems in MEMS devices because the strength of the magnetic field is closely related to the size of the electromagnet. Electrostatic and piezoelectric systems, however, work better in smaller size. Loosely, an electric field is inversely proportional to the device's dimension given the same voltage, while a piezoelectric device scales down very well until the material's piezoelectric domain size is reached. Though it is hard to evaluate all the energy harvesting approaches with a single figure of merit, the energy density of those approaches are compared to each other when their applications are constrained by the size.

Piezoelectric and electrostrictive polymer energy harvesting have stood out as preferred choices due to some of their unique properties, such as higher energy density, simple structure, and low cost. Piezoelectric materials are also readily available commercially. So we chose piezoelectric energy harvesting as a main focus of this thesis.

In the meantime, newly-developed electrostrictive materials have attracted a lot of attention in field of mechanical actuation and ultrasonic transducers. This thesis also studies their potential superiority in energy harvesting applications.

Without energy harvesting circuits, no matter how good a power conversion device is, it still cannot provide the appropriate form of power to be used for electronic devices and hardly achieves the best performance as a system. Energy harvesting devices, circuits, and sometimes energy storage work together as a system to provide the maximum possible power to meet certain requirements.

2.3 Mechanical energy harvesting applications

The typical mechanical sources used for energy harvesting include natural phenomena (wind, water flow and ocean wave), a human's daily activities (walking, keyboard strokes) and structural vibrations from machinery. Those mechanical sources can be further categorized into three types: quasi-static, harmonic and impulsive. Quasi-static mechanical excitation happens when the dominant frequency of excitation is much lower than the fundamental resonance frequency of the energy conversion device. Under such conditions, the mechanical dynamics of devices can usually be neglected in favor of the quasi-static assumption. On the other hand, if the mechanical excitation is in

sinusoidal, or harmonic, form and its dominant frequency falls into the vicinity of the resonant frequency of energy conversion devices, the mechanical dynamics of the device usually play an important role and should be considered. One major application of harmonic excitation is vibration energy harvesting.

Another type of mechanical excitation is impulsive. It happens when a repetitive force is exerted upon the device for a shorter period of time than its relaxation time. A typical application is rolling automobile tires. The sidewall of tire of an automobile traveling at high-way speeds often experiences an acceleration level of a few hundred g's (g being the acceleration due to gravity), while the duration of the acceleration is less than 10 percent of the period of the rotation.

2.3.1 Quasi-static excitation applications

Human motion is usually much slower than the resonance frequency of energy harvesting devices. For example, the frequency of walking or running is usually between 1 to 10 Hertz, while piezoelectric bimorphs have resonance frequencies of a few hundreds of Hertz. Numerous attempts have also been made to utilize the energy associated with human activities. Systematic work [33] done by MIT in early 1990's experimentally compared the power generation abilities of different devices inserted into the soles of jogging shoes. The three types of devices that were experimentally studied are piezoelectric bimorph, PVDF insertion, and electromagnetic generator (motor). They concluded that an electromagnetic generator was the best in terms of power generation (20mW), but it was too cumbersome to be practical. PVDF insertion was the easiest to

implant in the shoes because it was flexible and light weight. But its low piezoelectric coefficient resulted in a much lower power output (10 μ W) compared to the piezoelectric bimorph (2 mW). Using different types of devices, SRI based their 'power boots' [34] on an electrostatic generator, employing silicon rubber or soft acrylic. Their power boots yield 1.6W of total power for two steps a second. Unfortunately, the material needs a high bias voltage (5k volts) and is also limited in lifetime, which still needs to be improved before it can become a practical product. Besides walking, energy extracted from pushbutton or key strokes is enough for wireless remote controls. Reported by Paradiso, Jansen and Harmon [35], the feasibility of such applications has been demonstrated when short distance ON and OFF signals are transmitted wirelessly.

Low frequency or quasi-static energy harvesting is not unusual in natural phenomena. For example, Taylor and Burn studied an 'energy harvesting eel' [36] for harnessing energy from the flow of river water. They used a long strip of PVDF piezoelectric polymer that undulates under the pressure differences created by the force of vortices. Depending on the speed of current and the size of the eel, achieved power output was from tens of milliwatts to a few watts.

Quasi-static types of energy harvesting are also common in industry. Theurer [37] reported that energy can be extracted from an injection-mold pressure differential to power wireless pressure sensors.

Quasi-static energy harvesting usually has a low frequency and a high force input, which generally needs a mechanical impedance-matching structure for its optimal performance. These structures include cantilever, bimorph/unimorph, etc. Even hydraulic systems have been proposed for some applications. The quasi-static type excitation is the

simplest form of energy harvesting. For some applications it could be assumed that the input peak force or pressure is independent of the electrical boundary conditions of an energy conversion device, while it is often assumed that the mechanical strain or displacement is unaffected by the electrical boundary conditions to simplify the analysis.

2.3.2 Harmonic excitation

The majority of harmonic energy harvesting applications is in vibration energy harvesting. There are two methods that piezoelectric devices are coupled with vibrating structures. One is attaching, or bonding, the piezoelectric patches directly to the vibrating structure where strain concentrates. The vibration of the structure results in a deformation or strain of the piezoelectric devices. Because the structure is usually much larger and heavier than those of the piezoelectric device, the change of frequency and amplitude of the structural vibration due to the energy harvesting is often negligible, and vibration frequency is often much lower than the piezoelectric devices' resonant frequency. Thus this method is still a quasi-static energy harvesting. The helicopter blade energy harvesting is one such example.

The second method utilizes a proof mass to trap the kinetic energy or acceleration of the vibration body. This method is particularly suitable for harvesting energy from a rigid body vibration. Proof-mass and piezoelectric devices constitute a spring-mass-damper system, the resonance frequency of which is often designed to be close to the dominant frequency of vibration to be harvested. The dynamics of such a system are the determining factor of the energy harvesting performance. Illustrated in Figure 2-4 is the

process of vibration energy harvesting using an attached piezoelectric device and using a proof mass.

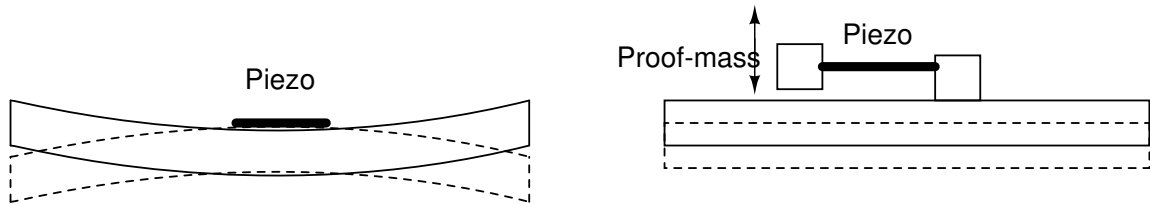


Figure 2-4: Vibration energy harvesting using an attached piezoelectric device (Left) and using proof-mass (Right)

2.3.3 Impulsive mechanical excitation

In some applications, the harvester is under impact of a relatively large force for a very short period of time, which results in a decaying vibration of the system until the next impact. Compared to the last two, there are fewer applications of this type. One of them is tire vibration harvesting. Traveling at normal highway speeds, the side wall of a tire often experiences a few hundred g's of acceleration when the closest face of the tire contacts the ground, but it only lasts for 10 percent of the period of rotation.

In this dissertation I will focus primarily on quasi-static and harmonic applications for active energy harvesting, due to their dominance in most of the applications. Mechanical energy, nevertheless, needs to be converted to electrical energy by some mechanism. The next section is dedicated to reviewing the most often employed approaches.

2.4 Energy harvesting system

An energy harvesting system usually consists of an energy conversion device (such as a piezoelectric element), energy harvesting circuit and control, and an energy storage unit. All of these subsystems play a crucial role, and none of them is more important than the others. It is also important to realize that each subsystem interacts with the others; therefore, global optimization of an energy harvesting system is preferred. For example, a piezoelectric device might generate good amount of power, say 20mW, but the peak voltage is 500 volts and the current is 40 μ A. For energy harvesting circuit design, it is often preferable to have a lower voltage, say 50 volts, and higher current (0.4mA) for better power efficiency.

2.4.1 The power flow of the system

A system diagram of a typical piezoelectric energy harvesting system is shown in Figure 2.5. From a power-flow point of view, the mechanical energy is coupled with the piezoelectric material through certain structures. Because the piezoelectric material has a small displacement and high force output, a monolithic piece is rarely used directly as a device. A mechanical impedance matching structure such as a biomorph is often employed, but sometimes the mechanical dynamics should also be included. The active material can be viewed as a two-port system. For the figure, we have chosen force and displacement as its input, and electrical voltage and current as its output. (The structure and dynamic and active material together constitute an energy harvesting device enclosed in the dash-lined box in the figure.) Power electronics, from a simple diode rectifier to a

more complex switch-mode power converter, and transfers the power from the harvester output into a usable DC voltage to an electrical load and sometimes also distributes the power between the storage unit and load. The energy harvesting circuit also enforces electrical boundary conditions to the device described by a certain control algorithm. Even for a simple diode rectifier, the control law is implemented implicitly through the voltage-current characteristic of diodes. For active energy harvesting, the control could be built in analog or digital circuits.

A storage unit, rechargeable battery or super capacitor, reserves energy in case the mechanical excitation is temporally absent or diminished. For a wireless sensor network, it is always necessary to be able to provide short bursts of power during radio transmission, because for most of the time the sensor nodes are in a 'sleep mode' and their power consumption could be as low as a few hundred microwatts, while during radio transmission the power requirement could reach a few hundred milliwatts for a duration of a few milliseconds.

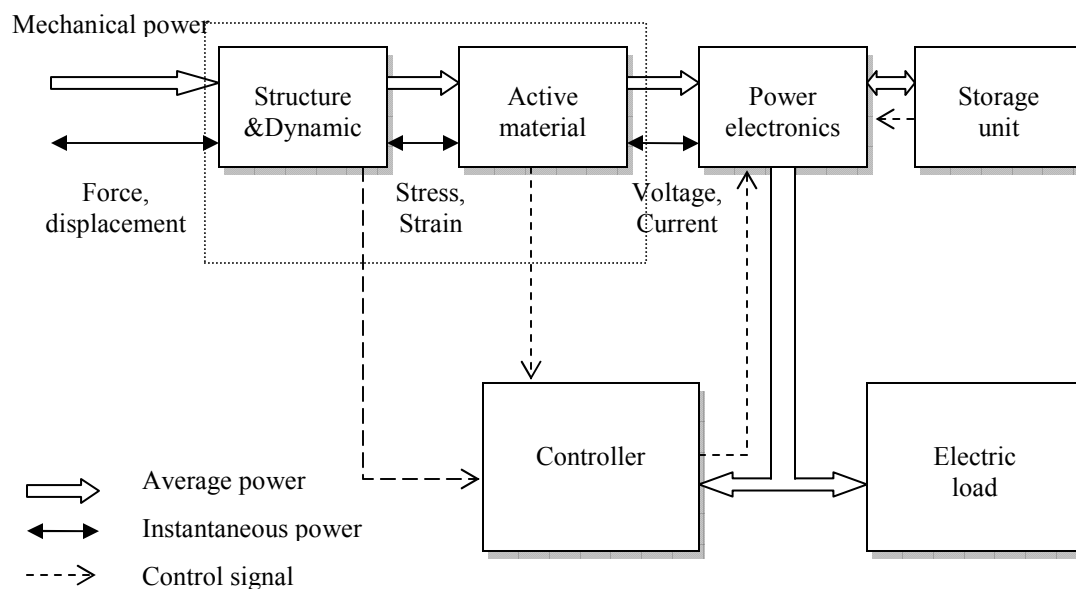


Figure 2.5: Energy harvesting system

We emphasize the instantaneous power flow in the system could be bi-directional between subsystems during energy conversion cycles. The net power or the average power flows from mechanical excitation to the storage unit and the electric load. Energy harvesting circuits could be categorized as three types based on their energy flow patterns during mechanical stimuli cycles: passive, semi-passive and active. A passive circuit, such as a diode rectifier, always transfers power (instantaneous power) from the piezoelectric devices to the energy storage cell (rechargeable batteries or super-capacitor). The semi-passive circuit uses a passive component, such as an inductor, to temporarily store and return part of the energy back to the piezoelectric devices during each cycle. For the semi-passive energy harvesting circuit, even though switches (MOSFET) are generally used, the current flow, therefore the power flow through the switch is always unidirectional. The active energy harvesting circuit, on the other hand,

utilizes bi-directional inverters and circulates part of energy back and forth between the piezoelectric device and the energy storage unit (rechargeable battery or super-capacitor) for each energy conversion cycle, resulting in a net flow of energy into the energy storage cell with a longer time average. Because bidirectional switch-mode power electronics are used, in most cases at least two switches have to be used in the circuit.

Typical passive harvesting circuits are diode rectifiers in half-bridge or full-bridge configurations with filter/reservoir capacitors. For this circuit, the power transfer is maximized if the reservoir capacitor voltage is kept at half of the open-circuit voltage under the same mechanical condition. A few different DC/DC converters that achieve such optimization were presented including adaptive control [13] and input impedance matching the DC/DC converter [49]. The limitation of passive circuits is that the voltage amplitude across piezoelectric device is limited by the open circuit voltage; hence, it constrains the amount of energy harvested.

Semi-passive energy harvesting circuits and their controls have been proposed to increase the voltage swing on the piezoelectric device by using an inductor to temporarily store and return part of the stored electrical energy back into the piezoelectric device. Semi-passive circuits include parallel synchronous harvesting on an inductor and series synchronous harvesting on inductor topologies. Both utilize an inductor with a combination of switches (such as MOSFET) and diode networks to realize sudden discharging and partial voltage reversion of the piezoelectric device. The switches' opening is synchronized with the peak voltage of the device. Since voltage amplitude on the piezoelectric device can be larger than that of passive circuits, the power conversion is also improved significantly. However, a semi-passive circuit relies on the inductor to

transfer the peak energy on the piezoelectric device. Since all the peak electrical energy in the piezoelectric device has to be stored in the inductor, the peak current is relatively high for the power level those energy harvesting system deal with; thus, the I^2R loss in the inductor becomes the major limitation of energy conversion efficiency. Increasing the value of the inductance could reduce the loss; however, in practice the value of inductor is constrained by its weight and size.

Furthermore, a sudden voltage transition across the piezoelectric device generates a rapid deformation of the device through unilateral electro-mechanical coupling of piezoelectricity. This deformation is equivalent to a step impact on the mechanical structure. Because the step impact comprises high frequency components that could easily cause mechanical systems to vibrate, its associated energy eventually dissipates as heat, further decreasing the efficiency of the system. Moreover, its simple control algorithm that synchronizes the opening of the switch with the peak voltage of the piezoelectric device is not optimized for the dynamic energy harvesting system that works at off-resonance.

In the field of active vibration control, researchers [18] have studied the power flow between piezoelectric device and power amplifiers. In some cases the power flow is actually from the piezoelectric device to a power amplifier. Were a linear amplifier used, this power would generally be dissipated through power transistors in the form of heat, but if a bi-directional switching amplifier is used to drive the piezoelectric device, this power could well be reclaimed and utilized, which already constitutes an active energy harvesting system. The only difference is the goal regarding their control laws. In energy

harvesting the controller is designed to maximize the power generation, while the goal of active vibration control is to suppress vibration. They are not always coincident.

In 2003, Hagood and Ghand [55] patented the general concept of actively controlling the voltage and/or charge across the terminals of a piezoelectric device to generate electrical power. Unfortunately, the systematic study of active energy harvesting using piezoelectric device is not known in academic literature. In this paper, we establish the modeling of active energy harvesting. Based on the model, the control algorithms are presented. For quasi-static cases, the control is much more straightforward than that in the case of dynamic applications, where searching for an optimized controller is more involved. Experiments were conducted demonstrating the superior performance of active energy harvesting systems.

2.4.2 Control of the energy harvesting circuit

We redraw the energy harvesting system in Figure 2.6 from a control system point of view. The controller is optimized for maximum power generation. In the figure, we arbitrarily choose force and current as inputs and voltage and speed as outputs. If the controller does not need the mechanical state and only voltage and current are used for control purposes, we call this a sensor-less control. Once the control loop is established, the system response to the mechanical excitation is, therefore, jointly determined by both the energy harvesting device and the circuit. Thus, we could alter the system response for the best harvesting effect with the power electronic circuit and its control.

The power is ultimately drawn from mechanical excitation. The design of energy harvesting systems is to optimize the interaction between the system and mechanical excitation in order to maximize mechanical power flow into the system, as well as minimize the power loss. If the mechanical excitation is described as force $f(t)$ and displacement $x(t)$, then the input mechanical power, can be represented as in Equation 2.12

$$P = \frac{1}{T} \int_0^T \dot{x}(t) f(t) dt \quad (2.12)$$

Noticing the displacement $x(t)$ is response to both mechanical force $f(t)$ and electrical voltage $v(t)$. Therefore the harvested power is jointly determined by mechanical and electrical boundary conditions.

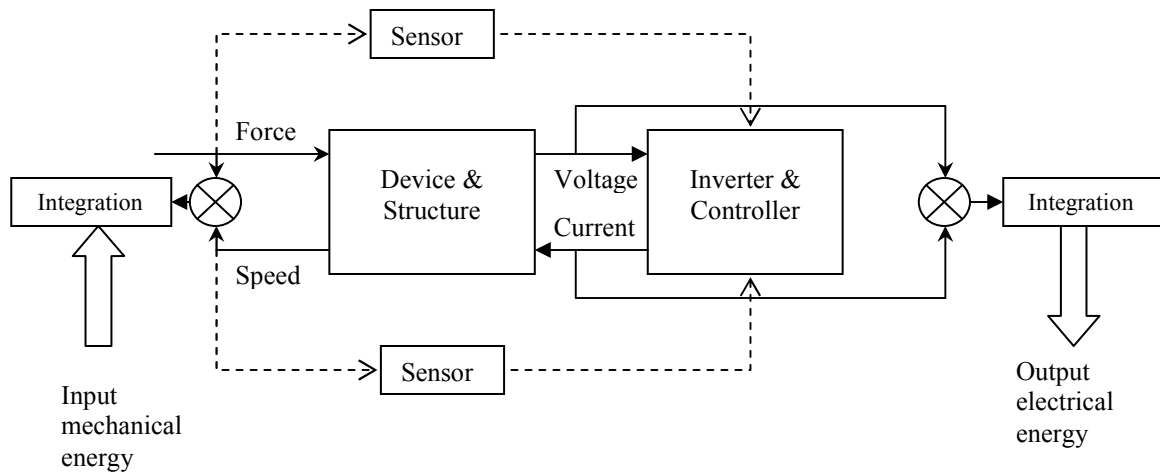


Figure 2.6: Control flow of energy harvesting system

In the following chapters, energy harvesting systems are studied from both power flow and control points of view.

Chapter 3

Quasi-static Linear Energy Harvesting Theory

Piezoelectric materials, including ceramics, single crystal, and polymer varieties, have been widely adopted for energy harvesting applications due to their high energy density, simple structure, and high frequency response. Many applications fall into the quasi-static excitation category. In this chapter, a theoretical model based on the analysis of electrical and mechanical boundary conditions is established. The model is used to examine passive, semi-passive and active energy harvesting circuits. Theoretically, it will be shown that active energy harvesting is well suited for quasi-static applications, for its higher energy output and better electromechanical coupling. The study also builds the foundation for investigating more complex systems, such as dynamic vibration energy harvesting.

3.1 Piezoelectric material and device

Piezoelectricity is a material constitutive property consisting of mutual coupling between mechanical strain/stress and electrical field/charge. Piezoelectricity could be described by the following linear constitutive equations [38]:

$$S_{ij} = s_{ijkl}^E T_{kl} + d_{ijm} E_m, \quad (3.1)$$

$$D_n = d_{nkl} T_{kl} + \varepsilon_{mn}^T E_m, \quad (3.2)$$

Where T_{kl} , S_{ij} are the mechanical stress and strain tensors, and D_n , E_m are the electric displacement and field vectors, respectively. In Equations 3.1 and 3.2 the Einstein summation convention is used.

Monolithic piezoelectric materials are rarely used as standalone devices. The generated strain of a piezoelectric material is small (usually $< 0.1\%$ for ceramics), even under high field. Furthermore, piezoelectric material, especially ceramics such as PZT, is relatively stiff and requires a large stress to be effectively strained. They are therefore often embedded into certain mechanical structures, constituting devices. Those structures include unimorph/bimorph cantilever beams [40], matrix composite structures [41], and cymbal structures [43]. Piezoelectric materials themselves are also often laminated into multilayer structures [42] or made into fibers to further reduce the required driving voltage or to enhance their robustness [44]. Although the constitutive equations of piezoelectricity are in tensor form, a piezoelectric device can often be described by scalar equations. Under the quasi-static assumption, linear, frequency-independent equations that represent the device behavior are written as follows:

$$\delta = s^V F + dV \quad (3.3)$$

$$Q = dF + C^F V \quad (3.4)$$

where δ is the deflection or displacement of the device, Q is the electrical charge on the electrodes of the device, F is the force exerted on the device, and V is the voltage across the electrodes. The s^V is the compliance under constant electrical field, d is the general piezoelectric coefficient and C^F capacitance under constant force. For many regularly-shaped devices, a closed-form expression of those parameters can be

derived through constitutive and structural equations [45]. For example, expressions for the parameters of a bimorph bending actuator shown in Figure 3.1 with length L , width w , and thickness t are provided in Equation 3.5, where s_{11}^E is the elastic compliance under constant electrical field, ϵ_{33}^T is the dielectric permittivity under constant stress, d_{31} is the transverse piezoelectric coefficient, and $k_{31}^2 = d_{31}^2 / \epsilon_{33}^T s_{11}^E$ is the transverse electromechanical coupling coefficient of the material.

$$k = \frac{wt^3}{4s_{11}^E L^3}, \quad d = \frac{3d_{31}L^2}{2t^2}, \quad C = \frac{\epsilon_{33}^T Lw(1 - k_{31}^2/4)}{t} \quad (3.5)$$

The finite element method (FEM) can be used to determine the parameters of more complicated geometries [46]. These parameters can also be determined experimentally [47].

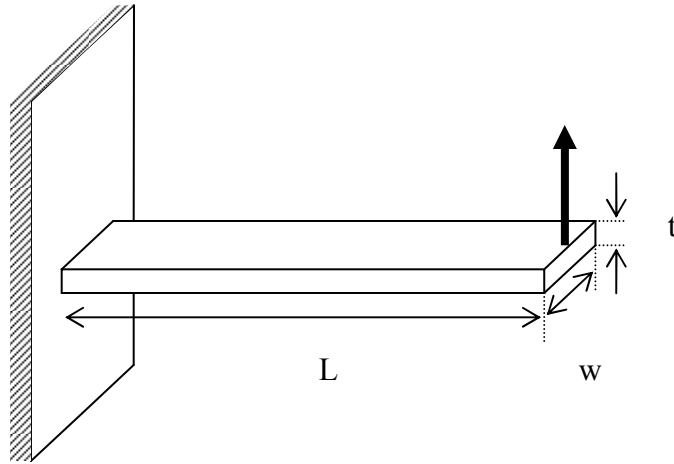


Figure 3.1: Bending actuator

Knowing the above parameters enables us to compare the relative performance of different devices. The piezoelectric coefficient d in Equations 3.3 and 3.4 is the coupling between electrical charge and mechanical force, but it does not always reflect the performance of the device from an energy point of view. A more often-used figure of merit is the electromechanical coupling coefficient k^2 , which is often used to characterize piezoelectric material as a transducer.

One definition of the coupling coefficient [48] is given by

$$k^2 = \frac{U_m^2}{U_e U_d} \quad (3.6)$$

where U_m is the mutual electromechanical energy density, U_e is the elastic energy density and U_d is the dielectric energy density. By this definition the coupling coefficient is only related to the initial and final state. So it could be directly related to the material properties. In fact, it summarizes in one parameter all the elastic, piezoelectric and dielectric constants for a specific configuration. For example, assuming the only non-zero component of electrical field and mechanical stress is along the polarization direction, a coupling coefficient is calculated as shown in Equation 3.7

$$k_{33}^2 = \frac{d_{33}^2}{\epsilon_{33}^T s_{33}^E} \quad (3.7)$$

Another often-seen definition [38] is related to a specific energy conversion cycle. Illustrated in Figure 3.2, the piezoelectric material is strained by stress T_3 component under short circuit condition. At maximum stress, the total stored energy per unit volume at maximum compression is corresponds to the total area of W_1 and W_2 in the figure.

Then stress is released under an open-circuit condition, during which a voltage is generated across the electrodes of the material. Finally at zero stress, the material is connected to an electric load to discharge the piezoelectric capacitance. As work is done on the electric load, the strain returns to its initial state. The energy dissipated on the resistor corresponds to the area W_1 , and the part of the energy unavailable to the electric load is therefore W_2 .

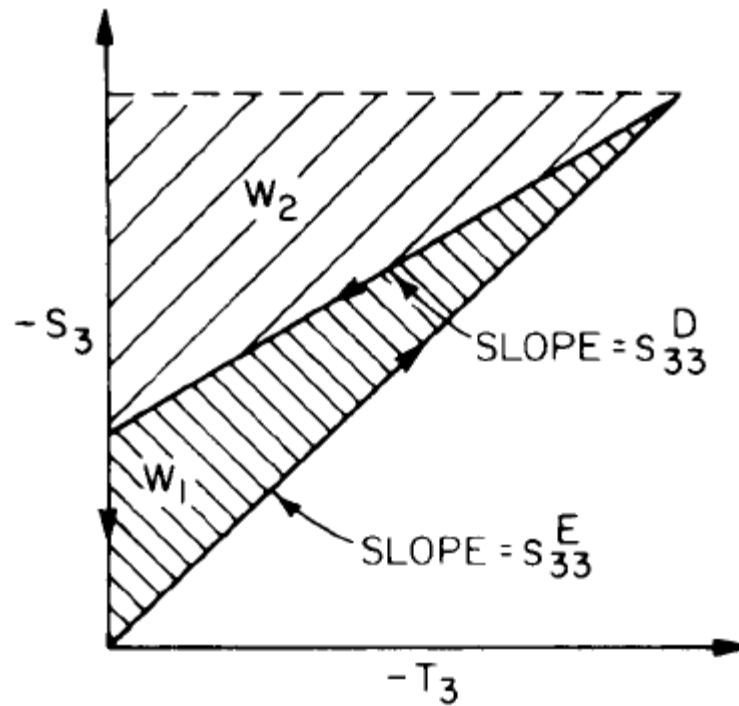


Figure 3.2: Energy harvesting cycle through open circuit and short circuit boundary conditions

Based on above energy conversion cycle the coupling factor is defined as follows:

$$k^2 = \frac{W_1}{W_1 + W_2} \quad (3.8)$$

It can be shown that based on the energy conversion cycle described above, the two definitions are mathematically the same.

The coupling coefficient of a device is similarly defined by 3.8, where the total energy is used instead of energy density. For a device described by Equations 3.3 and 3.4, the coupling coefficient is calculated to be:

$$k^2 = \frac{d^2}{s^V C^F} \quad (3.9)$$

The concept of efficiency of the piezoelectric material, on the other hand, is always associated with irreversible energy loss during the conversion process, and is usually defined using Equation 3.10

$$\eta = \frac{\text{Converted energy}}{\text{Input energy}} = \frac{\text{Input energy} - \text{loss}}{\text{Input energy}} \quad (3.10)$$

Energy conversion happens only when the device is under asymmetric electric boundary conditions. For example, if the device is open-circuited throughout the mechanical strain cycle, no net electrical energy is converted. Energy harvesting circuits have distinct electrical cycles, which greatly affect the energy harvesting process.

In the following section we will discuss in detail how different energy harvesting circuits interact with a piezoelectric device to achieve energy conversion. In this discussion we assume the mechanical excitation is given by a force with the same peak-to-peak variation for each circuit, but not necessarily in sinusoidal fashion. This is an advantage of this approach in comparison to the harmonic analysis modeling approach presented in [39].

3.2 Passive and Semi-passive Energy harvesting circuits

The piezoelectric energy conversion process can be graphically presented in the force-displacement and voltage-charge planes, as shown in Figure 3.3. An energy conversion cycle is the enclosed mechanical and electrical charge path the device traverses during one period of mechanical excitation. In the electrical domain illustrated in (a) of Figure 3.3, device voltage and charge path both traverse in a counter clockwise direction. The enclosed area is calculated as

$$\begin{aligned}
 A &= \oint QdV \\
 &= QV \Big|_{start}^{End} - \oint VdQ \\
 &= \int_0^T Vi dt
 \end{aligned} \tag{3.11}$$

Since Vi is the instantaneous electrical power, the last integration in Equation 3.11 represents total converted electrical energy in one period of time. Similarly, it can be proven that the enclosed area in the mechanical domain, (b) of Figure 3.3 represents the input mechanical energy in one cycle. Since no loss mechanism is modeled, the input mechanical energy is always equal to the output electrical energy. In other words, the two enclosed areas in both domains are equal, though of different shapes. To calculate the energy we could use either one or the other, whichever facilitates the calculation.

The plots can also tell us the instantaneous power flow direction at any state of the device. For example, a trajectory that is downwards in the I or IV quadrants or upwards in the II or III quadrants represent negative power, which indicates the power flows from the device to the electrical circuit, and vice versa. The average power

converted is understood as the energy converted in one cycle multiplied by the frequency of excitation.

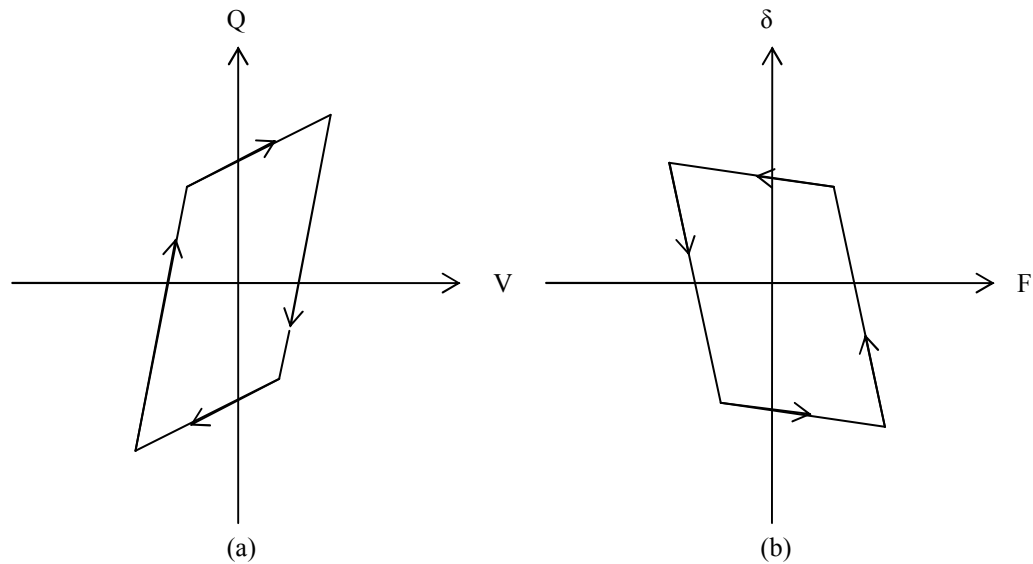


Figure 3.3: Energy conversion loop

Not only does this cycle portray the energy conversion process more intuitively than a harmonic analysis model, it is also helpful in finding optimized conditions for energy harvesting by revealing the fundamentals of the energy conversion. It is applicable for arbitrary mechanical excitation as well. More important is that harmonic analysis is not applicable for non-linear system such as electrostrictive energy harvesting, while the modeling approach we used for linear material (piezoelectric material) can be used for electrostrictive energy harvesting as well.

3.2.1 Passive circuits

One type of energy harvesting circuit is the so-called passive circuit, where the instantaneous power flow is always from the device to the electrical circuit. The traditional diode rectifiers and charge extraction circuits are typical passive circuit types.

3.2.1.1 Diode rectifier

A common energy harvesting circuit consists of a diode rectifier in full bridge (a) or half bridge (b) configurations, as shown in Figure 3.4. It is the most well known for piezoelectric energy harvesting.

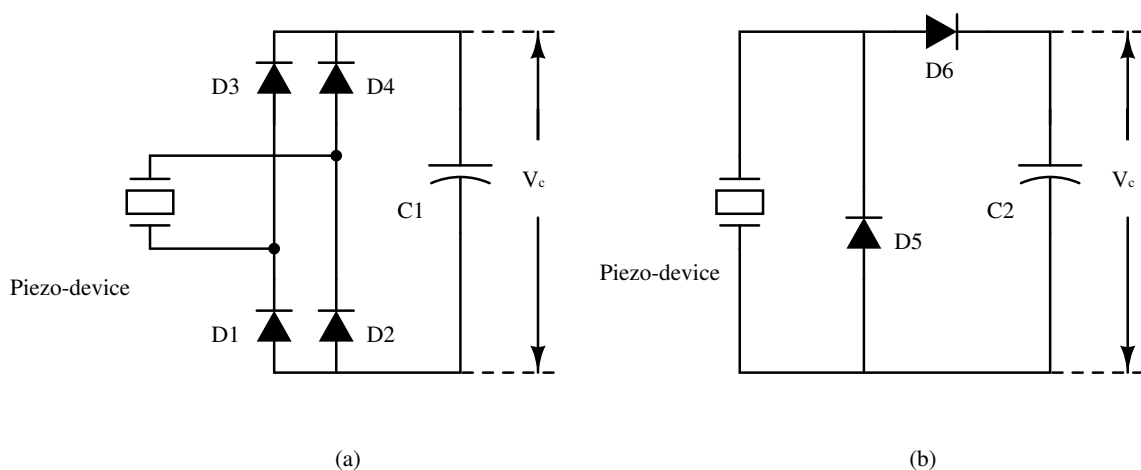


Figure 3.4: Full bridge diode rectifier (a) and half bridge diode rectifier circuit (b)

Diodes have unique unidirectional conduction. When configured as a rectifier, they are able to convert AC to DC voltage. Considering the half rectifier, in Figure 3.4 (b) as an example. When the piezoelectric device voltage is positive but lower than V_c , the voltage across capacitor C2, both D5 and D6 are reverse biased. A small leakage

current in the diode can typically be neglected. The piezoelectric device is therefore in an open-circuit condition. Under an applied mechanical force, the voltage on the device keeps increasing until slightly higher than V_c . Diode D6 is then forward biased and it starts to conduct, and therefore, except for a the forward voltage drop across diode, the piezoelectric device is connected to the capacitor voltage V_c . The diode D5's purpose is to prevent the device voltage from becoming negative when the opposite force is applied, and provides a necessary path for reverse current to flow.

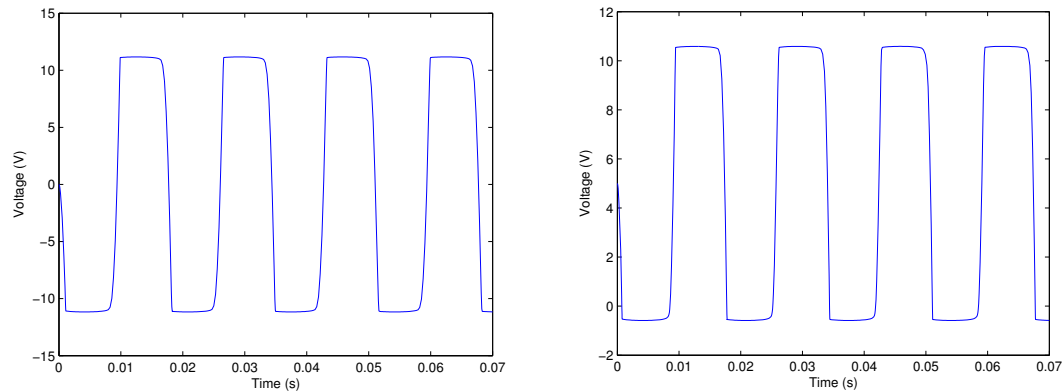


Figure 3.5: Voltage wave on the piezoelectric device using full bridge (left) and half bridge (right) rectifier

The voltage wave forms on the device for both configurations are shown in Figure 3.5. For both, the capacitor is much larger comparing to the piezoelectric device's capacitance, voltage is essentially content 10v. The swing of voltage for the full bridge is from -11 to 11, while for half bridge it is from -0.5 to 10.5V. The 0.5V diode voltage drops are also noticeable. If ideal diode is considered, both circuits could work equally well in term of output power. In practice, the half bridge's output voltage has less diode loss because only one of diode voltage drop is in the current path. Figure 3.6 shows an

experimental comparison between the two configurations. In the experiments the same piezoelectric device and diode (1N5450) were used. The capacitor voltage was controlled by a regulated DC voltage power supply operating as a load.

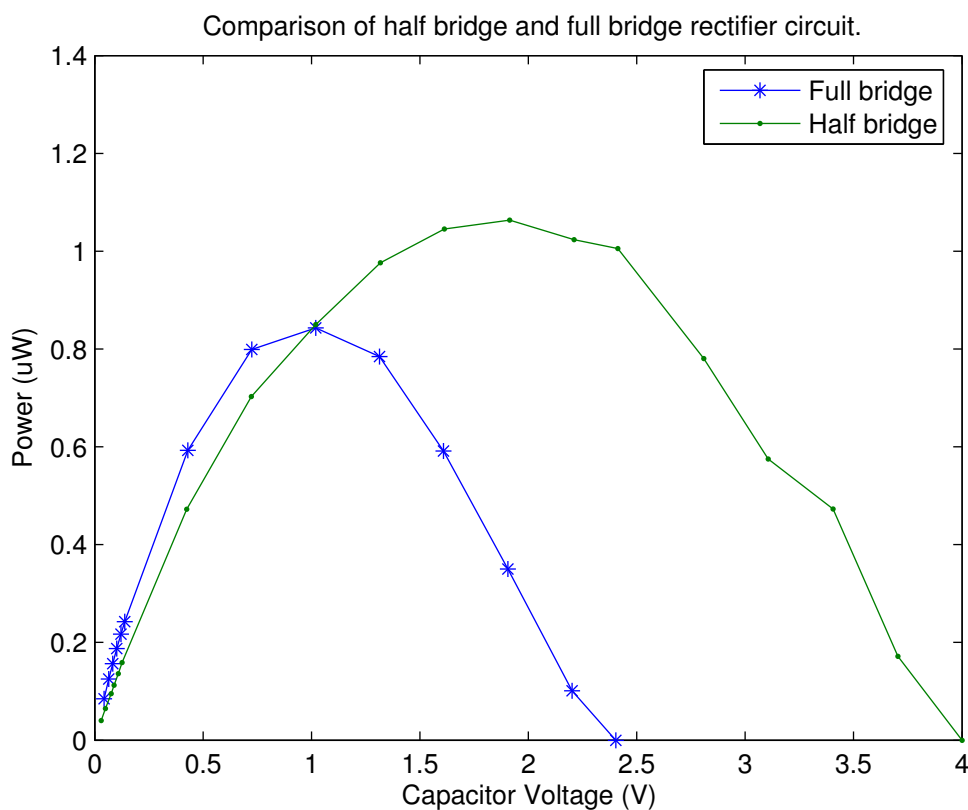


Figure 3.6: Experimental comparison of full bridge and half bridge rectifier. Half bridge rectifier has more optimized power and doubled optimized voltage.

From the experiment, we can see the half bridge rectifier has a higher output power and its optimized reservoir capacitor voltage is about twice that of the full bridge rectifier circuit. Generally speaking the half bridge rectifier is particularly suitable for low-voltage output devices for improved efficiency; while the full bridge rectifier is used to lower the result voltage across the capacitor for the devices open circuit voltage is high (a few hundred volts).

Since there are only slight differences in their operation, we only examine the full-bridge circuit in this study. An ideal diode is assumed unless stated otherwise for the analyses. The energy conversion cycle is plotted in Figure 3.7

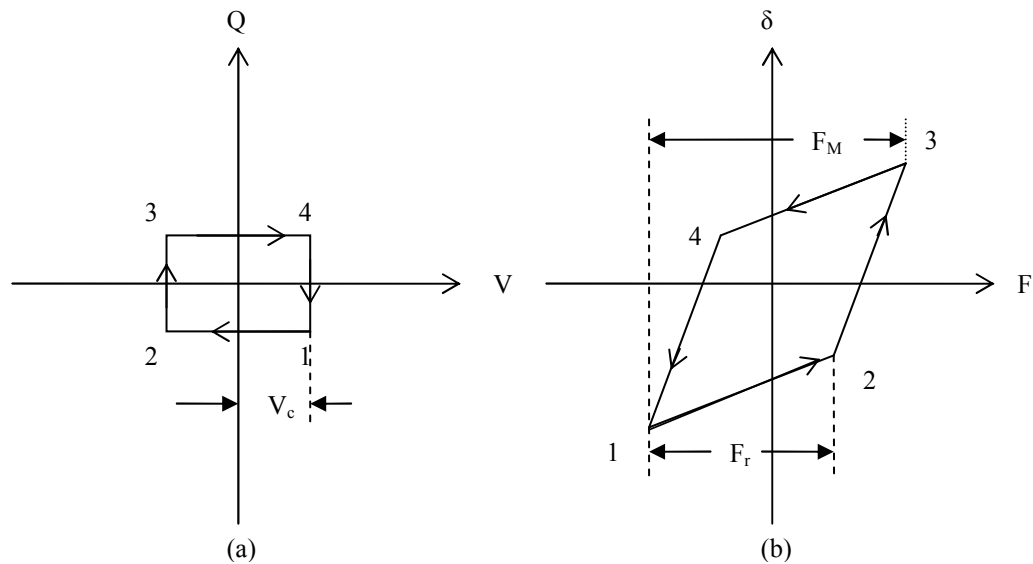


Figure 3.7: Energy conversion cycle for full bridge rectifier circuit (a) electrical domain, (b) mechanical domain

Suppose the mechanical excitation exerted on the device is a force with fixed peak-to-peak amplitude F_M . The device is described by Equation 3.3 and 3.4. The mechanical and electrical planes are plotted in Figure 3.7. In trajectories from 1-2 and 3-4, the rectifier is reverse biased, and the device is therefore in an open circuit condition. In the electrical plot those trajectories are horizontal paths and their slope in the mechanical domain is $s^V - \frac{d^2}{C^F}$. In the path 2-3 and 4-1, the diodes are forward biased so the voltage on the device is equal to the voltage on the capacitor, which can be assumed

to be constant. These paths are vertical in the electrical domain and have a slope of s^V in mechanical domain.

The force at which the device generates an open circuit voltage equal to the capacitor voltage is calculated from Equation 3.4 by letting $\Delta Q = 0$ and $\Delta V = 2V_c$ as follows,

$$F_r = 2 \frac{V_c C^F}{d} \quad (3.12)$$

From point 2 to 3 the device voltage is equal to V_c , and the change of the charge on the electrodes is calculated as

$$\Delta Q = d(F_M - F_r) = d \left(F_M - 2 \frac{C^F V_c}{d} \right) \quad (3.13)$$

The energy converted in one cycle is equal to the enclosed rectangular area in the electrical domain.

$$W = 2\Delta V_c \Delta Q = 2d \left(F_M - 2 \frac{C^F V_c}{d} \right) V_c \quad (3.14)$$

The energy is a function of the capacitor voltage and it maximizes when:

$$\frac{dW}{dV_c} = 2dF_m - 8C^F V_c = 0 \quad (3.15)$$

This leads to the optimized condition of the rectifier circuit.

$$V_c = \frac{dF_M}{4C^F} = \frac{1}{4} V_o \quad (3.16)$$

In Equation 3.16, V_o is the peak-peak open circuit voltage when the device is exposed to the same force, defined in Equation 3.17.

$$V_o = \frac{dF_M}{C^F} \quad (3.17)$$

At the optimized condition, the energy generated in one cycle is

$$W_{\max} = \frac{d^2 F_M^2}{4C^F} = \frac{1}{4} C^F V_o^2 \quad (3.18)$$

In the case of the half-bridge rectifier, it can be shown that the optimized condition become Equation 3.19

$$V_c = \frac{dF_M}{2C^F} = \frac{1}{2} V_o \quad (3.19)$$

Under ideal diode assumption the converted optimized energy of the half-bridge is the same as Equation 3.18, which could also be rewritten as Equation 3.20:

$$W_{\max} = 2k^2 \frac{F_M^2}{2k} = 2k^2 W_{mech} \quad (3.20)$$

Where W_{mech} is the peak mechanical energy stored in the device if same amount of force

F_M is exerted and the coupling factor $k^2 = \frac{d^2}{s^V C^F}$ is as defined in Equation 3.9. This

equation implies a good energy harvesting device must be compliant to obtain more energy when stressed, and should have a high coupling coefficient. The piezoelectric single crystal often out-performs ceramic material in harvesting power, because it has a better coupling and is less stiff.

The optimized condition of Equation 3.16 and Equation 3.19 can be implemented in practice using DC/DC converters [49]. The classical rectifier circuit remains to be the most adopted energy harvesting circuit due to its simplicity, low cost, and versatility.

Using the rectifier circuit, the voltage swing on a piezoelectric device is less than its open-circuit voltage. Therefore the electrically induced displacement is also limited. For a given mechanical force, if we could further increase the displacement by increasing the voltage swing on the device, we could effectively increase the converted energy for each cycle. One of the approaches is synchronous charge extraction.

3.2.1.2 Synchronous Charge Extraction

Another type of passive energy harvesting circuit, patented by Smalser [51], is a synchronous charge extraction circuit [50] that utilizes a peak detector to close a switch when the voltage across the piezoelectric device reaches its peak value. This circuit is similar to the synchronous switch damping on short (SSDS) [52] circuit used in the vibration control field. This circuit was later implemented [53] via an application specific integrated circuit (ASIC). Two implementation circuits are illustrated in Figure 3.8. The switch in circuit (a) uses a PMOS transistor with simple circuitry. To turn off a PMOS transistor, the gate voltage needs to be as high as the piezoelectric device voltage, which is often beyond the operation voltage of the control circuit. This makes design of the gate driving circuit difficult. The circuit (b) uses a fly-back transformer to simplify the gate drive circuit, where a NMOS transistor is used, therefore the gate voltage needs only to be higher than the transistor's threshold voltage relative to the ground.

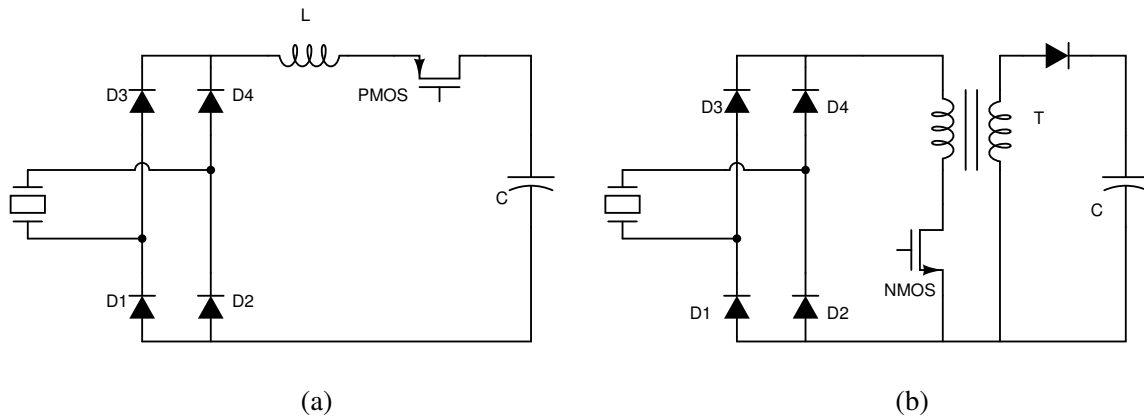


Figure 3.8: Synchronous charge extraction circuit

The control of this circuit involves a peak detector that turns on the switch at the peak voltage. Since the piezoelectric device is at open-circuit condition, the peak voltage happens at peak stress. When switch S1 closes, the piezoelectric device and inductor works as an LC resonance, and energy is temporarily stored in the inductor L as the device voltage drops to zero. After the voltage on the piezoelectric device drops to zero, the diodes are forward biased, and current continues to flow into the capacitor until all the energy stored in the inductor is transferred to the capacitor. The electrical and mechanical cycles of this approach are depicted in Figure 3.9, with the diode rectifier approach (dashed line) provided for comparison.

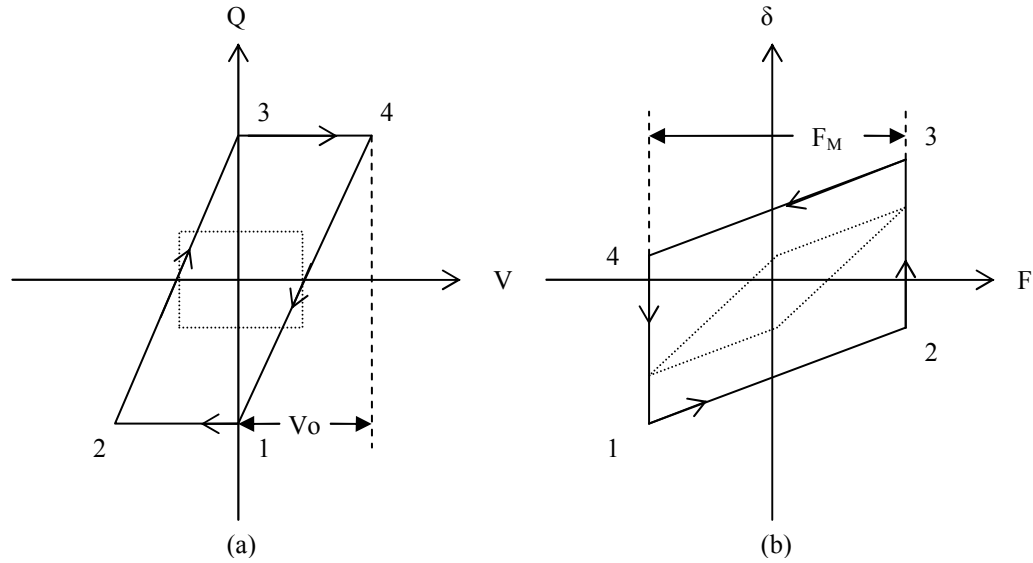


Figure 3.9: The energy conversion cycle of the synchronous charge extraction circuit. (a) electrical domain, (b) mechanical domain. The dash line is the full-bridge rectifier circuit under same force excitation, their enclosed area are 1/4 that of synchronous charge extraction.

In the conversion cycle, starting from the path 1-2, the switch is open and the device is in an open circuit condition. Hence the device voltage will increase proportionally to the applied force until it reaches its peak value

$$V_o = \frac{dF_M}{C^F} \quad (3.21)$$

At this moment the switch closes and the device is discharged into the inductor. From 2-3 the force on the device is assumed to be constant. The change in electrical charge on the device during these intervals is given by

$$\Delta Q = dF_M \quad (3.22)$$

The amount of the energy converted, therefore, is equal to area of the parallelogram in the electrical domain (a) of Figure 3.9.

$$W = \Delta Q V_o = \frac{d^2 F_M^2}{C^F} = C^F V_o^2 \quad (3.23)$$

Similarly, this energy could also be related to the device's coupling coefficient, which is four times as much as the diode rectifier case.

$$W = 8k^2 W_{mech} \quad (3.24)$$

A close scrutiny of the mechanical domain of the energy conversion cycle reveals that the mechanical energy input is also quadrupled, obeying the energy conservation of the system.

One apparent advantage of the synchronous charge extraction circuit is that the capacitor voltage does not need to be optimized as long as the switching is appropriately synchronized with the peak voltage for all levels of excitation. However, the voltage swing of the piezoelectric device is still constrained below or equal to the open circuit voltage. That in turn limits its energy conversion capability.

3.2.2 Semi-passive energy harvesting circuit

The semi-passive energy harvesting concept originally comes from the concept of impedance matching [54], which states that the maximum energy transfer from a piezoelectric device to the energy harvesting circuit is achieved when the input impedance of the circuit is the complex conjugate of the output impedance of the device. Because the piezoelectric device is largely capacitive, if the working frequency is low,

the matched impedance would be a prohibitively large inductance on the order of hundreds of henrys. The semi-passive approach was derived by thinking along the lines of reducing the value of the required inductor by performing time truncation, or disabling the induction path for most of the time, and allowing the resonance only at an appropriate moment in order to significantly reduce the value of the inductor. The resulting circuit configurations are serial and parallel SSHI circuits [61]

3.2.2.1 Serial SSHI circuit

Burns [62] patented an energy harvesting circuit that utilizes a resonance to partially reverse the voltage polarity of the piezoelectric device. Because the circuit includes an inductor in series with a piezoelectric device, it was named Serial Synchronized Switch Harvesting on Inductor (SSHI). The exact same circuit topology known as synchronized switch damping on inductor (SSDI) can be found in the structural damping literature [63]. This circuit configuration and its implementation are illustrated in Figure 3.10.

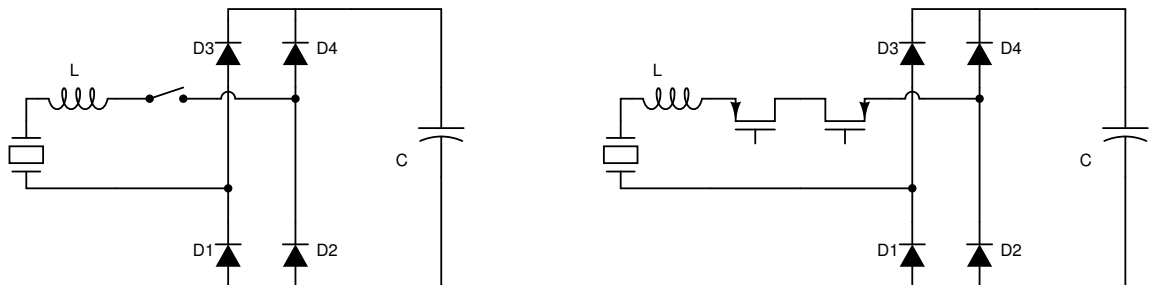


Figure 3.10: (a) serial synchronized switch harvesting on inductor circuit (b) implementation of serial synchronized switch harvesting on inductor circuit using bidirectional switch made of two back to back PMOS transistors

Two back-to-back transistors are used as a bidirectional switch, the gate drive of which usually needs a floating voltage source relative to the joint point of the two transistors. The optical coupler or boot trap circuitries are often adopted for the gate drive. Interestingly enough, this often cited SSHI circuit in the literature (Figure 3.10) actually could be implemented using a simpler circuit, shown in Figure 3.11, where only one transistor is necessary to block the unidirectional voltage. This circuit has the same functionality.

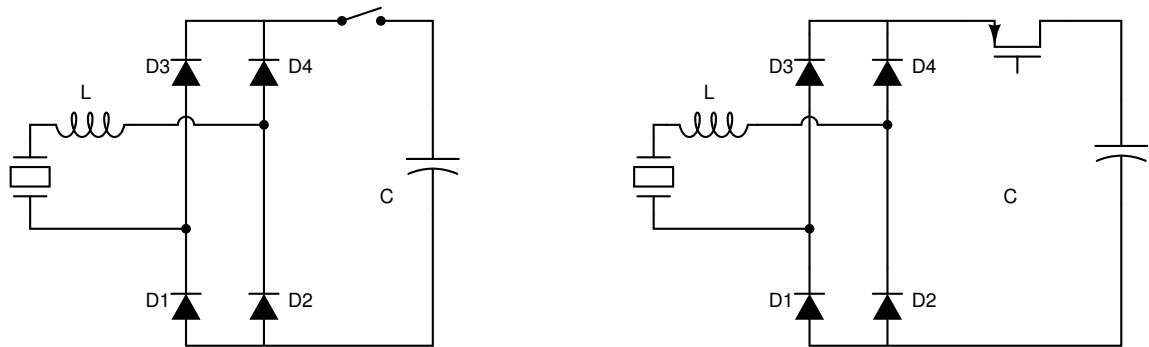


Figure 3.11: A simplified synchronized switch harvesting on inductor circuit (a) and its single PMOS transistor implementation

The control of the serial SSHI circuit is identical to that of the synchronous charge extraction circuit, in that the switch is closed at the positive or negative peak voltage of the piezoelectric device. The difference between the two circuits is that the current of the SSHI circuit will continue flowing through the device even if the device voltage drops to zero. As a result, part of the energy transfers back to the device, reversing its voltage polarity. Because electrical energy flows back in the device with assistance of a passive components, we categorize this circuit as semi-passive. The energy harvesting cycle is

shown in Figure 3.12. It is compared to the synchronous charge extraction technique shown with dashed lines.

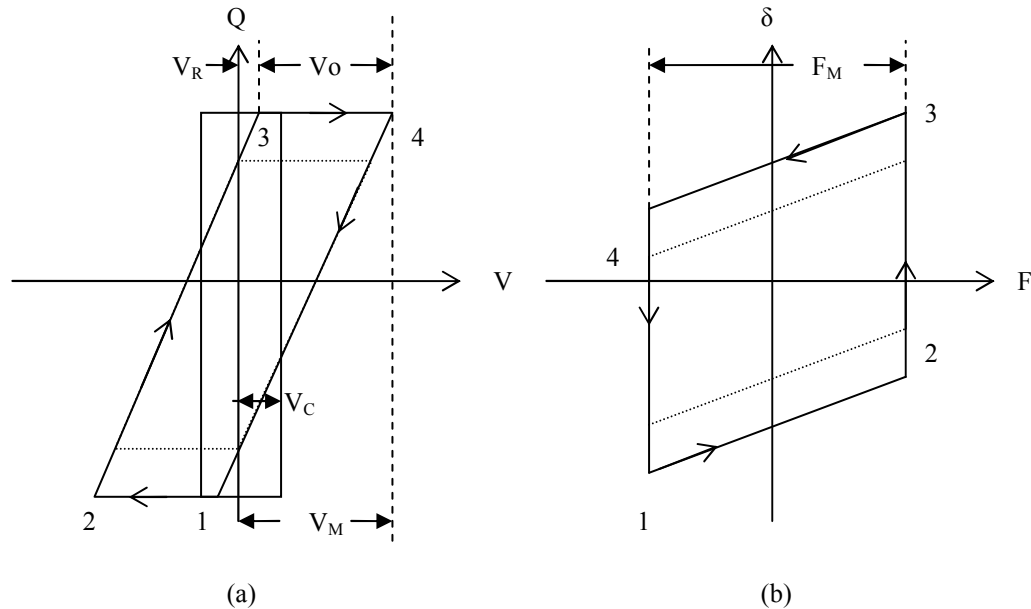


Figure 3.12: Conversion cycle of serial synchronized switch harvesting on inductor circuit (a) electric domain, (b) mechanical domain

In the path from 1-2, the switch is open and the piezoelectric device is therefore open circuited. As the applied force increases, the voltage on the device also increases. At the peak force (points 2 and 4), also the peak voltage, the switch is closed. During discharging, the capacitance of the device, inductor and voltage on the capacitor is equivalent to a LCR resonator shown in Figure 3.13. The inductor is chosen so that the period of the LCR resonator is much smaller compared to the period of the mechanical force. It can be assumed that during one period of resonance, the mechanical force stays the same and the capacitance of the device is also unchanging. In the resonator, a resistor

is added as a lumped electrical and mechanical energy dissipation during transition. The capacitor C is the capacitance of the device and L is the inductor used in the circuit.

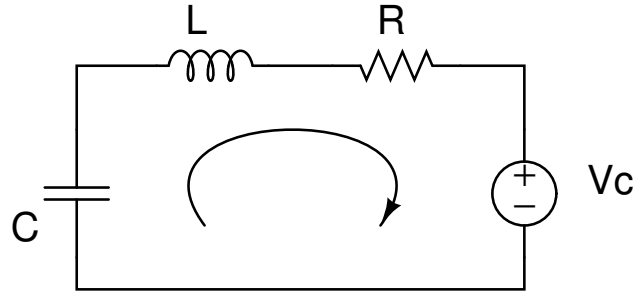


Figure 3.13: Equivalent circuit of serial synchronized switch harvesting on inductor circuit during transition

This is an initial condition problem with $v_{t=0} = V_M$, and its differential equation is written as

$$LC \frac{d^2 v}{dt^2} + RC \frac{dv}{dt} + v = V_c \quad (3.25)$$

By substitute v with $\mu = v - V_c$, and defining $\alpha = \frac{R}{2L}$ and $\omega_n^2 = \frac{1}{LC}$, then

Equation 3.25 becomes

$$\frac{d^2 \mu}{dt^2} + 2\alpha \frac{d\mu}{dt} + \omega_n^2 \mu = 0, \quad (3.26)$$

where ω_n is the undamped resonance frequency. The solution to Equation 3.27 for the under damped case (the over-damped and critically damped cases being too inefficient) that satisfies the initial condition is

$$\mu = (V_M - V_c) e^{-\alpha t} \cos \omega_d t \quad (3.27)$$

where $\omega_d = \sqrt{1 - \xi^2} \omega_n$ and $\xi = \alpha / \omega_n$. For a slightly damped system, $\omega_d \approx \omega_n$.

The circuit is usually designed so that current reverses only once for each transient, either via a blocking diode or timing the switch to precisely turn off at $t = \frac{\pi}{\omega_d}$.

Substitution yields Equation 3.28.

$$\mu = -(V_M - V_c) e^{-\alpha \frac{\pi}{\omega_d}} = -(V_M - V_c) e^{-\frac{\pi}{2Q}}, \quad (3.28)$$

where Q is known as the quality factor and is defined as $Q \triangleq \frac{\omega_n}{2\alpha} \approx \frac{\omega_d}{2\alpha}$. The reverse voltage therefore is

$$|v_R| = (V_M - V_c) e^{-\frac{\pi}{2Q}} - V_c \quad (3.29)$$

Under steady-state, the maximum voltage V_M stays the same for all cycles, and the relationship in Equation 3.30 holds.

$$V_M = V_o + |v_R| \quad (3.30)$$

In the above equation, the open circuit voltage $V_o = \frac{dF_M}{C}$ is defined the same as in Equation 3.21. By simultaneously solving Equations 3.29 and 3.30, we obtain V_M as a function of the open circuit voltage V_o and capacitor voltage V_c . The physical meaning of this result is that the equilibrium maximum voltage on the device is jointly determined by the amount of input energy, represented by V_o , and how much energy is removed from the system, which is proportional to V_c .

$$V_M = \frac{V_o - V_C \left(1 + e^{-\frac{\pi}{2Q}}\right)}{1 - e^{-\frac{\pi}{2Q}}} \quad (3.31)$$

Care should be taken when calculating the harvested energy, because we have included dissipation modeled as a resistor in the equivalent circuit. Even though the electrical energy coming out of the device is still represented by the parallelogram area, it is not equal to the energy collected by the capacitor. Since we know the charge going into the capacitor is

$$\begin{aligned} Q &= C(2V_M - V_o) \\ &= C(V_o - 2V_C) \left(\frac{1 + e^{-\frac{2\pi}{Q}}}{1 - e^{-\frac{2\pi}{Q}}} \right) \end{aligned} \quad (3.32)$$

And the capacitor is maintained at a constant voltage V_C , The energy is then represented by the shaded area in Figure 3.12.

$$\begin{aligned} W &= 2QV_C \\ &= 2C(V_o - 2V_C)V_C \left(\frac{1 + e^{-\frac{2\pi}{Q}}}{1 - e^{-\frac{2\pi}{Q}}} \right) \end{aligned} \quad (3.33)$$

For a given mechanical excitation this energy is a function of the capacitor voltage V_C , and it is maximized when

$$V_C = \frac{V_o}{4} \quad (3.34)$$

By substituting Equation 3.34 back into Equation 3.33, we find the optimized energy for a serial SSHI circuit.

$$\begin{aligned}
W_{\max} &= \frac{d^2 F_M^2}{4C} \left(\frac{1 + e^{-\frac{\pi}{2Q}}}{1 - e^{-\frac{\pi}{2Q}}} \right) \\
&= \frac{1}{4} C V_o^2 \left(\frac{1 + e^{-\frac{\pi}{2Q}}}{1 - e^{-\frac{\pi}{2Q}}} \right)
\end{aligned} \tag{3.35}$$

The optimized condition is given in Equation 3.36. The effectiveness of this circuit, as shown in Equation 3.35, highly depends on the quality factor Q of the resonator. The peak voltage at this condition is calculated as

$$V_M = \frac{1}{4} V_o \left(\frac{3 - e^{-\frac{\pi}{2Q}}}{1 - e^{-\frac{\pi}{2Q}}} \right) \tag{3.36}$$

For a lightly damped system, this voltage could become dangerously high for the device and electrical circuit.

3.2.2.2 Parallel SSHI circuit

As shown in Equation 3.31, the maximum voltage on the piezoelectric device in the serial SSHI could be high, especially for a lightly-damped circuit. This may sometimes impose a practical problem, such as dielectric break-down of the piezoelectric material, or a voltage higher than the rating of the power electronic devices. A parallel SSHI circuit, however, does not have this problem. It employs a parallel inductor to

partially reverse the voltage polarity as shown in Figure 3.19. In this configuration, the voltage on the device is constrained by the capacitor voltage.

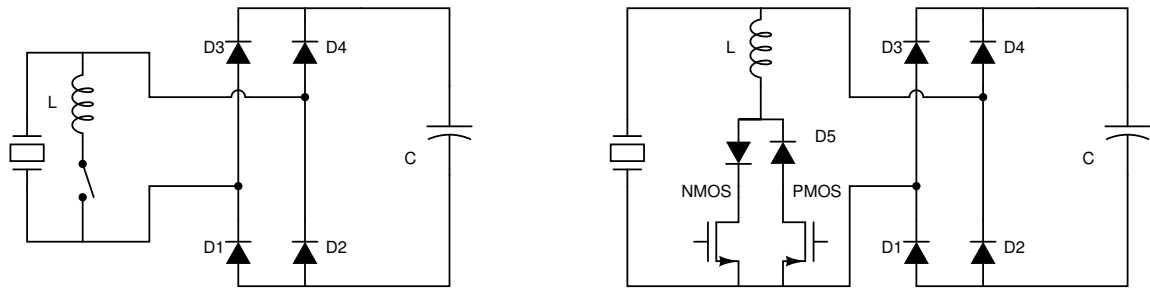


Figure 3.14: Parallel SSHI circuit and its implementation

The control of this circuit differs from the serial SSHI circuit. Ideally, the switch should be still turned on at the maximum mechanical force. However, as the voltage on the device is constrained by the capacitor voltage, the peak voltage of piezoelectric device does not coincide with the peak force. A circuit that compares voltage on the piezoelectric device with that of capacitor voltage is then used. The energy conversion cycle is plotted in Figure 3.15.

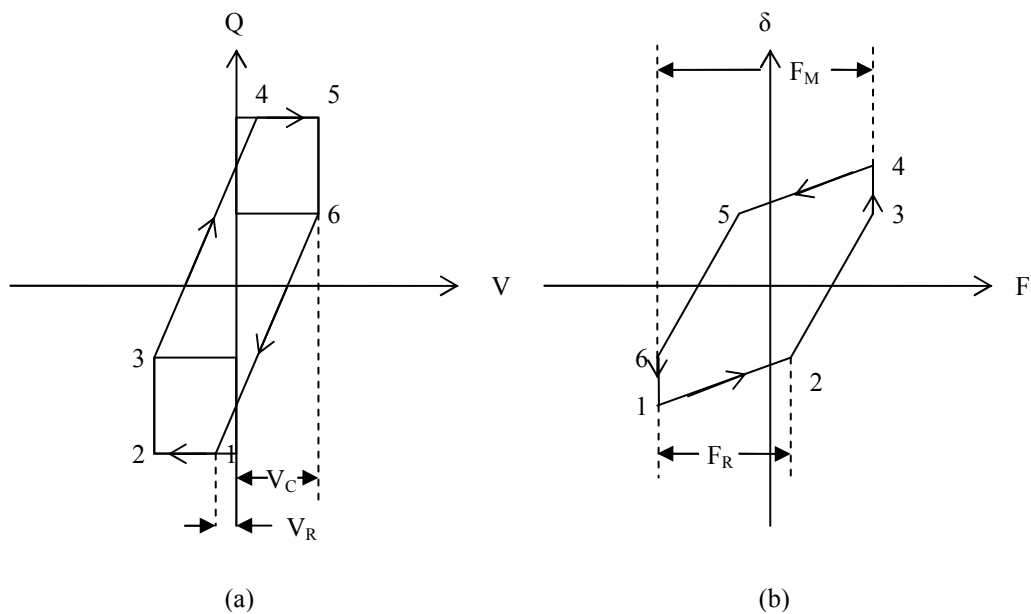


Figure 3.15: Energy conversion cycle of Parallel SSHI circuit (a) electrical domain (b) mechanical domain

In the figure, from 6-1 or 3-4 the switch turns on and the equivalent LCR discharging circuit is shown in Figure 3.16. Note it is similar to the serial SSHI circuit, but without the voltage source in series.

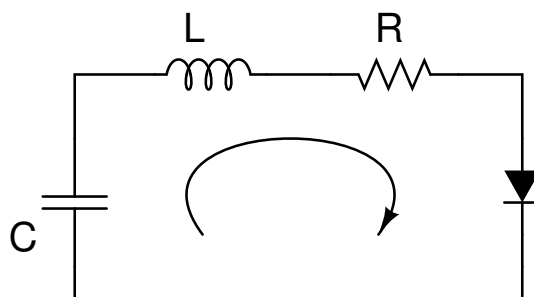


Figure 3.16: Equivalent Parallel SSHI discharging circuit, where diode blocks the reversion of the current

The differential equation (3.37) is solved with an initial condition of $v|_{t=0} = V_C$

$$LC \frac{d^2v}{dt^2} + RC \frac{dv}{dt} + v = 0 \quad (3.37)$$

Solving the above equation for the final state yields

$$V_R = -V_c e^{-\frac{\pi}{2Q}} \quad (3.38)$$

From the electric domain figure, the voltage change from 1-2 then is $V_c \left(1 - e^{-\frac{\pi}{2Q}}\right)$, so the

force corresponding to this change is

$$F_R = C \frac{V_c \left(1 - e^{-\frac{\pi}{2Q}}\right)}{d} \quad (3.39)$$

The energy collection only happens from 1-2 and 4-5, during which the charge flow into the capacitor is

$$\begin{aligned} Q &= d(F_M - F_R) \\ &= d \left(F_M - C \frac{V_c \left(1 - e^{-\frac{\pi}{2Q}}\right)}{d} \right) \end{aligned} \quad (3.40)$$

And the associated energy is the shaded rectangular areas in Figure 3.15.

$$\begin{aligned} W &= 2QV_c \\ &= 2C \left(V_o - V_c \left(1 - e^{-\frac{\pi}{2Q}}\right) \right) V_c \end{aligned} \quad (3.41)$$

This energy is optimized when

$$V_c = \frac{V_o}{2 \left(1 - e^{-\frac{\pi}{2Q}} \right)} \quad (3.42)$$

This gives

$$W = \frac{d^2 F_M^2}{2C \left(1 - e^{-\frac{\pi}{2Q}} \right)} = \frac{C V_o^2}{2 \left(1 - e^{-\frac{\pi}{2Q}} \right)} \quad (3.43)$$

In case the optimized voltage V_c still could be prohibitively high, the circuit is usually not designed to work at optimized conditions, and the output voltage is chosen for practical reasons.

As the above analysis shows, for both serial SSHI and parallel SSHI circuits the amount of energy converted from mechanical energy is larger than the passive approaches, depending on the quality factor Q . It works extremely well when structural damping is the main goal of the system. From an energy harvesting point of view, however, not all the absorbed mechanical energy actually converts to the electric form and a large portion is dissipated mechanically through structural damping and electrically as $I^2 R$ loss. Both SSHI circuits need optimization of the capacitor voltage as a function of input force for the best performance, which requires additional circuitry.

3.3 Active energy harvesting

Active energy harvesting, which utilizes a bidirectional switch-mode converter to actively apply voltage or current to the piezoelectric devices, has certain advantages over other approaches. For example, the voltage transition could be made arbitrarily smoother

than that of SSHI approaches, whose resonance frequency is dominated by the inductor value. A smooth transition has fewer high frequency components, therefore is unlikely to excite higher mode vibrations in the structure, thus resulting in less structural damping and energy loss. Secondly, the active energy harvesting uses a pulse-width-modulated switch amplifier, which moves energy through the inductor in a more continuous fashion, for the same amount of energy, the peak current in the inductor is orders of magnitude lower than that of an SSHI inductor, and hence results a much smaller I^2R loss.

The basic configuration of active energy harvesting was first patented by Hagood in 2003 [55], in which a bidirectional converter directly drives a piezoelectric device. However, as a patent is not supposed to be a systematic investigation of this topic, its work mechanism, comparison, and practical limitations were not given. Elsewhere there is no study on this specific topic. A few papers that investigate energy flow in the active structure damping could be a good reference in studying active energy harvesting [56], but their optimization goal is to suppress the vibration, while energy harvesting is a process to achieve the best electrical energy conversion. Their goals do not always coincide. In fact, for active vibration energy harvesting, the proof mass might experience larger vibration than that excited by the base vibration alone.

3.3.1 Fundamental limitations

Active energy harvesting is a technique that can push the energy harvesting limits of piezoelectric devices. Two major limits are mechanical and electrical, such as breakdown or depoling voltage, or forces and displacements that might crack the device. Those

limitations are plotted in Figure 3.17 as parallel dash lines perpendicular to their own axis.

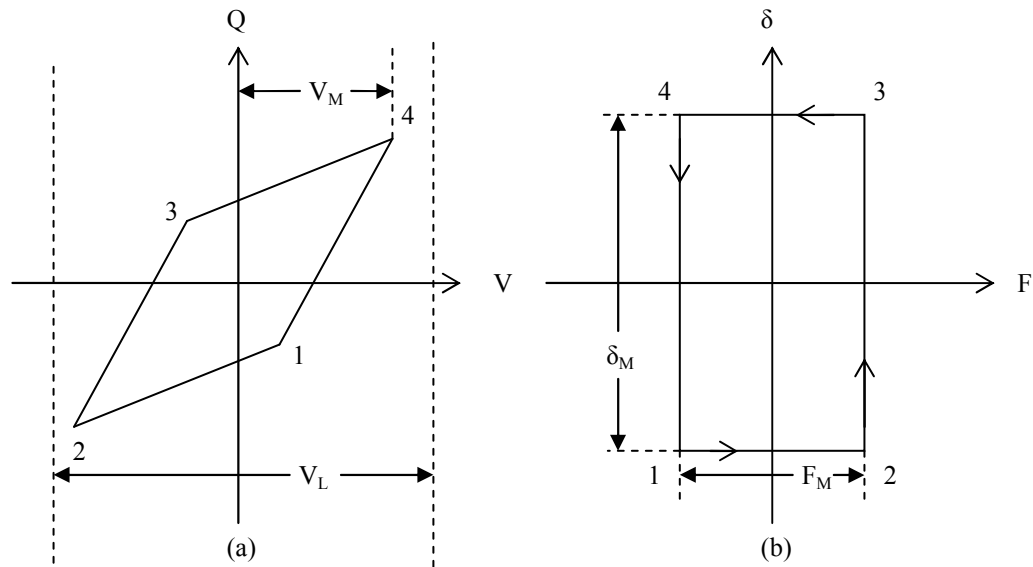


Figure 3.17: Mechanical limits bound the optimized energy conversion

If the device is only bounded by its mechanical limitations, (in other words, the device fails mechanically before electrical failure,) then

$$V_M = \frac{F_M}{dk} + \frac{\delta_M}{d} > V_L \quad (3.44)$$

In this case we could design the active harvesting cycle around the mechanical limitations, so that the energy harvesting cycle traverses along the device limitations for maximum energy conversion. The resulting conversion cycle is shown in Figure 3.17 and the energy is therefore is given by Equation 3.45

$$W_{\max} = F_M \delta_M \quad (3.45)$$

The slope of the path from 1-2 in the electrical domain is neither open circuit nor constant voltage. The voltage is a direct function of mechanical force and displacement. This indicates a sensor might be needed for its implementation.

3.3.2 Voltage controlled mode

In some cases, voltage is the limiting factor of the system, due to reasons such as the rating of the semiconductor switch. Under these conditions we could therefore design the active energy harvesting around its voltage boundary, which is called voltage-controlled mode. The first case is when

$$\frac{F_M}{dk} + \frac{\delta_M}{d} > V_L > 2 \left(\frac{F_M}{dk} - \frac{\delta_M}{d} \right) \quad (3.46)$$

Its conversion cycle is a truncated loop of Figure 3.17, shown in Figure 3.18.

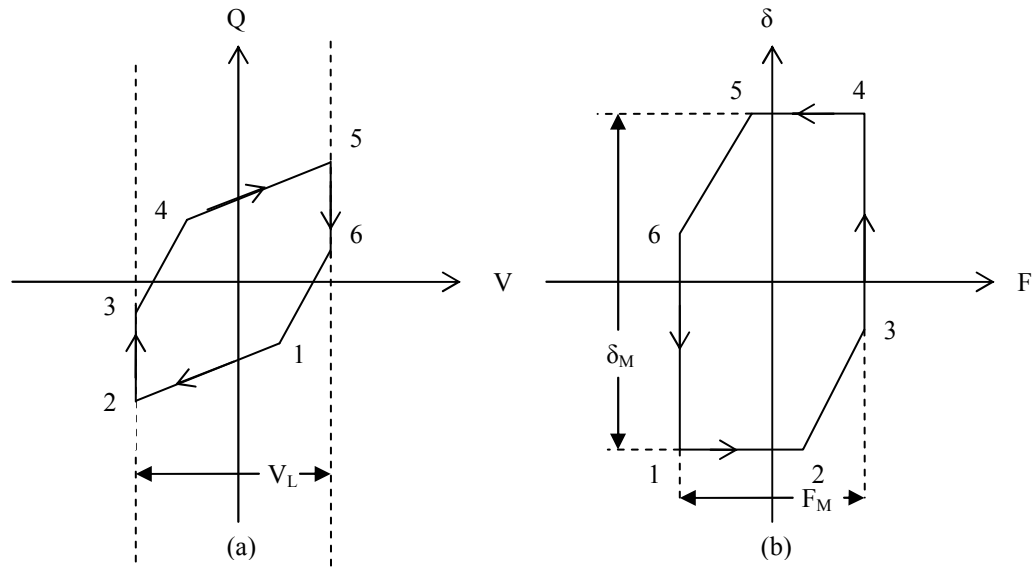


Figure 3.18: Voltage and displacement bounded energy harvesting cycle

Its converted energy is calculated as Equation 3.47

$$W = F_M \delta_M - \frac{1}{4k} (F_M - kdV_L + k\delta_M) \quad (3.47)$$

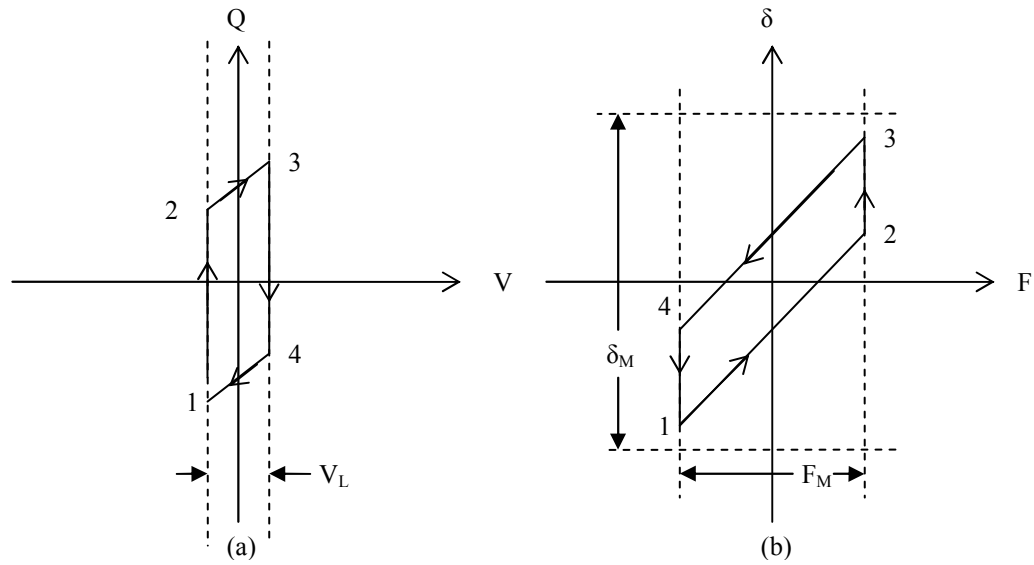


Figure 3.19: Voltage control of voltage controlled active energy harvesting

A condition often encountered in practice is when the voltage applied to the device is constrained purely by the electrical capability of the circuit and device. This can be summarized in Equation 3.48.

$$V_L < 2 \left(\frac{F_M}{dk} - \frac{\delta_M}{d} \right) \quad (3.48)$$

The converted energy is calculated from the area of either parallelogram in the electrical or mechanical domain in Figure 3.19.

$$W = dF_M V_L \quad (3.49)$$

We assume the following relationship holds

$$\delta_M > \frac{F_M}{k} + dV_L \quad (3.50)$$

This means we usually design the device to withstand the applied force and voltage at the same time.

Active energy harvesting in a voltage-controlled mode could also be accomplished with sinusoidal mechanical and electrical excitation. Suppose that the mechanical force takes the sinusoidal form $F = \text{Re}[\tilde{F}_0 e^{j\omega t}]$ and the voltage applied on the device is $V = \text{Re}[\tilde{V}_0 e^{j\omega t}]$. The electrical current is then found by

$$\tilde{I} = \dot{\tilde{Q}} = j\omega(d\tilde{F}_0 + C\tilde{V}_0) \quad (3.51)$$

The instantaneous power is therefore given by

$$P = \frac{1}{2} \text{Re}(V \times i^*) = \omega \frac{1}{2} d |\tilde{V}_0| |\tilde{F}_0| \sin \theta \quad (3.52)$$

where $\theta = \angle(\tilde{F}_0, \tilde{V}_0)$. This power is optimized when

$$|V_0| = \frac{V_M}{2}, |F_0| = \frac{F_M}{2}, \text{ and } \theta = -\pi \quad (3.53)$$

That gives the optimized power of

$$P = f \frac{\pi}{4} V_M F_M d \quad (3.54)$$

The converted energy is therefore less than the ideal voltage controlled mode by a factor of 0.785. However, the sinusoidal voltage will not generate high frequency harmonics in the mechanical system. The associated dielectric loss is also the smallest, which might be preferable if the material has a relatively large loss tangent.

3.3.3 Charge control

Instead of voltage, charge may be specified as a limiting factor on the device. Under these circumstances a charge-controlled approach to energy conversion could then be designed. Shown in Figure 3.20 is the conversion cycle when

$$C \frac{\delta_M}{d} - \left(d + \frac{C}{dk} \right) F_M < Q_L < C \frac{\delta_M}{d} \quad (3.55)$$

As depicted in Figure 3.20, the energy conversion cycles are bounded by both electrical charge and the mechanical displacement.

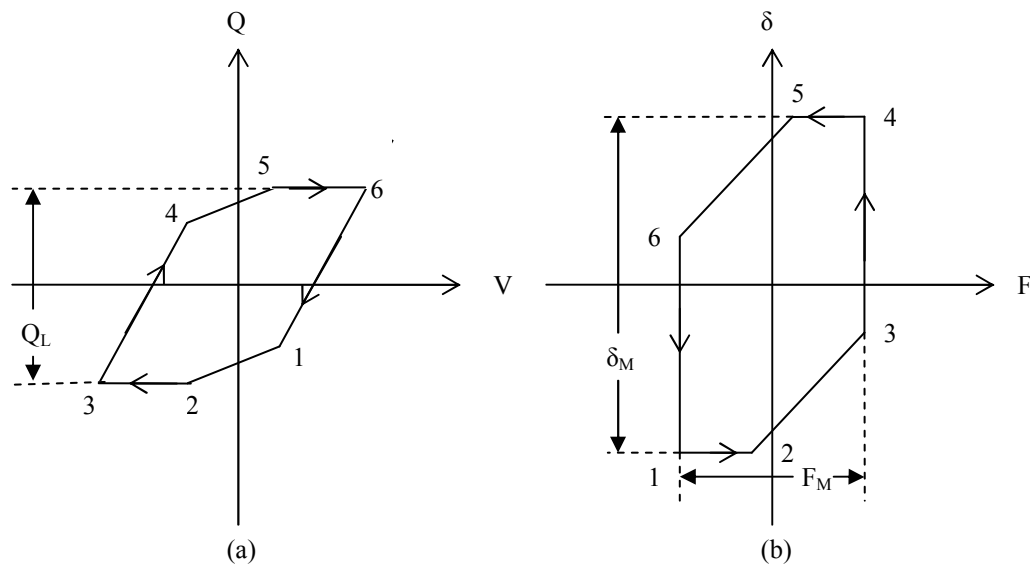


Figure 3.20: Charge controlled energy conversion cycle bounded by both electrical charge and the mechanical displacement

In this case, the energy is then given by

$$W = \delta_M F_M - \frac{1}{2} \left(\frac{1}{k} - \frac{d^2}{C} \right) \left(F_M - \frac{Q_L dk - Ck\delta_M}{d^2 k - C} \right)^2 \quad (3.56)$$

On the other hand, if the charge limit falls in the range of

$$Q_L < C \frac{\delta_M}{d} - \left(d + \frac{C}{dk} \right) F_M \quad (3.57)$$

The conversion cycle is then solely limited by the electrical charge on the device. A major benefit of this approach is that, during a constant charge period, the device is under open circuit condition and the electrical circuit is inactive. If we could design the circuit to be active for a small percentage of the energy conversion cycle, a very high efficiency could be achieved.

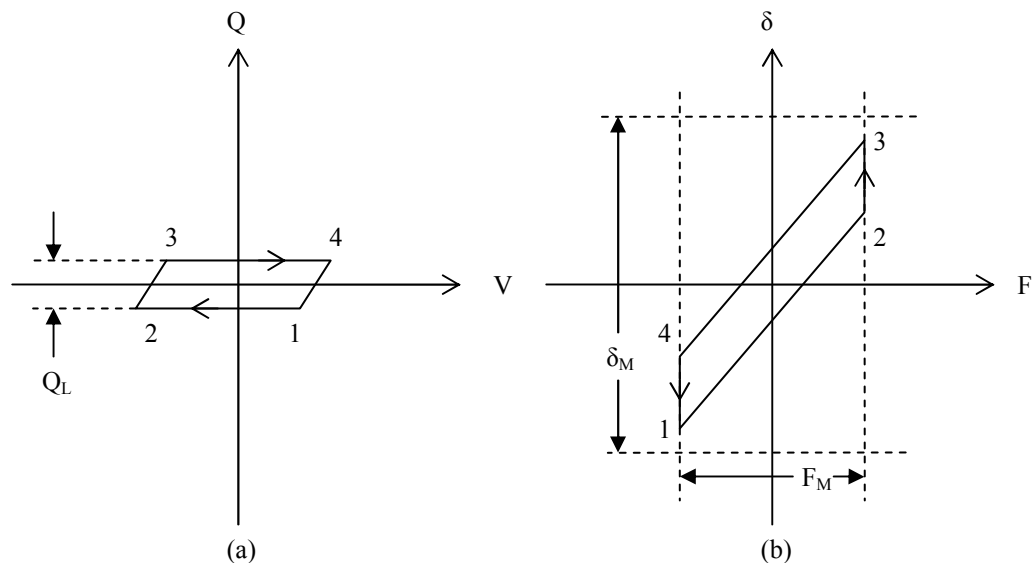


Figure 3.21: Charge controlled energy conversion cycle bounded only by both electrical charge

Similar to the voltage-controlled mode, the resulting net energy harvested is given by Equation 3.58.

$$W = \frac{dF_M Q_L}{C} \quad (3.58)$$

From the Equation 3.49 and 3.58, it seems that if the peak-to-peak mechanical force is independent of electrical boundary condition, we could boost the energy conversion arbitrarily high by increasing the voltage or charge swing on the device up to the piezoelectric device limit by using active energy harvesting. That is true only if the power electronic circuit has 100% efficiency. From a practical standpoint, however, the amount of energy that can be harvested, and the optimal voltage/charge waveform for a given mechanical excitation, depends heavily upon the efficiency of the power electronic circuitry. This is largely due to the fact that, during a mechanical excitation period, electrical power is flowing both into and out of the piezoelectric device.

3.3.4 efficiency of power electronics

Unfortunately, the amount of power that can be harvested is constrained by the fact that all power electronic circuits are lossy: therefore, a certain portion of its transferred energy dissipates in the form of heat. This characteristic is described by its efficiency.

$$\eta = \frac{\text{Output Energy/Cycle}}{\text{Input Energy/Cycle}} = 1 - \frac{\text{Loss/Cycle}}{\text{Input Energy/Cycle}} \quad (3.59)$$

In order to facilitate analysis, we choose a voltage and charge boundary with the following relations, so their energy conversion is the same.

$$V_L = \frac{Q_L}{C} < 2 \left(\frac{F_M}{dk} - \frac{\delta_M}{d} \right) \quad (3.60)$$

Both voltage-and-charge control conversion cycles that meet their own boundary are plotted in Figure 3.22

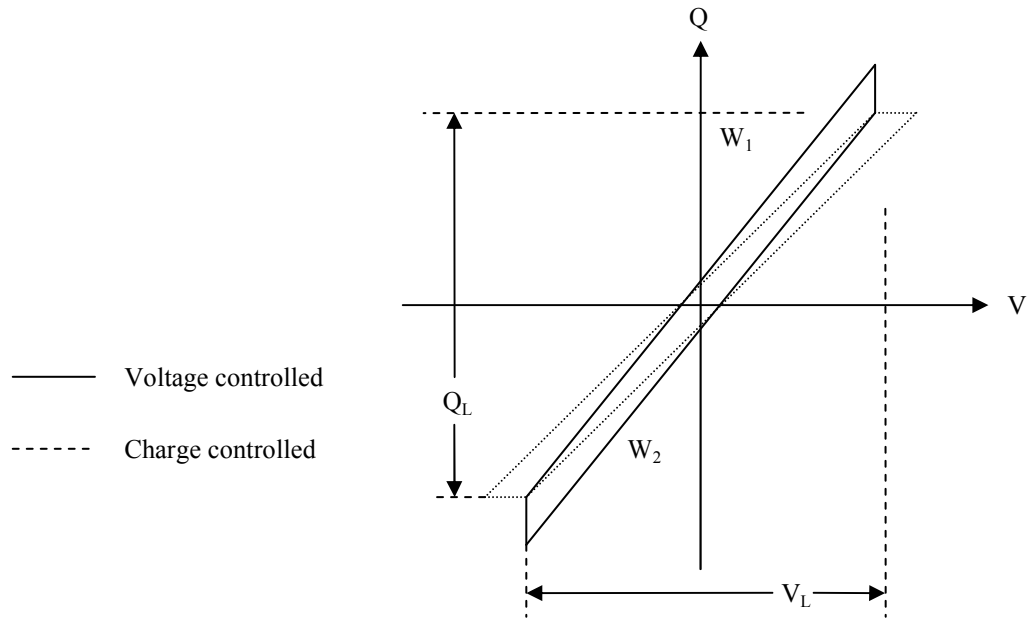


Figure 3.22: The voltage and charge controlled energy harvesting loops that have a equal amount of harvested energy. The shaded area represents the input electrical energy in one cycle

In the figure, the energy that is re-infused back to the device during the voltage reversion is represented by the shaded triangular areas W_1 and W_2 . They are related to the output energy as follows:

$$\frac{W_1}{W} = \frac{W_2}{W} = \frac{CV_L}{4dF_M} \quad (3.61)$$

Assuming the efficiency of the power electronic circuitry is independent of operating point, the actual electrical energy harvested is then given by Equation 3.62

$$\begin{aligned}
W^* &= W_{output}\eta - \frac{W_{1,2}}{\eta} \\
&= (W + W_{1,2})\eta - \frac{W_{1,2}}{\eta} \\
&= \left(1 - \frac{W_{1,2}}{W} \left(\frac{1}{\eta} - \eta\right)\right) W
\end{aligned} \tag{3.62}$$

The actual harvested energy during one conversion cycle is determined by substituting Equation 3.61 into the above equation.

$$\begin{aligned}
W^* &= \left(1 - \frac{CV_L}{4dF_M} \left(\frac{1}{\eta} - \eta\right)\right) dF_M V_L \\
&= C \left(V_o - \frac{V_L}{2} \left(\frac{1 - \eta^2}{\eta}\right)\right) V_L
\end{aligned} \tag{3.63}$$

For a given mechanical force and efficiency of the power electronics, the above energy could be optimized by varying the voltage swing V_L . This amplitude optimized condition is given by:

$$V_L = \frac{d}{2C} \left(\frac{\eta}{1 - \eta^2}\right) F_M = \frac{1}{2} \left(\frac{\eta}{1 - \eta^2}\right) V_o \tag{3.64}$$

At this voltage level, the optimized energy is

$$W^* = \frac{1}{2} \left(\frac{\eta}{1 - \eta^2}\right) \frac{d^2 F_M^2}{C} = \frac{1}{2} \left(\frac{\eta}{1 - \eta^2}\right) C V_o^2 \tag{3.65}$$

The above function is very sensitive to the efficiency, especially when it is high, as shown in Figure 3.23.

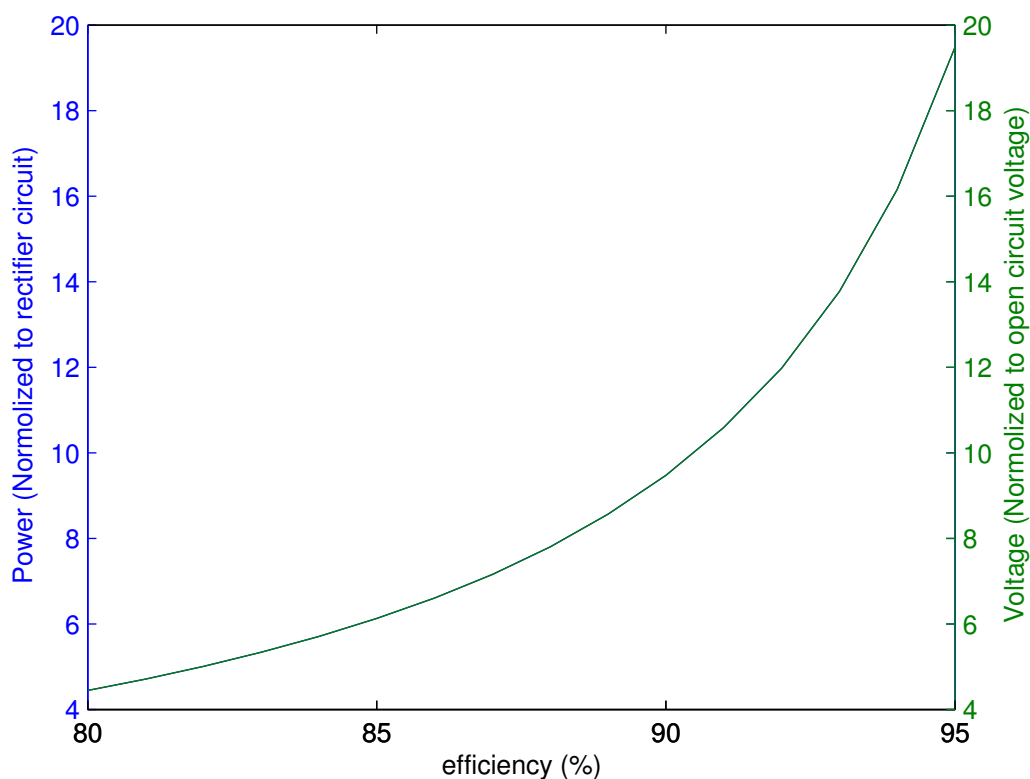


Figure 3.23: The performance of active energy harvesting as function of its efficiency.

The commercially available (from such as Linear Technologies and Analog Devices) DC-DC converters that voltage rated between 2 to 20 V and power rated between 1mW to 10mW usually have a power efficiency of 85% to 90%.

3.4 Theoretical Comparison of energy harvesting circuits

The theoretical comparison is summarized in Table 3.1. The passive circuits generally are poorest in terms of harvested energy, but they are also simplest in structure. The active energy harvesting circuit potentially could achieve much better performance, however they are the most complex energy harvesting circuit, which often requires

sensors and certain feedback control. In this regard there is no simply best circuit for all the applications. The significance of active energy harvesting might be for the application that demands more power when improvement of the piezoelectric device is difficult and the cost is not a big concern.

The presented analysis also indicates the semi-passive energy harvesting circuits have superior energy harvesting performance. The limiting fact of semi-passive circuit is the loss associated with the transient during a switching event.

Table 3.1

Table 3.1: Comparison of energy harvesting circuit

		Semi-passive Circuit			Active circuit	
Passive circuit		Serial SSHI	Parallel SSHI	Voltage controlled	Charge Controlled	
Energy	$2C(V_o - 2V_c)V_c$	$2C(V_o - 2V_c)V_c \left(\frac{1+e^{-\frac{\pi}{2Q}}}{1-e^{-\frac{\pi}{2Q}}} \right)$	$2C \left(V_o - V_c \left(1 - e^{-\frac{\pi}{2Q}} \right) \right) V_c$	$C \left(V_o - \frac{V_L}{2} \left(\frac{1-\eta^2}{\eta} \right) \right) V_L$	$\left(V_o - \frac{Q_L}{2C} \left(\frac{1-\eta^2}{\eta} \right) \right) Q_L$	
Rectifier	$2C(V_o - 2V_c)V_c$					
Charge extraction	1					
Optimized condition	$V_c = \frac{1}{4}V_o$	$V_c = \frac{1}{4}V_o$	$V_c = \frac{V_o}{2 \left(1 - e^{-\frac{\pi}{2Q}} \right)}$	$V_L = \left(\frac{\eta}{1-\eta^2} \right) V_o$	$Q_L = C \left(\frac{\eta}{1-\eta^2} \right) V_o$	
Optimized energy	$\frac{1}{4}$	$\frac{1}{4} \left(\frac{1+e^{-\frac{\pi}{2Q}}}{1-e^{-\frac{\pi}{2Q}}} \right)$	$\frac{1}{2} \left(\frac{1}{1 - e^{-\frac{\pi}{2Q}}} \right)$	$\frac{1}{2} \left(\frac{\eta}{1-\eta^2} \right)$	$\frac{1}{2} \left(\frac{\eta}{1-\eta^2} \right)$	

There hardly is a single criterion for all the energy harvesting circuit, because of the versatility of application. Each circuit has its performance and complexity. Every energy harvesting application is different in its size, weight and cost constraint on energy harvesting circuits.

Chapter 4

Active Energy Harvesting Experiment Using Piezoelectric

This chapter presents an experiment comparison between active energy harvesting and the standard diode rectifier circuit. The experiment results are also compared with the theoretical modeling developed in the previous chapter.

4.1 Mechanical excitation

A computer-programmable material testing system (MTS Systems Corporation's MTS810) was used in the following experiment to apply a compressive sinusoidal force to the piezoelectric device. The mechanical setup is shown in Figure 3.2. A load cell at the top measures the applied force and provides the feedback signal to the system computer so that the applied force is well-regulated. The weight of the structure above the sample device and below the load cell is added to the measured force. Alumina ceramic plates were used as a sample holder for their high electrical insulation abilities. Below the device a universal joint was inserted beneath the sample holder to achieve a uniform pressure on the device. Polyurethane foam of 20cm in thickness is attached to the machine's base and used as a cushion and damper to reduce the high frequency mechanical noise resulting from operation of the hydraulic system.

A static or minimum force of 15 lb was used throughout the experiment while energy harvesting was performed for multiple data points under a sinusoidal dynamic

force whose peak value (corresponding to the F_M in the theoretical part of this chapter) was between 45lb to 70lb. In order to satisfy the quasi-static assumption, the mechanical force frequency is set to be 10 Hz, low enough that no resonance is excited in the device.

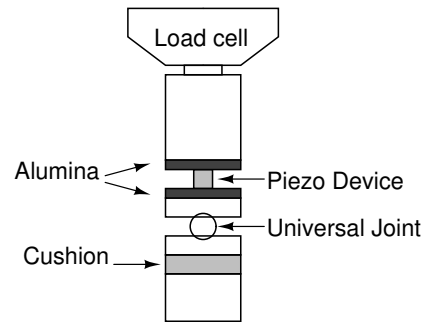


Figure 4.1: The mechanical setup for quasi-static energy harvesting

4.2 Determination of Device Parameters

A PMN-PT single crystal multilayer device, produced by TRS Ceramics Inc., was used in the following experiments. The single crystal, $\langle 001 \rangle$ cut, dimensions are 10mmx10mmx6.5mm, and its effective d_{33} is about 1100pC/N. This device is comprised of ten layers of 0.5mm thick single crystal (1cm X 1cm), which are sandwiched between gold electrodes. These layers are epoxied together. The piezoelectric single crystal has much higher coupling than the ceramic counterpart (i.e. PZT), so a relatively smaller force is required to generate enough power for the experiment. The multilayer structure also provides a favorably higher current-to-voltage ratio than a monolithic device of the same thickness, which is generally preferred by the power electronic circuit efficiency. The

material properties and geometric information of the single crystal are provided in

Table 4.1

Table 4.1: material properties and geometric information of the single crystal

Dielectric constant ϵ_3	Piezoelectric constant d_{33}	Elastic compliance s_{11}^E	Thickness t	Area A	# of layers
$4000\epsilon_0$	$1100pC/N$	$80 \times 10^{-12} m^2/N$	$0.5mm$	$100mm^2$	10

The device's parameters of Equation 3.3 and Equation 3.4 therefore can be theoretically determined to be

$$C = 10 \frac{\epsilon_{33}^S A}{t} = 70nF, d = 10d_{33} = 1.1 \times 10^{-8} m/V, k = \frac{A}{s_{11}^E 10t} = 3.3 \times 10^8 N/m \quad (4.1)$$

Experiments were performed to directly measure these device parameters. The capacitance of the device was measured under a free mechanical boundary condition using a multimeter to be 68nF, close enough to the theoretical calculation. In order to identify the piezoelectric coefficient, the open circuit peak-peak voltage is measured under a different mechanical load. The open-circuit voltage was measured using an oscilloscope whose input impedance is a 10M Ω and 12pf, which is 500 times larger than the internal impedance of device (about 0.2 M Ω at 10 Hz excitation). The results are shown in Figure 4.2.

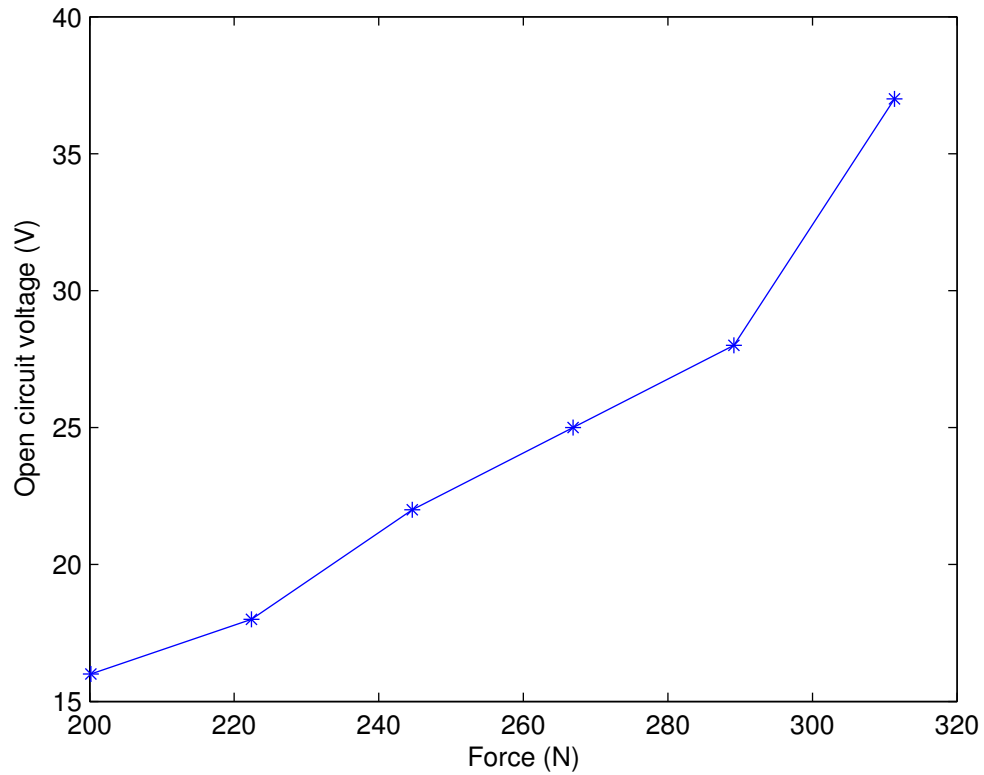


Figure 4.2: The open-circuit voltage at different levels of mechanical force

Assuming the open-circuit boundary condition ($Q=0$), the device's general piezoelectric constant is calculated using equation:

$$d = \frac{CV_o}{F_M} \quad (4.2)$$

Using the measurement data shown is in Figure 4.2, the results are given in the figure below

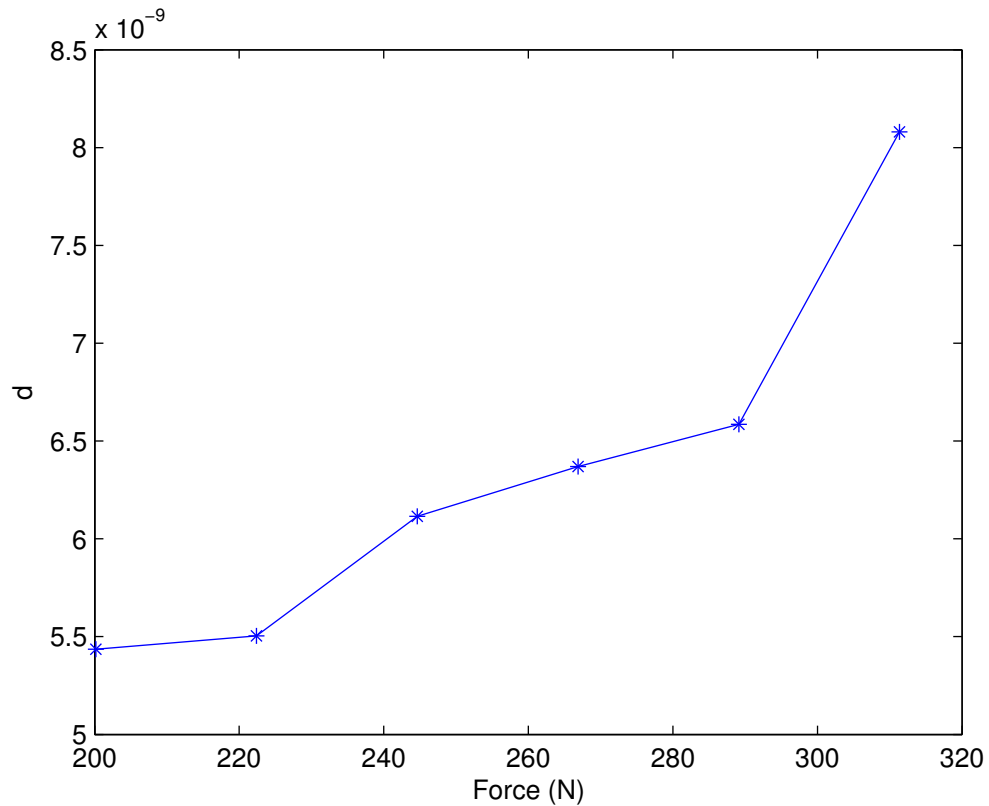


Figure 4.3: The piezoelectric coefficient changes under different mechanical load

The experiment measured general piezoelectric constant does not agree with the theoretically calculated value of 11×10^{-9} C/N. The data also shows that the general piezoelectric constant is a function of applied dynamic force. There are two perceived reasons for this result, the sample is partially clamped in the lateral direction by the sample holder during measurement, while in the theoretical calculation free mechanical boundary conditions are assumed. When partially clamped, the stress distribution in the sample is not uniform, and hence the piezoelectric contribution of each portion of the sample therefore is different. Secondly, PMN-PT single crystal is a complex system; once electrically poled, it has piezoelectric properties. However it also is intrinsically an

electrostrictive material. Our measurement counts both piezoelectric and electrostrictive effects as piezoelectricity.

4.3 The power electronic circuit

A half-bridge converter topology was chosen for the active power electronic circuit, shown in Figure 3.1. This topology is inherently bidirectional. For example, pulse-width modulating the upper MOSFET in the diagram allows the device to be charged to a positive voltage, while switch behavior of bottom MOSFET results in the device being charged to a negative voltage. The circuit was externally powered by a dual-voltage power supply of $\pm 15V$. The harvested power is calculated by multiply the voltage (30V) with the measured current. Negative power is harvested power.

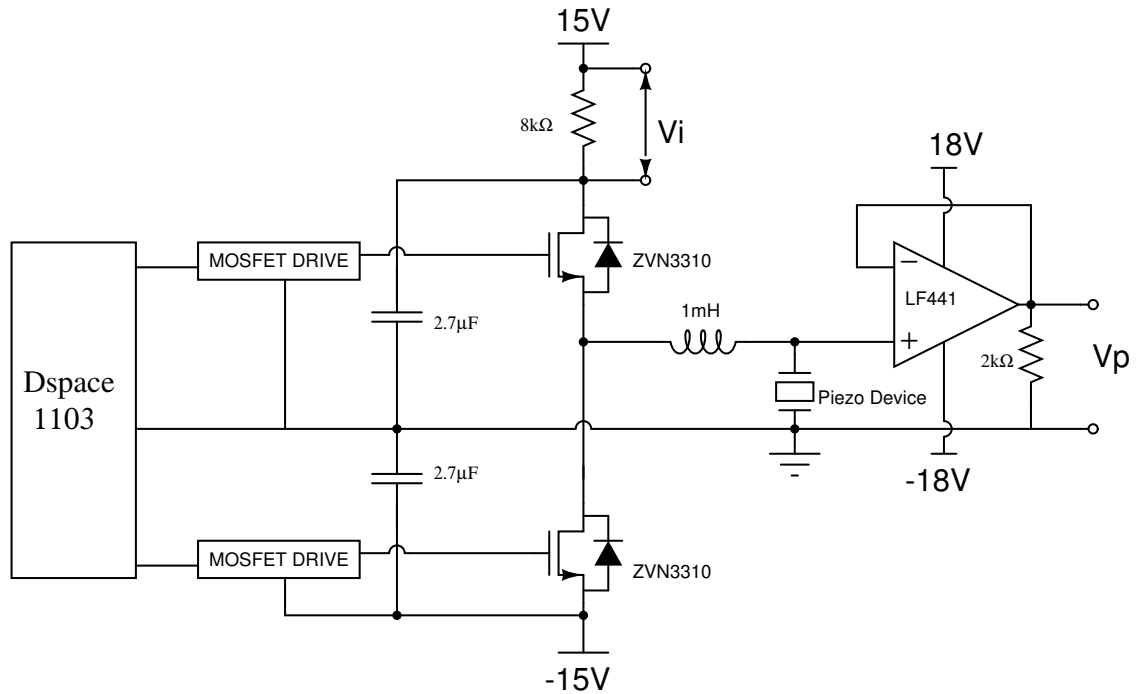


Figure 4.4: Half bridge converter used for active energy harvesting

The current that flows to the DC supply is monitored using an $8\text{k}\Omega$ sensing resistor whose voltage drop is insignificant compared to the bus voltage (30v). A high-input-impedance op-amp LF441 was configured as a voltage-follower and was used to measure the voltage across the piezoelectric device. Its leakage current is below 100fA , eliminating the interference of the amplifier on electrical measurement. A dSpace 1103 controller card was used to implement the active control technique and provide pulse-width modulation (PWM) to the circuit. For the purposes of this experiment the gate drivers for the MOSFETs were powered by an external power supply (battery). The switching signal is transferred through an optical coupler. For this experiment the power for gate drive and control system is not included in the power path. In the standalone active energy harvesting circuit, this part of the circuit is reasonably expected to have

ultra-low power consumption. If an Application Specific Integrated Circuit (ASIC) is used to implement the control of the active energy harvesting, the power consumption is expected to be less than one milliwatt.

In order to further reduce switching losses, the controller modulates the top and bottom MOSFET independently, depending upon whether the voltage across the device is being increased or decreased. A switching frequency of 2 kHz and constant duty cycle of 0.8% was used to shift the voltage across the device at the minimum and maximum values of the measured force.

The circuit efficiency was measured by charging and discharging a 50nF ceramic capacitor. The discharging efficiency is measured at 92%, and charging is measured at 95% at 1mW. The quiescent power consumption is measured to be below 10 uW without gate drive.

As a comparison, a half-bridge rectifier circuit using 1N5450 diodes and a 10uF film capacitor was built. The output of the circuit was connected to an HP voltage power supply as a load. A current sensing resistor of 21.5 k Ω is used for measuring the current flow into the power supply. The voltage across the sensing resistor and capacitor voltage were monitored by two 4½-digit multimeters. The harvested power is therefore the product of the current and the supply voltage. By varying the voltage across the capacitor using the power supply, we determine the optimized voltage for each mechanical load. This optimized power is used in the comparison of energy harvesting techniques.

4.4 Controller

The Simulink control code for the active energy harvesting circuit is shown in Figure 4.5. Mechanical force was measured by a load cell, and its signal was conditioned through a testing system and fed into an A/D channel of the DS1103. The load cell was recently calibrated to the equipment's specification, and its sensitivity is 600 lb/V. The force signal, however, was fairly noisy. If the signal is directly used by the controller, the applied voltage is poorly synchronized with the mechanical force. Adding a digital or analog filter might alleviate the signal to noise ratio. Unfortunately, filters usually introduce undesirable phase shift. To solve this problem a Phase-Locked Loop (PLL) is implanted in the Simulink code, shown in left bottom corner. It generates an ideal sinusoidal signal in phase with the applied force, and it is then used for the controller. The phase requirement of active energy harvesting described in previous chapters is to charge or discharge at the applied peak force. The threshold level of the 'switch' block in the Simulink code controls the duration of charging/discharging. The duty cycle of the PWM signal controls the rate of charging/discharging the device. These two parameters were manually chosen until the harvested energy was optimized for a 75 lb mechanical load, and were kept constant at these values for the rest of the experiments.

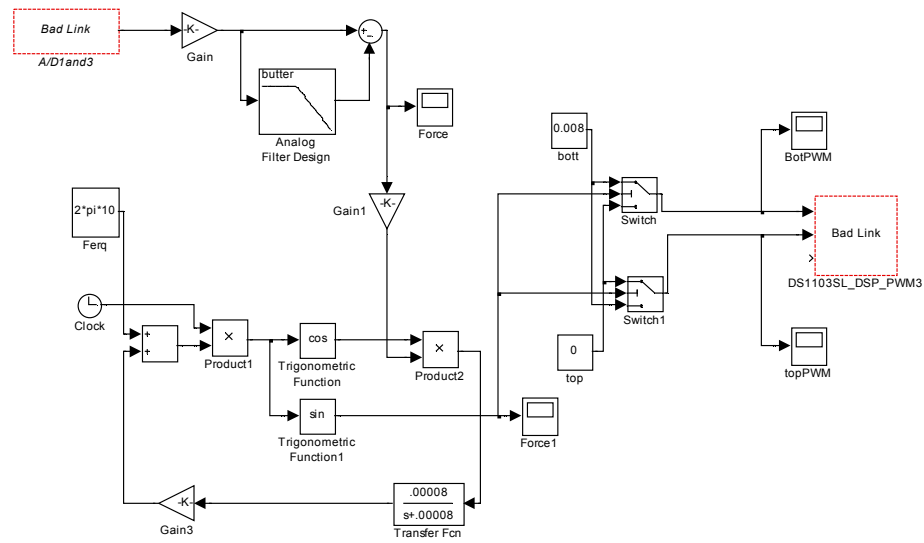


Figure 4.5: Active energy harvesting control using Simulink for Dspace system implementation

4.5 Results

By varying the mechanical excitation level and switching duty cycle, it is possible to achieve both the voltage-controlled and charge-controlled modes of operation. The voltage-controlled mode is shown in Figure 4.6 with an oscilloscope screen capture of the experiment, where the trapezoidal wave is the voltage on the piezoelectric device and the sinusoidal wave is the mechanical force (600lb/V). In this case the applied force is relatively large; hence, the active applied voltage and the voltage generated due to the applied dynamic force will add up to be larger than the bus voltage of the circuit. This relation is mathematically presented in Equation 3.46 , where the bus voltage of 30V is

the V_L . The voltage on the piezoelectric device is clamped to $\pm 15V$ shown in the figure through the flatness of the voltage wave.

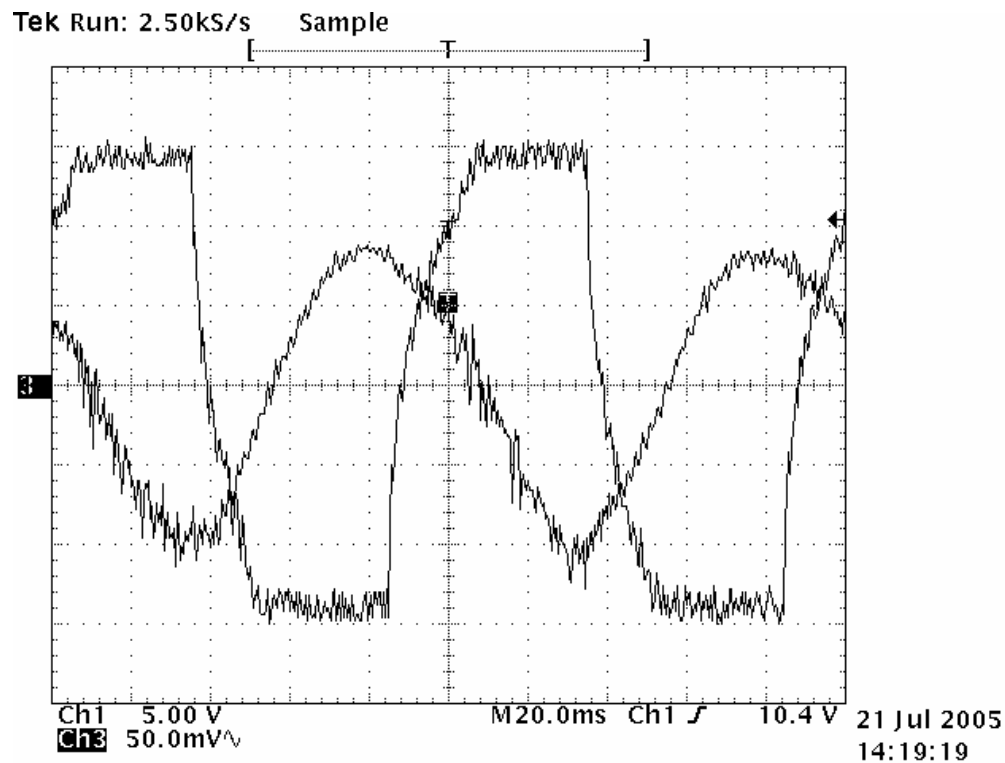


Figure 4.6: The voltage controlled mode operation. Channel 3 is the sinusoidal force (at 600lbf/V), while AC coupling of oscilloscope is used. Channel 1 is voltage across piezoelectric device,

On the other hand, if the sum of generated voltage from applied dynamic force and active applied voltage is smaller than the bus voltage of the circuit, the active energy harvesting operates in a charge-controlled mode. This condition is given by Equation 3.55, and its voltage wave is given in Figure 4.7 as a tooth wave. Note the steep raise and fall of the voltage is mainly from actively charging or discharging, while the less abrupt change of the voltage is from the mechanical force, during which both MOSFET switches of the circuit were open.

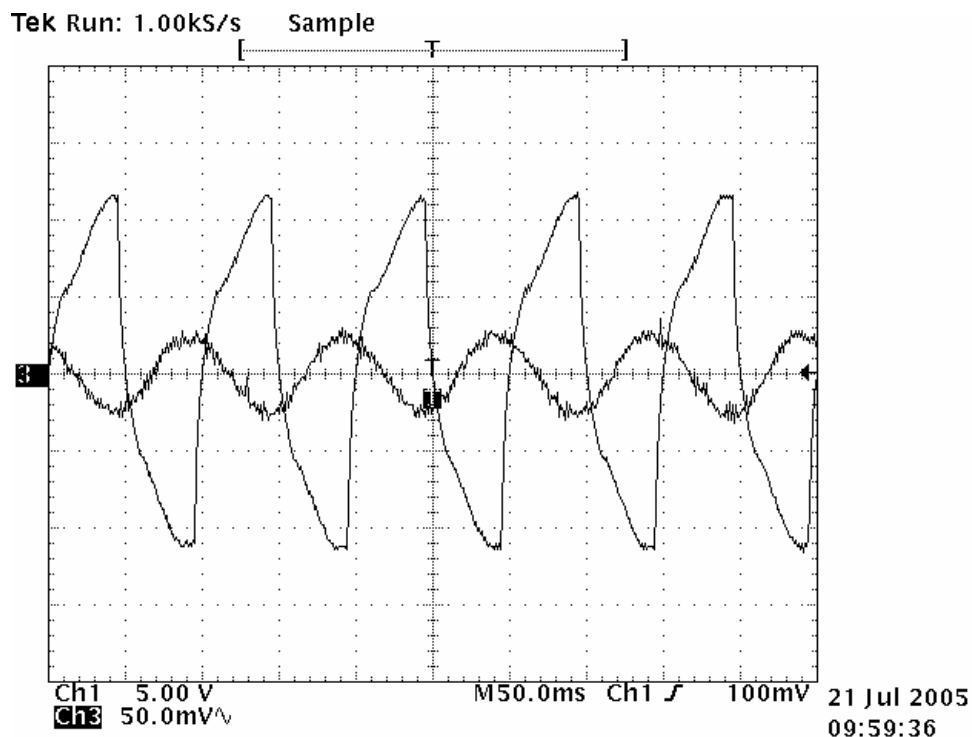


Figure 4.7: Sinusoidal wave is measured force (at 600lb/V), triangular wave is voltage across piezoelectric device. The charge controlled mode operation

Because this circuit is limited to a relatively low bus voltage of 30V, the charge-controlled mode occurs only under small mechanical force, and its generated power hardly surpasses the quiescent power consumption of the electrical circuit. We will therefore focus on the voltage-controlled mode for this experiment data collection.

The experimental data of both rectifier and active circuit is shown along with the theoretical model prediction. The experiment shows the active energy harvesting increases the harvested power by a factor of 45 under lower force of 45lb and 5 under 70 lb. The theoretical prediction of the active energy harvesting was based upon Equation 3.63, and the efficiency and device parameters measured in an earlier section. For the diode rectifier, Equation 3.18 was used to estimate the power harvested.

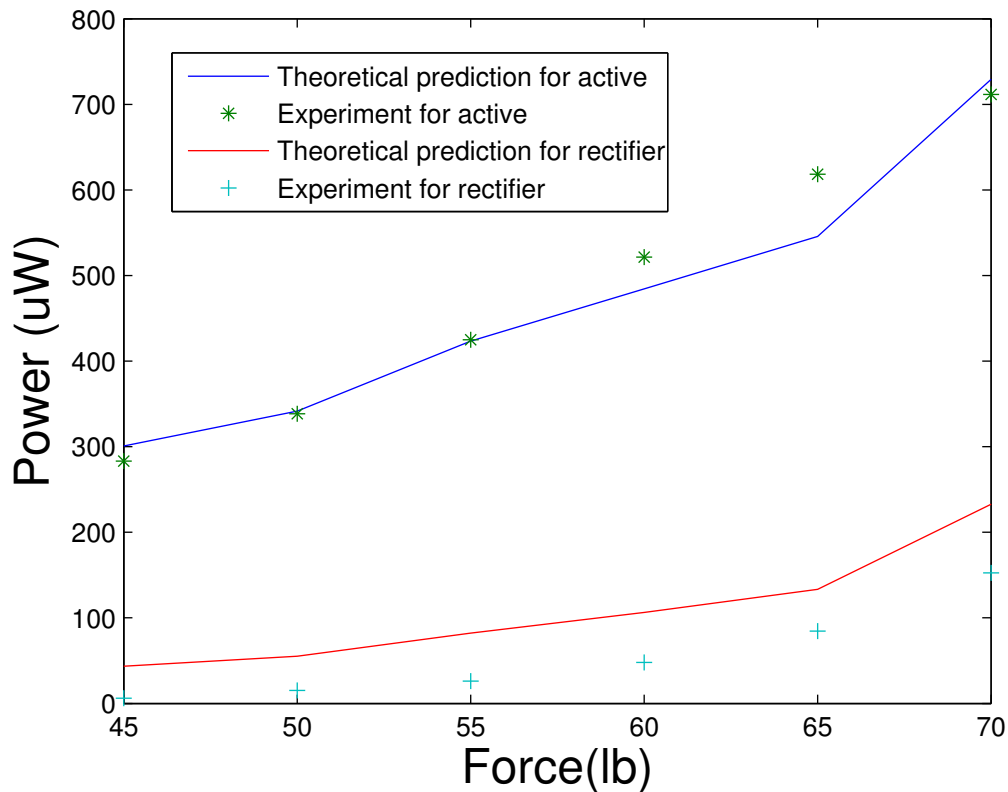


Figure 4.8: Active energy harvesting compared to diode rectifier circuit. Sinusoidal wave is measured force (at 600lbf/V), trapezoid wave is voltage across piezoelectric device.

There is, however, a discrepancy between theoretical predictions and the experimental results for the diode rectifier, as the experimentally harvested energy is lower than the prediction. This is likely because the calculation is based on the ideal diode. In practice the diode will consume some portions of the harvested power. These losses come from the diodes' forward voltage drop, and reverse current leakage.

That fact that active energy harvesting improves the performance much more for a smaller force can be explained as follows. The circuit efficiency is around 90%, therefore according to Equation 3.64 the optimized voltage limit should be 9 times the open circuit voltage. For a smaller force of 45lb the open-circuit voltage is 16V and 37V for the

higher force of 75lb. So for smaller force, the limiting voltage is closer to the optimized condition, therefore the improvement ratio is higher.

4.6 Comparison and conclusion

The diode rectifier circuit is the lower in energy, even under optimized conditions. However, the diode rectifier is the simplest circuit of all and it does not need a sensor. For certain applications the optimized working condition is not necessary, or the piezoelectric device and electrical load is so designed that in the power equilibrium it is close to the optimized condition. An ultra-low cost energy harvesting circuit only made of a few diodes and a capacitor could be realized at a cost of under a few dollars.

Active energy harvesting circuit by far is the most complex circuit, but it has superior performance, potentially better than even the SSHI circuits in harvested power. Furthermore, because the switching mode circuit is used as power stage, it uses high switching frequency, which could dramatically reduce the required inductor size and weight compared to that of SSHI circuits.

Active energy harvesting is also still in development, for fully standalone operation there are engineering challengers. The operation of those systems still needs to be thoroughly understood.

Chapter 5

Quasi-static Electrostrictive Energy Harvesting Theory

Electrostriction is generally defined as a quadratic coupling between strain/stress and electrical field/polarization [57]. The dipoles inside the material line up in the field direction under a DC bias field. Under an AC electrical field and mechanical strain, the phase transition occurs, which results in a change of electrical dipole moment. An electrical charge or current associated with this change is then generated across the electrodes, converting the mechanical energy to electrical energy. Because of the phase transition, the energy harvesting mechanism of the electrostrictive material is fundamentally different from that of the electro-elastomers [58][59], which uses electrostatic force for its energy conversion. Because of their quadratic nature, these materials are inert without electrical excitation. For example, an electrostrictive device does not generate any charge during a process of straining if the voltage across its terminals is zero, which differs from a piezoelectric device. In this sense, active energy harvesting is a mandatory approach if these devices are to be used as an electrical generator. This chapter is a study of active energy harvesting using this non-linear material. We discuss the mechanical and electrical boundary conditions for maximizing the harvested energy density and mechanical-to-electrical coupling of electrostrictive materials. Mathematical models for different energy harvesting approaches were developed under quasistatic assumptions. Harvested energy densities are then determined for representative electrostrictive material properties using these models. Experimentally

using sinusoidal voltage active energy harvesting, a very high energy harvesting density for this material was achieved.

5.1 Electrostrictive materials and devices

The recent development of electrostrictive polymers has generated new opportunities for high-strain actuators. At the current time, the investigation of using electrostrictive polymer for energy harvesting, or mechanical to electrical energy conversion, is beginning to show its potential for this application. Electrostriction can be described as a quadratic coupling between strain and electrical field using Equations 5.1 and 5.2, where the strain S_{ij} and the electric flux density D_m are expressed as independent variables of the electric field intensity $E_{m,n}$ and the stress T_{ij} ,

$$S_{ij} = s_{ijkl}^E T_{ij} + M_{mnij} E_n E_m, \quad (5.1)$$

$$D_m = \varepsilon_{mn} E_n + 2M_{mnij} E_n T_{ij}, \quad (5.2)$$

where s_{ijkl}^E is the elastic compliance under constant field, M_{mnij} is known as the electric-field-related electrostriction coefficient, and ε_{mn} is the linear dielectric permittivity. One observation of the equations reveals that mechanical energy couples with electrical charge only when the electric field is non-zero. Otherwise, Equation 5.2 degrades into a normal dielectric equation.

An isotropic electrostrictive polymer film contracts along the thickness direction and expands along the film direction when an electric field is applied across the

thickness. Assuming that the only nonzero stress is that applied along the length of the film, the constitutive relation then could be simplified as:

$$S = sT + ME^2 \quad (5.3)$$

$$D = \varepsilon E + 2MET \quad (5.4)$$

where:

$$\begin{aligned} E &= E_3, D = D_3, S = S_1, \\ T &= T_1, s = s_{11}^E, M = M_{31}, \\ \varepsilon &= \varepsilon_{33} \end{aligned} \quad (5.5)$$

Because our analysis is based on these simplified relations, we will no longer specify the orientation of parameters and field variables in the following. We also will neglect the effects of dimensional changes of the material on the electrical boundary conditions. For example, a constant voltage applied to an electrostrictive device will be assumed to be equivalent to the constant electric field in the material. As the strains in these materials tend to be less than 5%, deformation contribution therefore is small. This assumption is reasonable and dramatically simplifies the analysis.

5.2 Energy Harvesting Cycle and Boundary Conditions

The mechanical-to-electrical energy harvesting in electrostrictive materials is illustrated by example in the mechanical stress/strain and electric field density/flux density plots shown in Figure 5.1 . Initially, the material shown in part (a) of the figure has no applied stress, then stress is applied and the state travels along path A. The applied stress then is reduced. If the electrical boundary conditions have changed at the apex of

path A, the contraction path will not follow path A but path B. Both in the mechanical and electrical planes, the material state traverses a closed loop. In the mechanical plane (a) the rotation is counterclockwise, and in the electrical plane (b) in the figure the rotation is clockwise. This rotation designates that the net energy flow is from the mechanical terminals to the electrical. The areas enclosed in the loops of the mechanical and electrical planes are both equal to the converted energy density in units of J/m^3 .

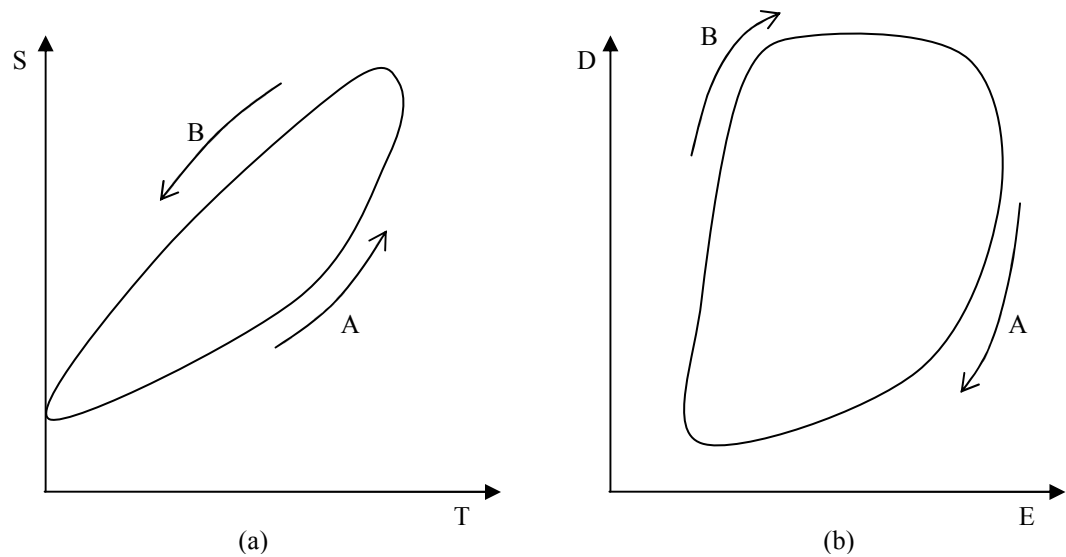


Figure 5.1: Type Caption Here

For quasistatic mechanical-to-electrical energy harvesting, one can apply various electrical boundary conditions during the stress variation cycle to break the elastic symmetry of stretching and contraction of the electrostrictive polymer, and thereby harvest energy. In order to maximize the energy harvesting density, the boundary conditions have to be designed so that the area enclosed in the loop is as large as possible

without exceeding the limitations of the polymer material (e.g., maximum stress, breakdown field). One approach is to adjust the mechanical boundary conditions through the design of a mechanical transformer—such as a cantilever, bimorph structure, or hydraulic coupler—to modify the mechanical stresses applied to the material in order to create a better match with the material’s elastic properties. Another approach is to control the electrical boundary conditions in certain relations with the mechanical force. Ideally the energy harvesting cycle consists of the largest possible loop, bounded only by the limitations of the material. However, actual implementation of the optimal energy harvesting cycle in an energy harvesting circuit may be difficult to achieve. In the following, we will analyze electrical boundary conditions that can be applied to the device fairly easily with power electronic circuitry. The concept of the coupling factor, as defined in the IEEE standard [38] for piezoelectric materials, is useful as a figure of merit for energy harvesting, and is given below

$$k^2 = \frac{W_1}{W_1 + W_2}, \quad (5.6)$$

where area $W_1 + W_2$ is the input mechanical energy density, and area W_1 is the output electrical energy density. The coupling factor often is associated with a specific set of electrical boundary conditions, as will be discussed in the following. In this work we shall use the general definition above and consider several different cases of electrical boundary conditions. The mechanical excitation in each case will be the same: the application of stress is from zero to a maximum value T_{\max} , which then returns to zero.

5.2.1 Coupling Factor Determined from Linearized Model of Electrostriction

For many transducer and actuator applications, electrostrictive materials often are exposed to a large direct current (DC) bias field and a smaller alternating current (AC) perturbation. Under these conditions, local linearization, based on Taylor expansion, is often used to simplify the quadratic nature of electrostriction, which then takes the same form as the piezoelectric equations. Therefore, an equivalent piezoelectric constant as a function of the bias field can be determined for the electrostrictive material. The linearization of the constitutive relation defined in Equation 5.3 and Equation 5.4 about its bias values E_0 and T_0 can be written as:

$$\begin{aligned} S &\approx S_0 + s(T - T_0) + 2ME_0(E - E_0), \\ D &\approx D_0 + (\varepsilon + 2MT_0)(E - E_0) + 2ME_0(T - T_0) \end{aligned} \quad (5.7)$$

Using S_0 , D_0 , T_0 and E_0 as the equilibrium points and the deviations from those points as the (linearized) variables, the equivalent piezoelectric constant is then given by:

$$d' = 2ME_0 \quad (5.8)$$

and the equivalent dielectric constant is given by:

$$\varepsilon' = \varepsilon + 2MT_0 \quad (5.9)$$

Equation 5.8 indicates the equivalent piezoelectric constant is nontrivial only when a certain bias field E_0 is applied. The coupling coefficient, or the ratio of electrical energy output to mechanical energy input, for the linearized system then can be calculated using the standard quasistatic coupling factor for piezoelectric materials as:

$$k^2 = \frac{d'^2}{\varepsilon' s} = \frac{4M^2 E_0^2}{s(\varepsilon + 2MT_0)} \quad (5.10)$$

However, in order to maximize the energy conversion, large variations in applied stress and electric field are required. Hence, the linearized model may provide inaccurate or misleading conclusions as to how to achieve the highest harvesting energy density and harvesting efficiency. In energy harvesting applications the quadratic model, therefore, will provide a more accurate understanding; hence, the following analysis will be based upon the electrostrictive equations provided in Equations 5.3 and 5.4

5.2.2 Energy Harvesting Cycle #1: Constant Field and Open-Circuit Electrical Boundary Conditions

The standard coupling factor expressed above for piezoelectric materials is based upon electrical boundary conditions in which the device is electrically short circuited as stress is applied, and open circuited as the stress is removed. In the case of electrostrictive materials, such boundary conditions would not result in energy harvesting. However, a similar excitation that would generate electrical energy would consist of a constant, nonzero electric field applied to the device as stress is applied; then open-circuit conditions as the stress is removed. This electromechanical cycle is shown in Figure 5.2 . The material is stress free at state 1 of the cycle, and an electric field E_0 is applied and kept constant as the stress is increased to T_{\max} , ending in state2. The electrostrictive device is then open circuited when the stress is removed, ending in state 3. From state 3 the electric field E_0 is re-established in the material, returning to the original state 1. The

total mechanical input energy density available for the energy harvesting for such a cycle

can be shown to be $W_1 + W_2 = \frac{1}{2} s T_{\max}^2$, and the energy W_1 can be calculated as follows.

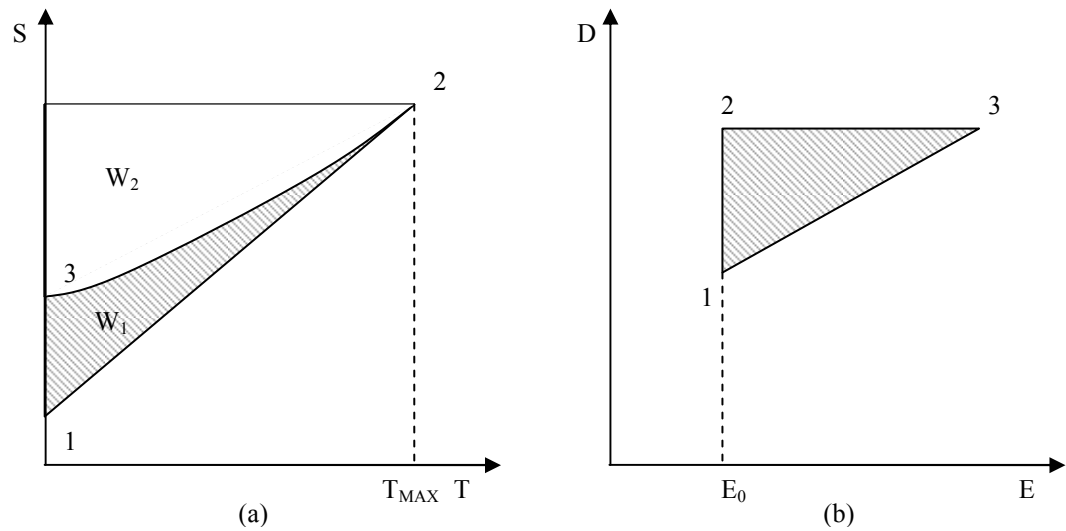


Figure 5.2: Energy harvesting cycle under constant field 1-2 and open circuit 2-3 electrical boundary conditions.

As the material is in open-circuit condition from state 2 to 3, the electric flux density is constant and is given by

$$D = \varepsilon E_0 + 2ME_0 T_{\max} \quad (5.11)$$

the electric field intensity as the stress is removed, therefore, is given by:

$$E = E_0 \frac{\varepsilon + 2MT_{\max}}{\varepsilon + 2MT} \quad (5.12)$$

this field intensity reaches its peak value E_p when the applied stress becomes zero, or:

$$E_p = E_0 \left(1 + \frac{2MT_{\max}}{\varepsilon} \right) = E_0 (1 + \gamma) \quad (5.13)$$

where γ corresponds to the relative change in dielectric constant due to applied stress and is defined as follows:

$$\gamma = \frac{2MT_{\max}}{\varepsilon} \quad (5.14)$$

For existing electrostrictive materials, γ is usually less than 1. Now:

$$\begin{aligned} W_2 &= -\int_2^3 TdS = \frac{1}{2} sT_{\max}^2 - 2M^2T_{\max}^2 E_0^2 \frac{1}{\varepsilon} \\ &= \frac{1}{2} (sT_{\max}^2 - \varepsilon\gamma^2 E_0^2) \end{aligned} \quad (5.15)$$

The harvested energy is corresponding to the area $W_1 = \frac{1}{2} sT_{\max}^2 - W_2$, and is calculated as

$$W_1 = 2 \frac{E_0^2}{\varepsilon} MT_{\max}^2 \quad (5.16)$$

Therefore, the coupling factor is given by: Equation 5.17

$$k^2 = \frac{4M^2 E_0^2}{s\varepsilon} \quad (5.17)$$

The above result is the same as the linearized equivalent coupling of Equation 5.10, but we should notice that the electrical field E_0 in Equation 5.17 is the lowest field during the cycle, but for Equation 5.10 E_0 is the middle or average field of the cycle.

If E_0 is so chosen that the peak electric field intensity is the maximum allowable due to material constraints, E_{\max} , the maximum harvesting energy density is given by:

$$W_{1\max} = \frac{\gamma}{(1+\gamma)^2} MT_{\max} E_{\max}^2 \quad (5.18)$$

The coupling factor associated with this energy density is given by:

$$k^2 = \frac{4M^2 E_{\max}^2}{(1 + \gamma)^2 s \varepsilon} \quad (5.19)$$

5.2.3 Energy Harvesting Cycle #2: Constant-Field Boundary Conditions During stressing and Unstressing of Material

Another possible method of imposing electrical boundary conditions is to keep the electric field constant as the material is stressed, then change the field to a different value that is kept constant as the stress is removed. Such a cycle is shown in Figure 5.3

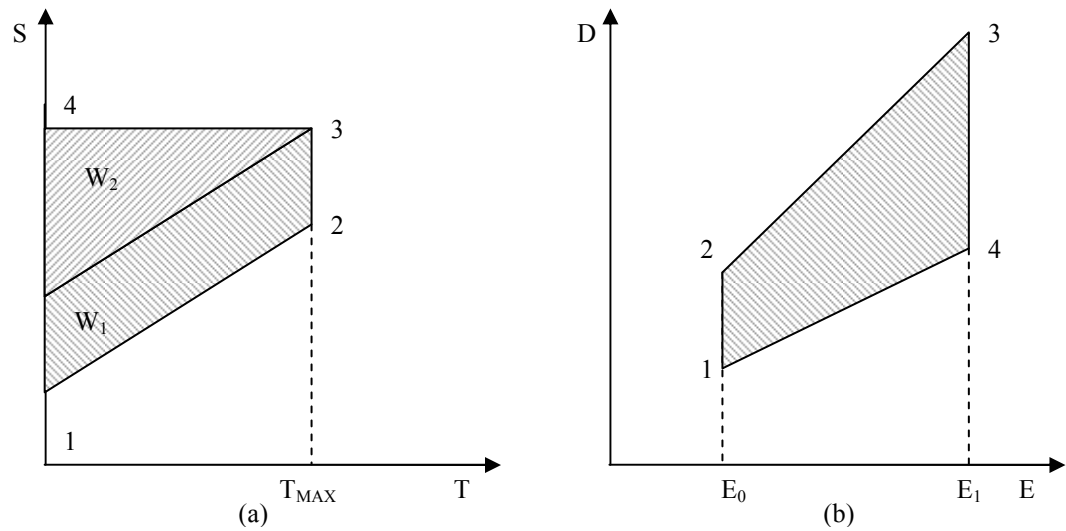


Figure 5.3: Energy harvesting cycle under constant electrical field conditions as the material is stressed and unstressed.

As in Section 5.2.2 , a constant electric field E_0 exists from state 1 to state 2 as the stress is increased to T_{\max} . From state 2 to state 3 the electric field is increased from E_0 to

E_1 , then kept constant until the stress is reduced from T_{\max} to 0 from state 3 to state 4. At zero stress the electric field is reduced to E_0 , returning to state 1. In the dielectric-field plot, paths 1–4 and 2–3 are not parallel, which is due to the stress dependence of the dielectric constant. The converted energy can be shown to be:

$$W_1 = T_{\max} M (E_1^2 - E_0^2) \quad (5.20)$$

Since the input energy density $W_2 = \frac{1}{2} s T_{\max}^2$, the coupling factor is given by:

$$k^2 = \frac{M (E_1^2 - E_0^2)}{\frac{1}{2} s T_{\max}^2 + M (E_1^2 - E_0^2)} \quad (5.21)$$

The maximum energy harvesting density and coupling occurs when E_0 is set to be zero and E_1 is set to E_{\max} . Then,

$$W_{1\max} = T_{\max} M E_{\max}^2, \quad (5.22)$$

and its coupling factor is

$$k^2 = \frac{M E_{\max}^2}{\frac{1}{2} s T_{\max}^2 + M E_{\max}^2} \quad (5.23)$$

5.2.4 Energy Harvesting Cycle #3: Open-Circuit Boundary Conditions During Stressing and Unstressing of Material

Instead of keeping constant field, open-circuit electrical boundary conditions could be applied as the stress is applied and removed. This energy conversion cycle is shown in Figure 5.4 .

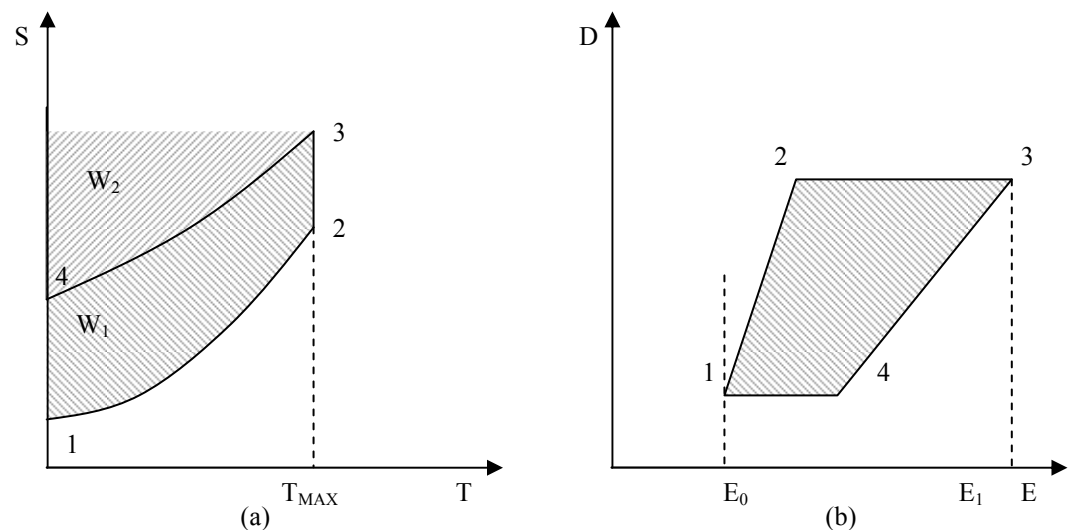


Figure 5.4: Energy harvesting cycle under open-circuit conditions as stress is applied and removed.

From state 1 to state 2 and state 3 to state 4, the electric field changes as the stress changes. From state 2 to state 3 and from state 4 to state 1, the electric field is changed through the electrical interface. We define the field at state 1 to be E_0 and the field at state 3 to be E_3 .

The energy harvesting density then is:

$$W_1 = \frac{MT_{\max}}{1+\gamma} (E_3^2 - E_0^2) \quad (5.24)$$

And its associated coupling factor is given by:

$$k^2 = \frac{(1+\gamma)M(E_3^2 - E_0^2)}{\frac{1}{2}(1+\gamma)^2 sT_{\max} + (1+\gamma)(E_3^2 - E_0^2)M - \frac{2}{\varepsilon}M^2T_{\max}E_3^2} \quad (5.25)$$

The maximum harvesting density then occurs when $E_0 = 0$ and $E_3 = E_{\max}$.

$$W_{1\max} = \frac{MT_{\max}E_{\max}^2}{1+\gamma} \quad (5.26)$$

The coupling factor under these conditions is given by:

$$k^2 = \frac{(1+\gamma)ME_{\max}^2}{\frac{1}{2}(1+\gamma)^2 sT_{\max} + ME_{\max}^2} \quad (5.27)$$

5.2.5 Energy Harvesting Cycle #4: Passive Diode Circuit for Energy Harvesting

A circuit that has been proposed for electrostatic-based energy harvesting [10] also can be used with electrostrictive materials and is shown in Figure 5.5. The circuit uses high voltage diodes as passive switching devices. The main advantage of this circuit design is simplicity.

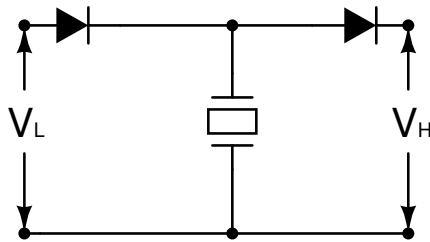


Figure 5.5: Passive diode circuit for energy harvesting.

Its energy harvesting cycle is shown in Figure 5.6 .

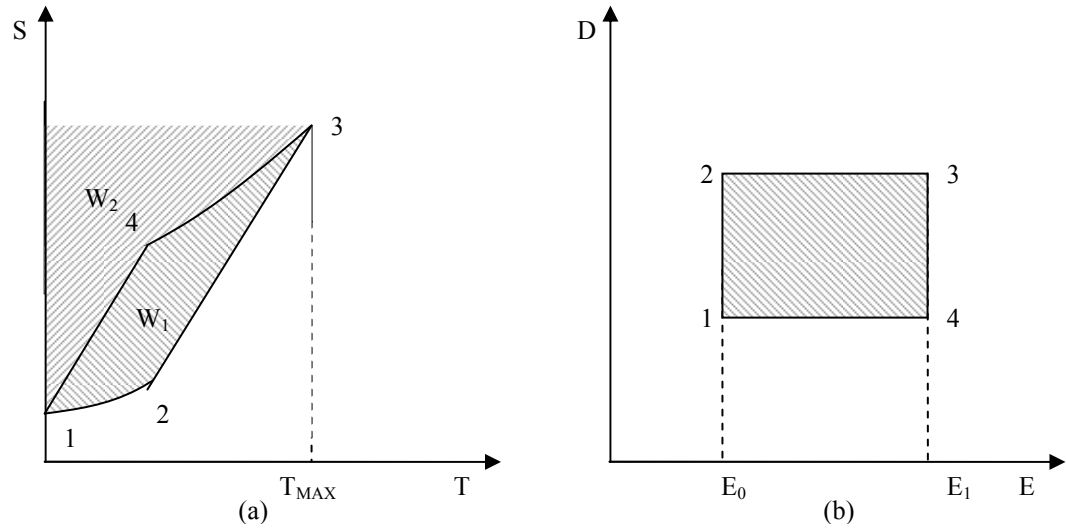


Figure 5.6: Energy harvesting cycle for passive diode circuit.

However, as the circuit is passive, the voltage change across the device occurs only due to the electrostrictive effect. As a result, it can be shown that the voltages V_L and V_H are constrained by the following condition:

$$V_L < V_H < \gamma V_L \quad (5.28)$$

These constraints severely impair the energy harvesting density and coupling factor when γ is small.

The harvesting energy density in this system is given by:

$$W_1 = \varepsilon (E_H - E_L) ((1 + \gamma) E_L - E_H) \quad (5.29)$$

where E_L and E_H are the electric fields associated with V_L and V_H , respectively. The coupling factor is given by:

$$k^2 = \frac{2\varepsilon(E_H - E_L)((1 + \gamma)E_L - E_H)}{sT_{\max}^2 - \varepsilon(E_H - E_L)^2} \quad (5.30)$$

The energy conversion density and coupling is maximized when:

$$E_L = \frac{2 + \gamma}{2(1 + \gamma)} E_H \quad (5.31)$$

If we set $H_H = E_{\max}$, density is given by:

$$W_{1\max} = \frac{\gamma}{2(1 + \gamma)} MT_{\max} E_{\max}^2 \quad (5.32)$$

and its associated coupling factor is:

$$k^2 = \frac{2(1 + \gamma)\gamma ME_{\max}^2}{2(1 + \gamma)^2 sT_{\max} + ME_{\max}^2 \gamma} \quad (5.33)$$

5.2.6 Sinusoidal excitation

In this section we analyze the case where the mechanical and electrical excitations both consist of constant components and sinusoidal-varying components of the same frequency, as shown in the following

$$\begin{aligned} E &= E_0 \sin(\omega t) + E_1, \\ T &= T_0 \sin(\omega t + \varphi) + T_1 \end{aligned} \quad (5.34)$$

The current density is the derivative of flux density with respect of time, and is calculated as

$$i = \omega \varepsilon E_0 \cos(\omega t) + 2\omega M (E_0 T_0 (\cos(2\omega t + \varphi)) + E_0 T_1 \cos(\omega t) + E_1 T_0 \cos(\omega t + \varphi)) \quad (5.35)$$

In order to simplify the calculation, we choose $\sin(n\omega t)$ and $\cos(m\omega t)$ as orthogonal bases of a Hilbert space, where m and n are integers, and define the inner product as,

$$\langle a, b \rangle = \int_0^T a \times b dt \quad (5.36)$$

we have $\langle a, b \rangle \neq 0$, only when $a = b$, so the only term that contributes to the electrical power is $E_1 T_0 \cos(\omega t + \varphi)$. The power density is therefore

$$P = \frac{1}{T} \int_0^T E i dt = \frac{2\omega M E_0 E_1 T}{T} \int_0^T \sin(\omega t)_0 \cos(\omega t + \varphi) = \omega M E_0 E_1 T \sin \varphi \quad (5.37)$$

The energy harvesting density under these conditions is therefore:

$$W_1 = 2\pi M E_0 E_1 T_0 \sin \varphi \quad (5.38)$$

Assuming electric field and stress are constrained between zero and their maximum values $E_0 = E_1 = \frac{1}{2} E_{\max}$ and $T_1 = \frac{1}{2} T_{\max}$, this energy harvesting density will be

maximized when $\varphi = -\frac{\pi}{2}$, which is

$$W_{1\max} = \frac{\pi}{4} M E_{\max}^2 T_{\max} \quad (5.39)$$

5.3 Comparison of Different Boundary Conditions

Inspection of the expressions for maximum energy harvesting density for different electrical boundary conditions reveals that they can be compared directly through a normalization process based upon maximum applied stress and electric field

$$W_{1\max}^* = \frac{W_{1\max}}{MT_{\max} E_{\max}^2} \quad (5.40)$$

With this definition, the normalized value of energy harvesting density becomes solely a function of the term γ . Figure 5.7 presents this comparison over a range of γ from 0 to 1, which is well over the maximum limit achievable by existing electrostrictive materials. Inspection of Figure 5.7 reveals that the constant-field condition has the best energy harvesting density, with the open-circuit condition being comparable at low levels of γ . The constant-field-and open- circuit condition and the passive-diode-circuit condition increase with γ , but they fall well below that of the constant-field condition over the range of γ presented here.

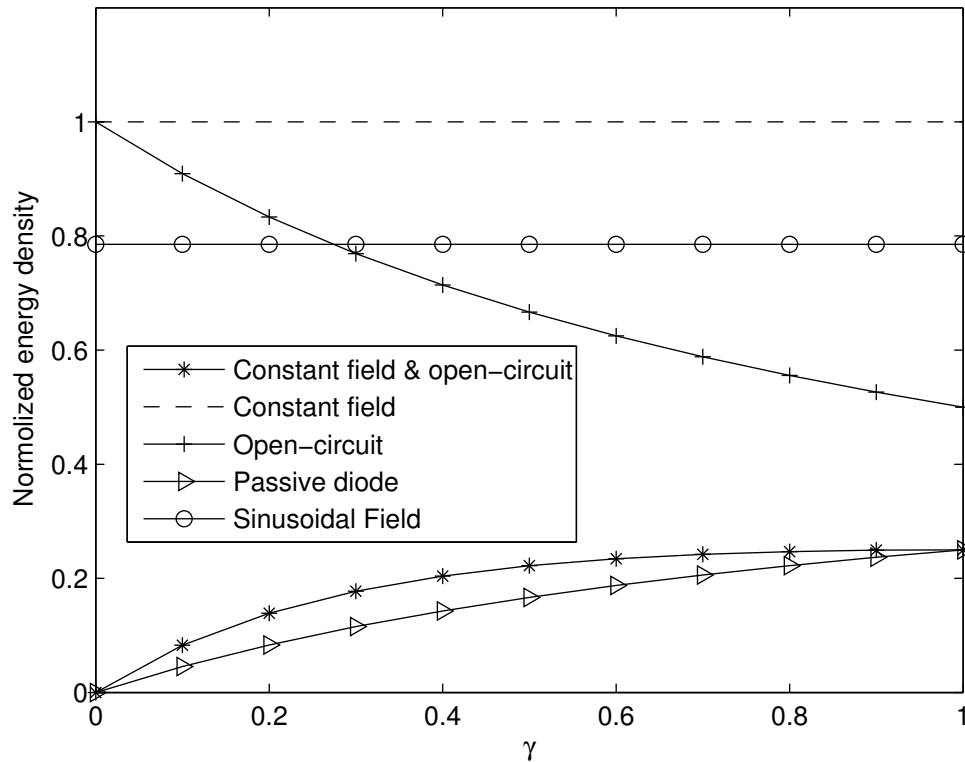


Figure 5.7: Theoretical prediction of Electrostrictive energy harvesting under different harvesting circuits

In order to compare the effectiveness of the above electrical boundary conditions, electrostrictive material properties based on experimental data were assigned to the calculation, along with allowable electric field and stress values for safe operation. Representative material parameters and limitations of two electrostrictive polymers, PVDF based terpolymer and a polyurethane, are provided in Table 5.1 [7], [11].

Table 5.1: Electrostrictive Material Parameters and Their Operation Limitations.

Electrostrictive Material	ϵ_{33}	M_{13} (V/m) ⁻²	S_{11} (Pa ⁻¹)	E_{\max} (MV/m)	T_{\max} (MPa)	γ
Terpolymer	$50\epsilon_0$	2×10^{-18}	2.5×10^{-9}	150	20	0.181
Polyurethane	$7.5\epsilon_0$	3.6×10^{-18}	5.9×10^{-9}	175	2	0.217

Resulting energy harvesting densities (the maximum energy density harvested $W_{1\max}$) and their associated coupling factors are provided in Table 5.2 and Table 5.3 below. It can be seen that, even for the same polymer, different electric boundary conditions can result in quite different values of harvested energy.

Table 5.2: Maximum Energy Harvesting Density and Associated Coupling Factor for Various Electrical Boundary Conditions, Terpolymer Material.

Electrical boundary conditions	$W_{1\max}(\text{J}/\text{cm}^3)$	k^2
Constant field & open-circuit	0.117	0.233
Constant field	0.900	0.643
Open-circuit	0.762	0.665
Passive diode	0.069	0.130
Sinusoidal field	0.706	N/A

Table 5.3: Maximum Energy Harvesting Density and Associated Coupling Factor for Various Electrical Boundary Conditions, Polyurethane Material.

Electrical boundary conditions	$W_{1\max}(\text{J}/\text{cm}^3)$	k^2
Constant field & open-circuit	0.032	0.283
Constant field	0.221	0.651
Open-circuit	0.181	0.679
Passive diode	0.020	0.156
Sinusoid	0.173	N/A

So far, electrostrictive materials have been theoretically shown to possess significant electric energy harvesting densities. Of the electrical boundary conditions investigated, the best harvested energy density occurs when the electric field in the material is increased from zero to its maximum value at maximum stress, then returned to zero at minimum stress. In the case of a small value of γ , a similar set of boundary conditions in which the device is open circuited during the stressing and unstressing of the material provides similar energy harvesting densities. Boundary conditions related to

the standard definition of coupling factor, and to a passive diode circuit, are shown to provide relatively low energy harvesting density over the range of γ achievable by existing electrostrictive materials. While sinusoidal voltage excitation does not perform best, its smooth transition of voltage and easy implementation might be advantageous for certain applications and when dielectric loss are not considered. In the next section we will use this approach as a demonstration.

Chapter 6

Quasi-static Electrostrictive Energy Harvesting Experiment

6.1 Experimental Setup

An experiment was performed to demonstrate the very high energy harvesting density of electrostrictive polymer material using an active approach. Because only high voltages (up to 1000V) and small currents (tens micro-amperes) are generated by available samples, we did not use a power electronic inverter as a driving circuit. Instead, a commercially available high-voltage amplifier is used. Its current and voltage are closely monitored to calculate the power flow between the electrostrictive device and the voltage amplifier.

6.1.1 MECHANICAL SYSTEM AND EXPERIMENTAL SETUP

The mechanical driver of the energy harvesting system consisted of a loudspeaker (6 Ω , Aiwa) driven by an 300W audio amplifier (PM175, Carver) with a load cell (ELPM-T3E-1KL, Entran Device Inc) to measure the force applied on the polymer film. One end of the electrostrictive thin film was attached to the loudspeaker's voice coil, and the other end is clamped to a fixed sample holder. The motion of the voice coil applies tensile stress to the sample. Its displacement is measured by a photonic sensor (MTI 2000, MTI Instruments). Using the transverse strain and the stress calculated from load cell and photonic sensor, the material's compliance can be calculated by

$$S_{11} = \frac{\text{Strain}}{\text{stress}} = \frac{S_1}{T_1} \quad (6.1)$$

The electrical boundary condition is controlled by the high voltage amplifier (Model 610D, Trek Inc), which is capable of providing voltage and current up to 10 kV and 2mA, respectively. The monitoring signals for the applied current or voltage are given through analog output ports of the amplifier. The mechanical and electrical excitation is controlled by a signal conditioning system (SC-2345, National Instruments). The Labview software environment is used for programming the control and data acquisition of the active energy harvesting process. This experimental setup is shown in Figure 6.1

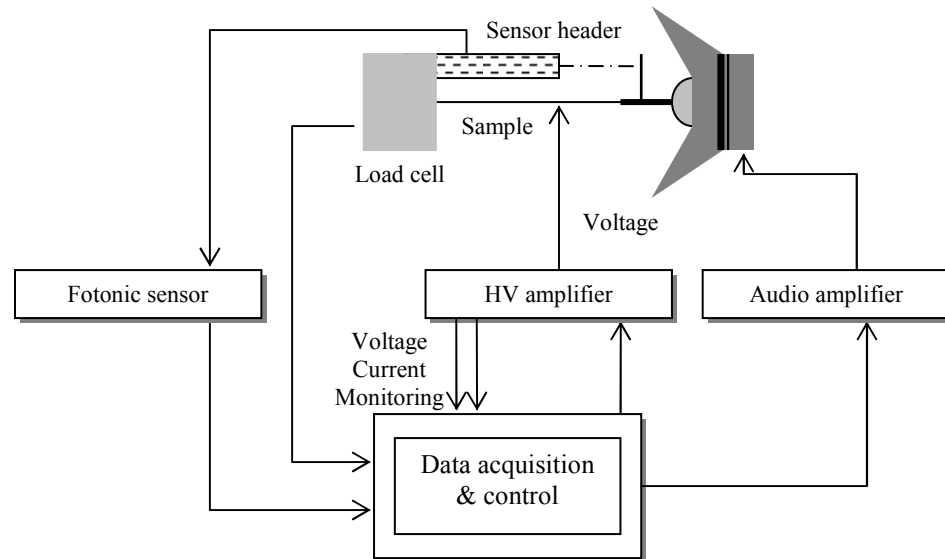


Figure 6.1: Experiment setup for electrostrictive materials

The electrostrictive terpolymer film (vinylidene fluoride-trifluoroethylene) dimensions of 23.04mm x 7.72mm x 13 μ m, is prepared by a solution cast method. It's material properties are given in Table 5.1. To prevent the breakage of the aluminum electrode during the stretching process, a thin polypyrrole conducting polymer electrode is deposited on the both sides of the film before the evaporation of aluminum electrodes of 20 nm in thickness. The presence of aluminum greatly enhances the conductivity of the electrodes.

To measure the energy harvested in the experiment, a Labview program is used to measure the voltage and current of the sample simultaneously. Then the product of current and voltage yields the instantaneous power. We digitally integrate the current as a representation of charge generated during the mechanical cycles. Also, the integration of the instantaneous power during for one second gives us the generated power.

6.1.2 Experiment and results

All dielectric materials have losses that are associated with the relaxation behavior of the dipoles when an AC voltage is applied. This energy is dissipated as heat when electrostrictive polymers are used as an energy harvesting material. In the experiment, we first determine the loss as a function of frequency, applied AC, and DC bias field. These losses were then subtracted from ideal lossless models and compared to the experimental results.

6.1.2.1 Determined the loss

The electrostrictive polymer sample is fixed on both ends to sample holders so the mechanical influence is kept to a minimum, and then an AC voltage is applied using a high voltage amplifier. The input current and voltage is closely monitored to calculate the power loss by integrating the product of current and voltage. The results are shown in Figure 6.2.

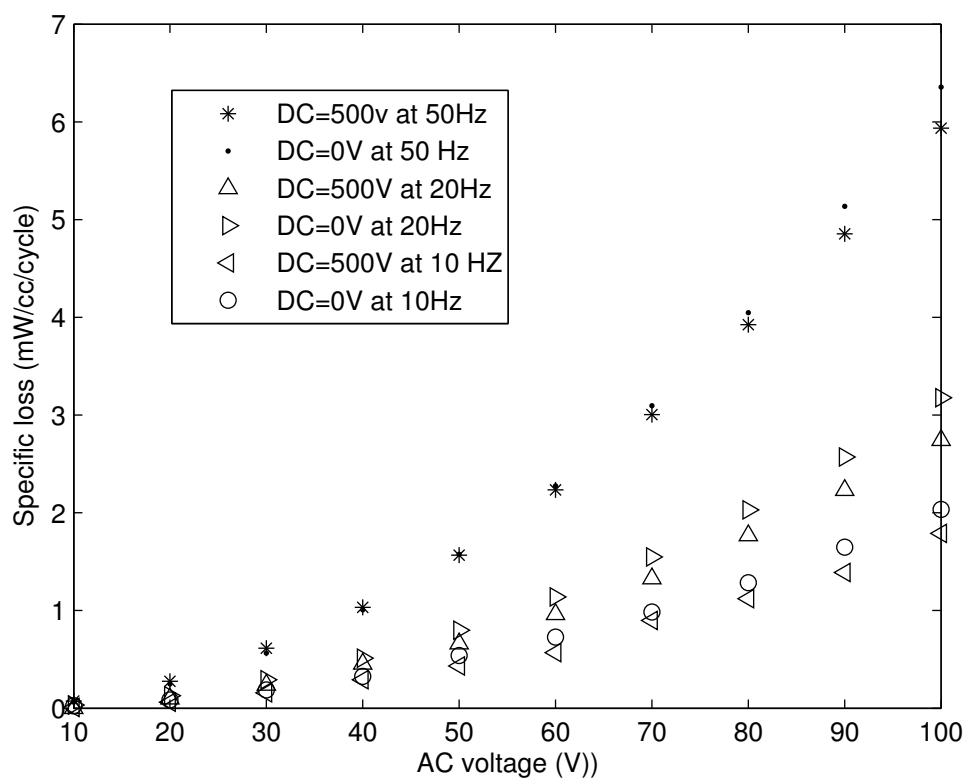


Figure 6.2: Power loss under different electrical excitation under a the fixed strain mechanical boundary condition.

The data shown here is the loss energy density during one cycle. The loss is not only a function of applied AC voltage and frequency, but also depends on the DC bias field. For the same AC voltage excitation, as the DC bias field increases, the loss decreases. For a DC bias voltage of 500V, we fit the experimental data to Equation 6.2 using the least square curve fitting method.

$$P_{loss} = AE^m f^n \quad (6.2)$$

Where A, m and n is determined to be $A = 5.3 \times 10^{-2}$, $m = 1.8$, $n = 0.84$, and E is electric field and f is the frequency. The curve fitting results are shown in Figure 6.3. The estimation of the losses for frequency and amplitude that does not coincide with known measurement is then based on the curve fitting function of Equation 6.2.

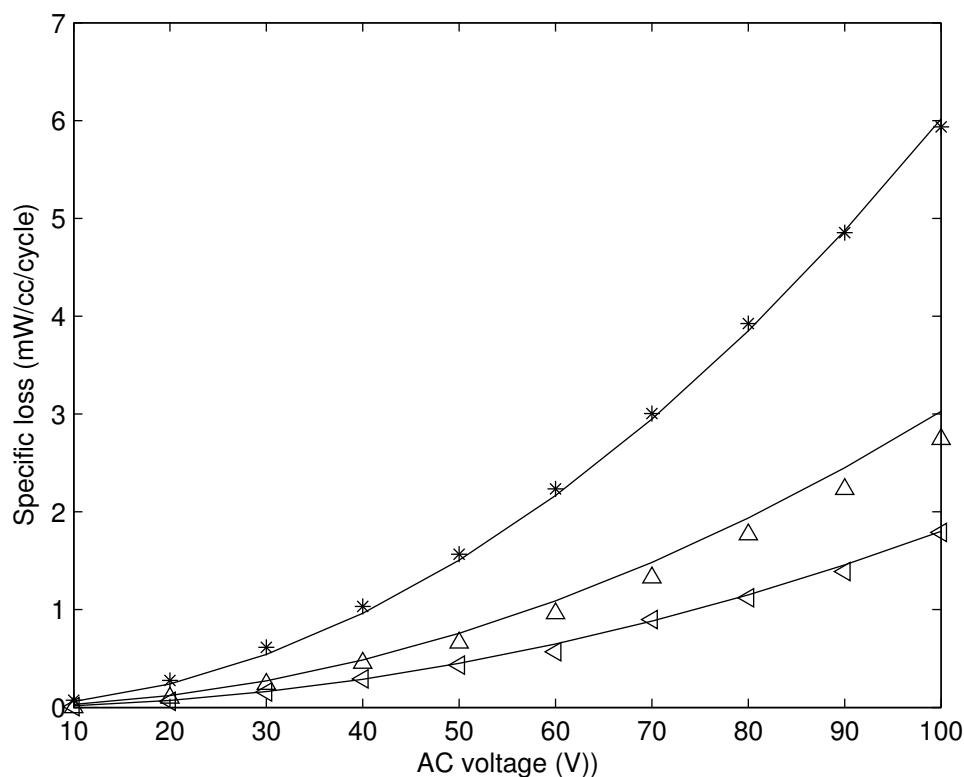


Figure 6.3: Cure fitting of loss measurement data to Equation 6.2

6.1.2.2 Energy harvesting

Energy harvesting was then performed by applying sinusoidal mechanical longitudinal stress to the sample, with a resulting maximum strain of 0.7%. The phase and amplitude of applied electrical AC voltage and DC voltage to the sample is manually controlled through the Labview interface. The phase is relative to the signal that is fed into the audio amplifier. We found there is a phase shift of 65 degrees between the signal feed into audio amplifier and the actual force exerted on the sample. This phase shift is due the dynamics of the audio amplifier and the speaker.

Figure 6.4 is a plot of flux density or charge density vs. electrical field during one energy harvesting cycle of the experiment. The shape of the closed curve is similar to the hysteresis loop often seen in dielectric experiments. However, the loop in this energy harvesting experiment rotates in the reverse direction, indicating an energy gain instead of loss. The enclosed area in this figure corresponds quantitatively to the converted electric energy during one cycle.

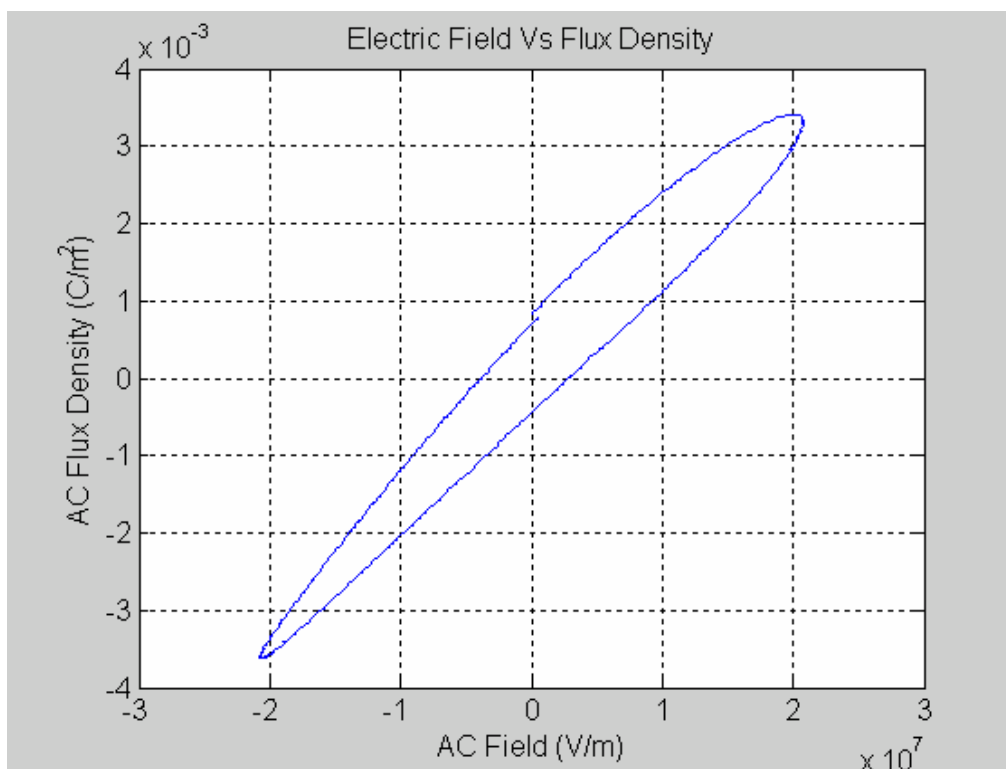


Figure 6.4: The energy harvesting cycle of electrical field and flux density.

The mechanical stress and strain loop is shown in Figure 6.5. The flatness of the curve at low stress occurs when the film is totally relaxed, due to the nature of the experimental setup. With the DC offset of the strain or stress being subtracted, the reference point or origin of the strain or stress in the figure is the average value so the

negative stress value does not correspond to compressive strain or stress but zero stress.

The enclosed area of the loop represents the input mechanical energy of one cycle.

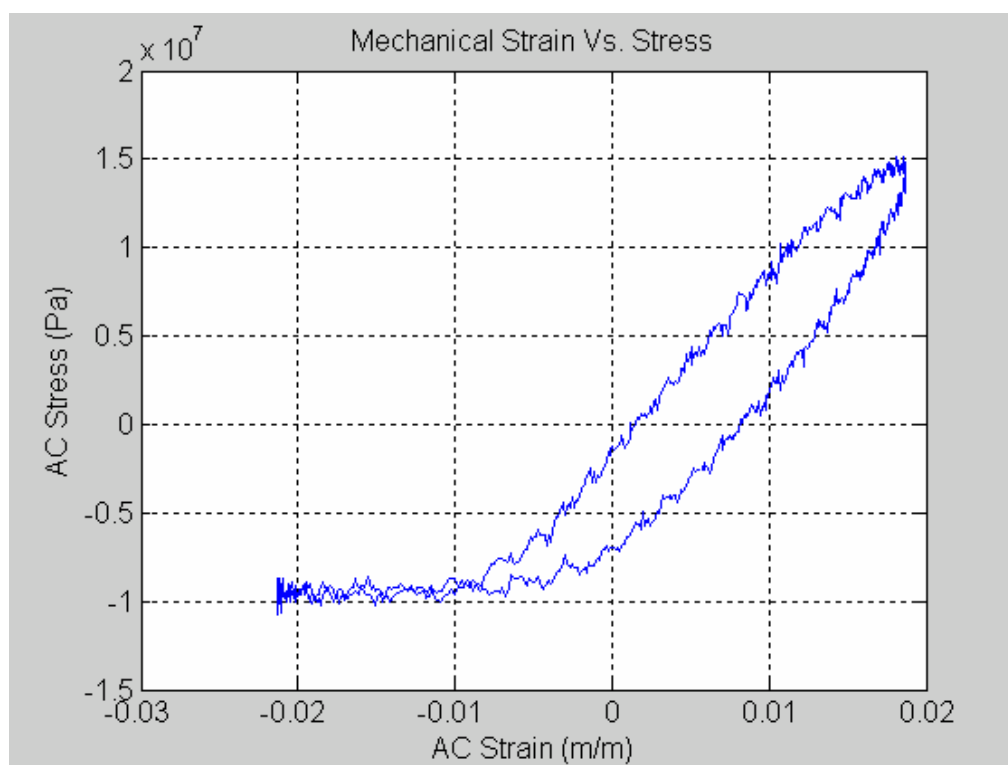


Figure 6.5: Strain stress plot of electrostrictive energy harvesting

The energy harvesting experiment is conducted with 0.7% maximum strain, and a 500V DC bias voltage is applied to the film. We vary the amplitude and phase of the AC voltage at a frequency of 1 Hz. The average power flow into the device is plotted in Figure 6.6.

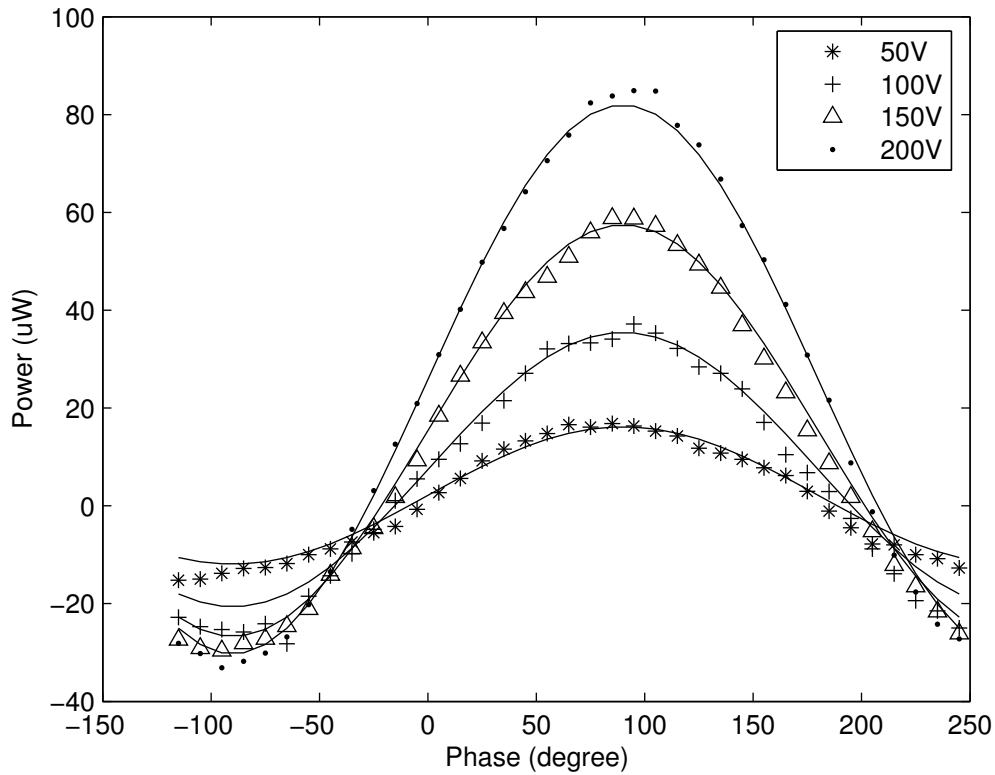


Figure 6.6: Theoretical and experimental results, in which the solid lines are theoretical prediction

In the figure, negative power represents harvested power, while positive power is the electrical input power when the electrostrictive acts as a mechanical actuator. The phase angle is the voltage relative to the mechanical force. When the phase is -90 degrees, the harvested power reaches its maximum or negative minimum in the figure. We have theoretically predicted the active energy harvesting using sinusoid voltage control in Equation 5.38. Now we include the energy loss measured in previous section, The harvested energy is then presented in Equation 6.3

$$W_1 = 2\pi M E_0 E_1 T_0 \sin \varphi - A E_0^{1.8} f^{0.84} \quad (6.3)$$

This theoretical prediction is also plotted in the figure in the solid lines in comparison to the experimental data points.

The voltage and mechanical force waveforms of the experiment at this optimized condition are shown in Figure 6.7

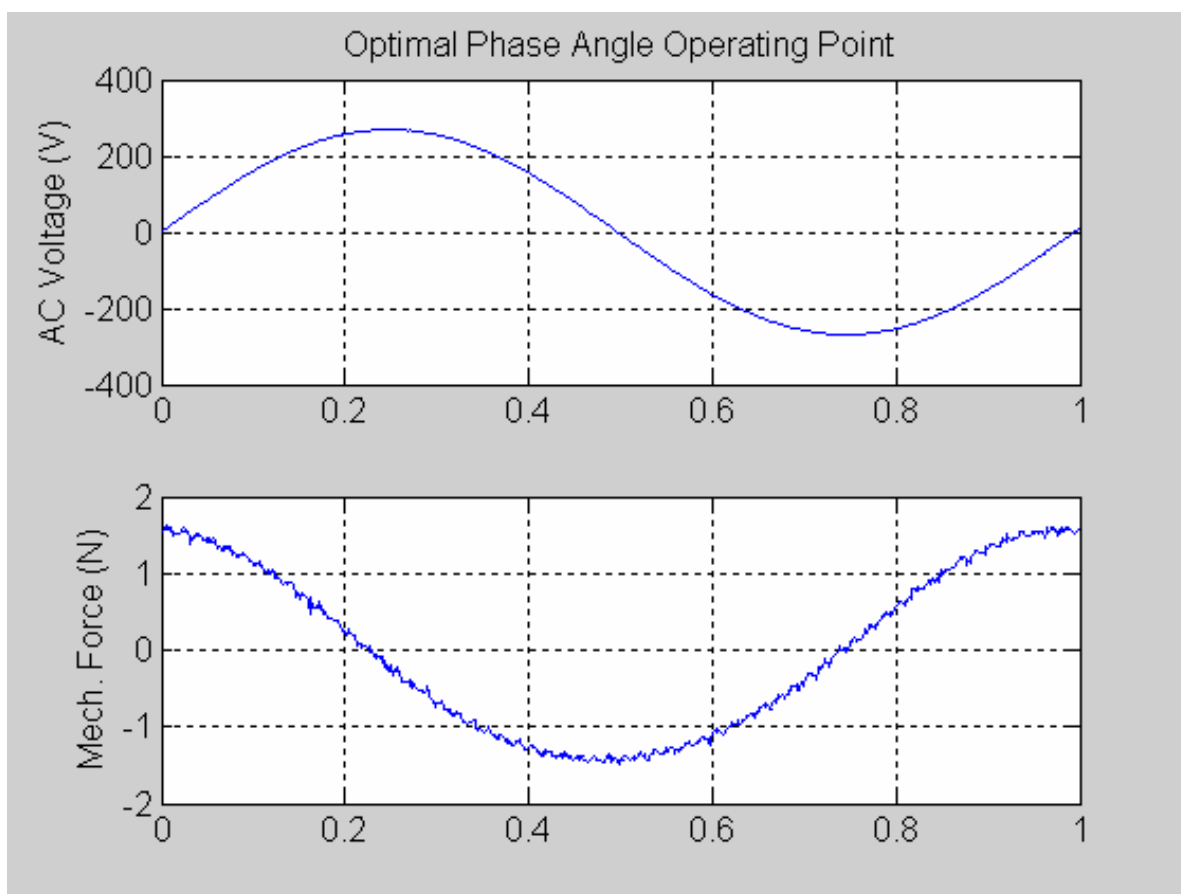


Figure 6.7: Mechanical force and voltage wave on the sample during active energy harvesting experiment. (For both channels AC coupling was used in data acquisition)

The experimental data of the voltage and force also indicate the optimized phase condition, that the voltage lead the mechanical force by 90 degrees. The Fourier transformation of the voltage and current wave of the energy harvesting under optimized conditions is given in Figure 6.8

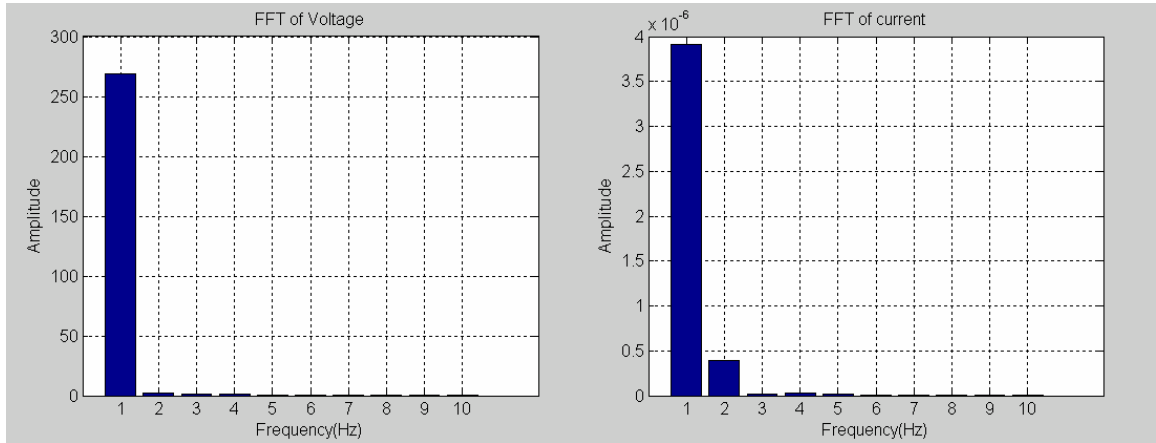


Figure 6.8: Frequency domain of current and voltage wave during active energy harvesting, only 0~10 Hz is shown in figure

It is interesting to note in the above figure that, while the voltage is almost purely sinusoidal at 1 Hz, the current has a noticeable component at a harmonic frequency of 2 Hz. This is due to the non-linear effect of the electrostrictive material. According to Equation 5.35, the magnitude of this current is

$$|i|_{double} = 2\omega ME_0 T_0 \quad (6.4)$$

From the above equation the electrostrictive coupling coefficient M could therefore be calculated from the AC electrical field and mechanical stress as $2.2 \times 10^{-18} (V/m)^{-2}$, which is close to the known number tabulated in Table 5.1. The existence of the harmonic current is due to the inherently non-linear characteristic of electrostrictive material.

Finally, the results of the electrostrictive energy harvesting experimental are compared to the other energy harvesting materials in Table 6.1

Table 6.1: Electrostrictive energy harvesting experimental results comparison

Material	Coupling efficiencies	Harvested energy density (mJ/cc)
PVDF*	0.5 [60]	0.044
PZT*	1.5-5	2.1
Electrostrictive (PVDF-TrFE)**	10	39.4

The active energy harvesting has achieved an extremely high energy density and coupling coefficient compared to conventional materials. The fact that the electrostrictive polymer has a superior electromechanical coupling is fundamental to the resulting good energy harvesting results. Active energy harvesting, used to excite the material at optimized electrical boundary conditions has liberated the potential of this material. The experiment, however, used a high voltage amplifier as driving circuit, therefore the harvested energy was not converted to usable format. Instead it is dissipated by the amplifier. A multilayer structure electrostrictive device with much higher output current and lower voltage requirement is needed for practical applications of this outstanding material. The high-voltage, high-efficient power electronics that enable active energy harvesting for the electrostrictive polymer also need to be designed specifically for such applications.

Chapter 7

Conclusions and Future Work

7.1 Summary

This thesis has established a modeling technique that is unique in that it uses electrical mechanical boundary integration methods to analyze the energy conversion process. As we gain better understanding of how mechanical energy is converted to electrical energy in piezoelectric and electrostrictive materials, it is intuitive to think along the lines of actively controlling the electrical boundary conditions (voltage/charge) for better energy harvesting effects. This directly leads to the concept of active energy harvesting.

As detailed theoretical analysis shows, the key for a successful active energy harvesting system relies on three aspects of the system. First, the power electronics circuit must be able to apply higher voltage to the device than the open circuit voltage of a piezoelectric device. For optimized operation, the power electronics might need to apply substantially higher voltage to the device. Second, the power efficiency of power electronics directly impacts the performance of the system. This is because the capacitive nature of a piezoelectric device results in a large portion of reactive power in the energy conversion process. Lastly, the voltage and mechanical excitation must be in certain phase relations for optimized power, which might need a mechanical sensor.

Experimental study also confirms that active energy harvesting outperforms the traditional diode rectifier circuit by a large margin. The experimental data matches the theoretical analysis quite well.

The study of electrostrictive polymers as energy harvesting material is also highly interesting. We theoretically determined the energy harvesting circuits that best fit to this kind of material. And more exciting is that the experiment also shows exceptional high energy harvesting density, which could be achieved using actively controlled electrical boundary conditions. The data is explained by the theoretical model if the experimentally measured dielectric loss is subtracted from the ideal lossless model.

7.2 Future Work

From a theoretical side, this thesis developed the model under a quasi-static assumption. In fact, it is highly desirable to include the structural dynamics in the model. Some preliminary work has indicated that active energy harvesting is also highly attractive for vibration energy harvesting. It can increase the power output at resonance frequency and also broadens the half-power bandwidth.

For practice, highly efficient, high voltage power electronics need to be developed along with ultra-low power control circuits. One major obstacle of an active energy harvesting circuit is the ‘cool start’ problem. That is, when the storage unit is depleted, how can one design a system that could still power the control circuit and accumulate energy? This is more difficult for electrostrictive materials, which always need certain bias fields to be active.

Bibliography

1. Vieira, M.A.M.; Coelho, C.N., Jr.; da Silva, D.C., Jr.; da Mata, J.M., "Survey on wireless sensor network devices", Emerging Technologies and Factory Automation, 2003. Proceedings. ETFA '03. IEEE Conference p 36-38
2. G. J. Pottie and W. J. Kaiser, "Wireless Integrated Network Sensors," Commun. ACM, May 2000, p 51-58
3. Satyanarayanan, M., "Avoiding dead batteries" IEEE Pervasive Computing, v 4, n 1, January/March, 2005, p 2-3
4. Sikora, Axel, Ottesteanu, Marius, "Power consumption models for wireless grid networks with special regard of energy autonomous systems", WSEAS Transactions on Systems, v 4, n 12, December, 2005, p 2189-2195
5. Rahimi, Mohammad; Shah, Hardik; Sukhatme, Gaurav S.; Heideman, John; Estrin, Deborah, "Studying the feasibility of energy harvesting in a mobile sensor network" Proceedings - IEEE International Conference on Robotics and Automation, v 1, 2003, p 19-24
6. Sodano, Henry A. (Ctr. Intelligent Mat. Syst./Struct., Virginia Polytech. Inst./Stt. Univ.); Park, Gyuhae; Leo, Donald J.; Inman, Daniel J., "Use of piezoelectric energy harvesting devices for charging batteries", Proceedings of SPIE - The International Society for Optical Engineering, v 5050, 2003, p 101-108
7. Liu, Yiming; Ren, Kai Liang; Hofmann, H.F.; Zhang, Qiming, "Investigation of electrostrictive polymers for energy harvesting", IEEE Transactions on Ultrasonics, Ferroelectrics, and Frequency Control, v 52, n 12, December, 2005, p 2411-2417
8. Mateu, Loreto (Department of Electronic Engineering, Polytechnical University of Catalonia); Moll, Francesc, "Optimum piezoelectric bending beam structures for energy harvesting using shoe inserts", Journal of Intelligent Material Systems and Structures, v 16, n 10, October, 2005, p 835-845
9. Kim, Sunghwan (Department of Mechanical Engineering, University of Pittsburgh); Clark, William W.; Wang, Qing-Ming, "Piezoelectric energy harvesting using a diaphragm structure", Proceedings of SPIE - The International Society for Optical Engineering, v 5055, 2003, p 307-318
10. Yoon, Hwan-Sik (Mechanical Engineering, Ohio State University); Washington, Gregory; Danak, Amita, "Modeling, optimization, and design of efficient initially

curved piezoceramic unimorphs for energy harvesting applications", *Journal of Intelligent Material Systems and Structures*, v 16, n 10, October, 2005, p 877-888

11. Roundy, Shad (Australian National University, Dept. of Engineering); Zhang, Yang, "Toward self-tuning adaptive vibration based micro-generators", *Proceedings of SPIE - The International Society for Optical Engineering*, v 5649, n PART 1, Smart Structures, Devices, and Systems II, 2005, p 373-384
12. Datasheet PMG7-6 Perpetuum Ltd <http://www.perpetuum.co.uk/products.htm>
13. Ottman, Geoffrey K. (Applied Physics Laboratory, Johns Hopkins University); Hofmann, Heath F.; Bhatt, Archin C.; Lesieutre, George A., "Adaptive piezoelectric energy harvesting circuit for wireless remote power supply", *IEEE Transactions on Power Electronics*, v 17, n 5, September, 2002, p 669-676
14. Shenck, N.S.; Paradiso, J.A., "Energy scavenging with shoe-mounted piezoelectrics", *IEEE Micro*, v 21, n 3, May/June, 2001, p 30-42
15. Guan, Mingjie (Smart Materials and Structures Laboratory, Department of Automation and Computer-Aided Engineering, Chinese University of Hong Kong); Liao, Wei-Hsin, "On the energy storage devices in piezoelectric energy harvesting", *Proceedings of SPIE - The International Society for Optical Engineering*, v 6169, Smart Structures and Materials 2006: Damping and Isolation, 2006, p 616-619
16. Nye, T.W. (TRW Space and Electronics Group); Manning, R.A.; Qassim, K., "Performance of active vibration control technology: The ACTEX flight experiments", *Smart Materials and Structures*, v 8, n 6, Dec, 1999, p 767-780
17. Radcliffe, C.J. (Michigan State Univ); Wang, K.-W; Tzou, H.S.; Hendricks, E.W. eds., "Active Control of Noise and Vibration - 1992", American Society of Mechanical Engineers, Dynamic Systems and Control Division (Publication DSC, v 38, Active Control of Noise and Vibration - 1992, p 363-367
18. Vujic, Nikola (Ctr. Intelligent Mat. Syst./Struct., Mechanical Engineering Department, Virginia Tech); Leo, Donald J.; Lindner, Douglas K., "Power regeneration in active vibration isolation systems", *Proceedings of SPIE - The International Society for Optical Engineering*, v 5052, 2003, p 368-379
19. Miles, R.W. (Northumbria Photovoltaics Applications Centre, School of Informatics, Engineering and Technology, Northumbria University) "Photovoltaic solar cells: Choice of materials and production methods" *Vacuum*, v 80, n 10, Aug 3, 2006, p 1090-1097

20. Tse, K.K. (Department of Electronic Engineering, City University of Hong Kong); Ho, Billy M.T.; Chung, Henry Shu-Hung; Hui, S. Y. Ron "A comparative study of maximum-power-point trackers for photovoltaic panels using switching-frequency modulation scheme" *IEEE Transactions on Industrial Electronics*, v 51, n 2, April, 2004, p 410-418
21. Mi, Minhong (Department of Electrical Engineering, University of Pittsburgh); Mickle, Marlin H.; Capelli, Chris; Swift, Harold "RF energy harvesting with multiple antennas in the same space" *IEEE Antennas and Propagation Magazine*, v 47, n 5, October, 2005, p 100-106
22. Duffy, M. (National University of Ireland); Carroll, D. "Electromagnetic generators for power harvesting" *PESC Record - IEEE Annual Power Electronics Specialists Conference*, v 3, 2004 *IEEE 35th Annual Power Electronics Specialists Conference, PESC04, 2004*, p 2075-2081
23. Seemann, Kay (Institute of Electronics Engineering, University of Erlangen-Nuremberg); Weigel, Robert "Ultra-low-power rectification in passive RFID tags at UHF frequencies" *Frequenz*, v 59, n 5-6, May/June, 2005, p 112-115
24. Despesse, Ghislain (CEA/DRT-LETI/DCIS); Jager, Thomas "Exploitation of the thermotunnel effect for energy scavenging" *Journal of Applied Physics*, v 96, n 9, Nov 1, 2004, p 5026-5031
25. E.M. Yeatman, "Advance in Power Source for Wireless Sensor Node," *Proc. Int'l Workshop Wearable and Implatable Body sensor Networks, 2004*, pp. 20-21.
26. A.S. Holmes et al., "Axial-Flow Microturbine with Electromagnetic Generator: Design, CFD Simulation, and Prototype Demonstration," *Proc. 17th IEEE int'l Micro Electro Mechanical Systems Conf. (MEMS 04)*, IEEE Press, 2004 pp.568-571.
27. O. Yaglioglu, "Modeling and Design Considerations for a Micro-Hydraulic Piezoelectric Power Generator," master's thesis. Dept. Electrical Eng. And Computer Science, Massachusetts Inst. Of Technology, 2002
28. R.D. Kornbluh et al., "Electroelastomers: Applications of Dielectric Elastomer Transducers for Actuation, Generation and Smart Structures," *Smart Structure and Materials 2002: Industrial and Commercial Applications of Smart Structures Technologies*, Proc. SPIE, vol. 4698, Int'l Soc. Optical Eng., 2002, pp. 254-270.
29. Chandrakasan, Anantha (Massachusetts Inst of Technology); Amirtharajah, Rajeevan; Cho, Seong Hwan; Goodman, James; Konduri, Gangadhar; Kulik, Joanna; Rabiner, Wendi; Wang, Alice "Design considerations for distributed microsensor systems" *Proceedings of the Custom Integrated Circuits Conference, 1999*, p 279-286

30. Peano, Fabio (Politecnico di Torino, Department of Energetic); Tambosso, Tiziana "Design and optimization of a MEMS electret-based capacitive energy scavenger" *Journal of Microelectromechanical Systems*, v 14, n 3, June, 2005, p 429-435
31. Sommer-Larsen, Peter (Danish Polymer Centre, RISO National Laboratory); Kofod, Guggi; Benslimane, Mohammed; Gravesen, Peter; Shridhar, M.H. "Performance of dielectric elastomer actuators and materials" *Proceedings of SPIE - The International Society for Optical Engineering*, v 4695, 2002, p 158-166
32. Ting, Robert Y. (Univ of Central Florida); Zhang, Qiming "New electrostrictive PVDF copolymers for large-strain actuator application" *Proceedings of SPIE - The International Society for Optical Engineering*, v 4073, 2000, p 48-58
33. Mateu, Loreto (Department of Electronic Engineering, Polytechnical University of Catalonia); Moll, Francesc "Optimum piezoelectric bending beam structures for energy harvesting using shoe inserts" *Journal of Intelligent Material Systems and Structures*, v 16, n 10, October, 2005, p 835-845
34. Pelrine, R. (SRI International); Kornbluh, R.; Eckerle, J.; Jeuck, P.; Oh, S.; Pei, Q.; Stanford, S. "Dielectric elastomers: Generator mode fundamentals and applications" *Proceedings of SPIE - The International Society for Optical Engineering*, v 4329, 2001, p 148-156
35. Laibowitz, Mathew (MIT Media Laboratory); Paradiso, Joseph A. "Parasitic mobility for pervasive sensor networks" *Lecture Notes in Computer Science*, v 3468, *Pervasive Computing: Third International Conference, PERVASIVE 2005, Proceedings*, 2005, p 255-278
36. Taylor, George W. (Ocean Power Technologies Inc.); Burns, Joseph R.; Kammann, Sean M.; Powers, William B.; Welsh, Thomas R. "The energy harvesting Eel: A small subsurface ocean/river power generator" *IEEE Journal of Oceanic Engineering*, v 26, n 4, October, 2001, p 539-547
37. Theurer, Charles B. (Department of Mechanical Engineering, University of Massachusetts Amherst); Kazmer, David; Zhang, Li; Gao, Robert X. "Self-Energized Wireless Pressure Sensor Using Energy Extraction from Injection Mold Pressure Differential" *Proceedings of IEEE Sensors*, v 1, n 2, 2002, p 942-949
38. IEEE standard on piezoelectricity 29 Jan 1988
39. Yoon, Hwan-Sik (Mechanical Engineering, Ohio State University); Washington, Gregory; Danak, Amita "Modeling, optimization, and design of efficient initially

- curved piezoceramic unimorphs for energy harvesting applications": *Journal of Intelligent Material Systems and Structures*, v 16, n 10, October, 2005, p 877-888
40. Mossi, Karla (Virginia Commonwealth University); Green, Christopher; Ounaies, Zoubeida; Hughes, Esther, "Harvesting energy using a thin unimorph prestressed bender: Geometrical effects," *Journal of Intelligent Material Systems and Structures*, v 16, n 3, March, 2005, p 249-261
 41. Ren, Kailiang (Department of Electrical Engineering, Pennsylvania State University); Liu, Yiming; Geng, Xuecang; Hofmann, Heath F.; Zhang, Qiming M. "Single crystal PMN-PT/epoxy 1-3 composite for energy-harvesting application", *IEEE Transactions on Ultrasonics, Ferroelectrics, and Frequency Control*, v 53, n 3, March, 2006, p 631-637
 42. Danak, Amita D. (Intelligent Struct. and Systems Lab, Ohio State University); Yoon, Hwan-Sik; Washington, Gregory N. "Optimization of electrical output in response to mechanical input in piezoceramic laminated shells": *American Society of Mechanical Engineers, Aerospace Division (Publication) AD*, v 68, *Proceedings of the ASME Aerospace Division - 2003*, 2003, p 309-315
 43. Kim, Hyeoung Woo (Intl. Ctr. Actuators and Transducers, Materials Research Institute, Pennsylvania State University); Batra, Amit; Priya, Shashank; Uchino, Kenji; Markley, Douglas; Newnham, Robert E.; Hofmann, Heath F. "Energy harvesting using a piezoelectric "cymbal" transducer in dynamic environment": *Japanese Journal of Applied Physics, Part 1: Regular Papers and Short Notes and Review Papers*, v 43, n 9 A, September, 2004, p 6178-6183
 44. Sodano, Henry A. (Department of Mechanical Engineering - Energy Mechanics, Michigan Technological University); Inman, Daniel J.; Park, Gyuhae "Comparison of piezoelectric energy harvesting devices for recharging batteries": *Journal of Intelligent Material Systems and Structures*, v 16, n 10, October, 2005, p 799-807
 45. Wang, Qing-Ming (Lexmark Int, Inc); Du, Xiao-Hong; Xu, Baomin; Cross, L. Eric "Electromechanical coupling and output efficiency of piezoelectric bending actuators": *IEEE Transactions on Ultrasonics, Ferroelectrics, and Frequency Control*, v 46, n 3, 1999, p 638-646
 46. Lim, Kee-Joe (Sch. of Elec. and Comp. Engineering, Chungbuk National University); Kang, Seong-Hwa; Lee, Jong-Sub "Design and properties of piezoelectric vibrator with generating function by FEM analysis": *Journal of Electroceramics*, v 13, n 1-3, July, 2004, p 429-432
 47. Kim, Sunghwan (University of Pittsburgh, Mechanical Engineering); Clark, William W.; Wang, Qing-Ming "Piezoelectric energy harvesting using a clamped circular plate: Experimental study": *American Society of Mechanical Engineers*,

- Aerospace Division (Publication) AD, v 68, Proceedings of the ASME Aerospace Division - 2003, 2003, p 461-469
48. Richard Feynman, Robert B. Leighton, Matthew L. Sands "The Feynman lecture on physics" Vol. II, 17-7 Welsey 1989
 49. Ottman, Geoffrey K. (Dept. of Electrical Engineering, The Pennsylvania State University); Hofmann, Heath F.; Lesieutre, George A. "Optimized piezoelectric energy harvesting circuit using step-down converter in discontinuous conduction mode" PESC Record - IEEE Annual Power Electronics Specialists Conference, v 4, 2002, p 1988-1994
 50. Lefevre, Elie (Laboratoire de Genie Electrique et Ferroelectricite, INSA de Lyon); Badel, Adrien; Richard, Claude; Guyomar, Daniel "Piezoelectric energy harvesting device optimization by synchronous electric charge extraction" Journal of Intelligent Material Systems and Structures, v 16, n 10, October, 2005, p 865-876
 51. P. Smalser, "Power transfer of piezoelectric generated energy," U.S. Patent, 5 703 474, 1997.
 52. Badel, A. (Institut National des Sciences Appliquees de Lyon, Laboratoire de Genie Electrique et Ferroelectricite); Sebald, G.; Guyomar, D.; Lallart, M.; Lefevre, E.; Richard, C.; Qiu, J. "Piezoelectric vibration control by synchronized switching on adaptive voltage sources: Towards wideband semi-active damping" Journal of the Acoustical Society of America, v 119, n 5, 2006, p 2815-2825
 53. Richard, Claude (Inst Natl des Sciences Appliquees); Guyomar, Daniel; Audigier, David; Bassaler, Henri "Enhanced semi passive damping using continuous switching of a piezoelectric device on an inductor" Proceedings of SPIE - The International Society for Optical Engineering, v 3989, 2000, p 288-299
 54. Brennan, M.J. (Univ of Southampton); Garcia-Bonito, J.; Elliott, S.J.; David, A.; Pinnington, R.J. "Design of a piezoelectric actuator for active vibration control" American Society of Mechanical Engineers, Design Engineering Division (Publication) DE, v 93, Active Control of Vibration and Noise, 1996, p 315-322
 55. Hagood, N.W. and Ghandi, K. 2003. "Electrical power extraction from mechanical disturbances", U.S. Patent 6,580,177.
 56. Alsweify, Khaled A. (California Polytechnic State Univ); Kolkailah, Faysal A.; Farghaly, Said H. "Active and passive damping control of intelligent structure vibration" International SAMPE Symposium and Exhibition (Proceedings), v 43, n 1, 1998, p 413-425

57. Kloos, Gerhard (Eindhoven Univ of Technology) "Quadratic electrostriction in polymers" Annual Technical Conference - ANTEC, Conference Proceedings, v 2, Materials, 1996, p 2365-2368
58. R. Pelrine, R. D. Kornbluh, J. Eckerle, P. Jeuck, S. Oh, Q. Pei, and S. Stanford, "Dielectric elastomers: Generator mode fundamentals vol. 4329, pp. 148–156, Mar. 2001.
59. Q. M. Zhang and J. Scheinbeim, "Electric EAP," in *Electroactive Polymer [EAP] Actuators as Artificial Muscles*. Y. Bar-Cohen, Ed. 2nd ed. Bellingham: SPIE Press, 2004, pp. 95–150.
60. Lee, C.S. (Department of Physics, Ctr. Electro/Photo Responsive Molec., Korea University); Joo, J.; Han, S.; Koh, S.K. "Multifunctional transducer using poly (vinylidene fluoride) active layer and highly conducting poly (3,4-ethylenedioxythiophene) electrode: Actuator and generator" *Applied Physics Letters*, v 85, n 10, Sep 6, 2004, p 1841-1843
61. Makihara, Kanjuro, Onoda, Junjiro, Miyakawa, Takeya, "Low energy dissipation electric circuit for energy harvesting" *Smart Materials and Structures*, v 15, n 5, Oct 1, 2006, p 1493-1498
62. Burns, J.R., Smalser, P., Taylor, G.W. and Welsh, T.R. 2003. "Switched resonant power conversion electronics", U.S. Patent 6,528,928 .
63. Faiz, A. (Laboratoire de Genie Electrique et Ferroelectricite (LGEF), INSA de Lyon); Guyomar, D.; Petit, L.; Buttay, C. "Semi-passive piezoelectric noise control in transmission by synchronized switching damping on voltage source" *Journal De Physique. IV : JP*, v 128, September, 2005, p 171-176

VITAE

Yiming Liu

Education

PhD Candidate, Electrical Engineering

GPA 3.7/4.0 Pennsylvania State University *August 1999–December 2006*

Bachelor of Science, Physics

GPA 3.8/4.0 Nanjing University *August 1992–May 1996*

Work Experience

KCF Technologies State College, PA *August 2004– December 2006*

Embedded Software & System Design Engineer

- Energy Harvesting circuit design
- Smart Tether embedded system design
- Robotic arm for sound intensity measurement system integration

Awards and Honors

- Braddock Fellowship (1999-2000)
- People's Scholarship (1992-1994)
- Duncan Fellowship (1999-2000)
- Yinsong Scholarship (1992-1993)